QUANTITATIVE INFRARED MULTICOMPONENT ANALYSIS OF MINERALS OCCURRING IN COAL

Patricia A. Estep, John J. Kovach, and Clarence Karr, Jr.

U.S. Department of the Interior, Bureau of Mines,
Morgantown Coal Research Center, Morgantown, West Virginia

INTRODUCTION

The recent development of a new low-temperature ashing technique (12) for obtaining unaltered mineral matter from coal, combined with the extension of the mid-infrared region to 200 cm^{-1}, has shown clearly that infrared spectroscopy is a valuable tool for use in coal mineralogical studies (15). The direct infrared analysis of minerals in coal has been hindered previously by the broad background absorption of the coal itself (11) as shown in Figure 1, curve (b), coupled with the paucity and often nonspecificity of mineral absorption bands in the rock-salt region of 5000 to 650 cm^{-1}. However, when the coal substance, approximately 90% of the sample, is removed at low temperatures in an oxygen plasma (12), there remains unaltered mineral matter with an infrared spectrum exhibiting many diagnostic and analytically useful absorption bands as shown in Figure 1, curve (c). The disappearance of organic absorption bands indicates complete removal of the coal substance. The improved quality of the spectrum obtained on this enriched mineral matter has increased the possibilities for quantitative analysis. In this paper we describe the development of an infrared solid state quantitative analysis for five commonly occurring coal minerals--quartz, calcite, gypsum, pyrite, and kaolinite. The presence of many other minerals in coal in a wide range of concentrations has been shown (6, 9, 16, 28). However, those included in this analysis were selected on the basis of their frequency of occurrence and relative abundance in the coal samples examined in this laboratory. We anticipate that in this continuing broad program using infrared spectroscopy for coal mineralogical studies, qualitative and quantitative analysis can be developed for other minerals.

A large part of the published infrared data for minerals (1, 14, 30) and inorganic compounds (26) is limited to the rock-salt region of 5000 to 650 cm^{-1}. Recently, spectral data in the extended region of 650 to 400 cm^{-1} has been presented for some minerals (31, 37) and down to 240 cm^{-1} for some inorganic compounds (24, 25, 32, 38). However, these collections offer very few high-resolution spectra for naturally occurring minerals to 200 cm^{-1}. The published papers on quantitative infrared analysis of minerals have dealt with a single mineral or the detailed studies of sampling parameters, while very little has appeared on multicomponent mixtures (14, 23).

EXPERIMENTAL

Several specimens of each of the five minerals were obtained from different localities and their infrared spectra checked qualitatively for associated mineral contamination and phase purity by three means: common agreement of the spectra for samples from several sources, literature infrared data, and X-ray powder data. On the basis of this qualitative screening, two sources were selected for detailed grinding studies in order to establish the infrared absorptivity calibration data. The mineral was placed with an agate ball into an agate vial, approximately one-third full, and ground mechanically in a Spex Mixer Mill. A sample was removed from the vial for infrared analysis at five-minute intervals with a five-minute cooling period. The grinding was continued until measured band absorptivities became constant, at which point a particle size determination was made using a Coulter Counter, Model A (Coulter Electronics). Pellets for the infrared analysis were prepared by weighing one milligram of the pregound mineral and 500 milligrams of cesium iodide powder (Harshaw, 100 to 325 mesh, median particle size 62μ) on a microbalance and blending by hand for five minutes in a mullite mortar. This mixture was transferred quantitatively to a die and pressed into a pellet according to a triple press method (13). For this the pellet was placed under vacuum, pressed for five minutes at a pressure of 23,000 pounds total load, the pressure relaxed for five minutes, and the procedure repeated twice. The additional pressing steps presumably relieve the strain introduced by the original pressing. The resulting pellet of 0.80 by 13 mm was then scanned immediately on a Perkin-Elmer 621 infrared grating spectrophotometer purged with dry air.

Enriched mineral samples from coal were prepared by low-temperature oxidation at 145° C in an oxygen plasma using Tracerlab's Model LTA-600. Each of the five minerals was exposed to the same ashing conditions as the coal samples. There were no sample alterations, except for the partial dehydration of gypsum to the hemihydrate.

RESULTS AND DISCUSSION

Sampling Parameters

Tuddenham (35) has shown the application of the potassium bromide pellet method to mineral analysis and demonstrated its quantitative potentialities. Most infrared spectroscopists conclude that it is possible to achieve acceptable solid state analysis only with rigorously standardized conditions of sample preparation. The many difficulties encountered in quantitative solid phase spectroscopy have been reviewed by Duyckaerts (10), Kirkland (17), and Baker (5).

Particle Size. Probably the most important single physical factor to be considered in quantitative solid state spectroscopy is that of particle size. This problem has been investigated both theoretically and experimentally by several workers (10, 19, 34, 35). As particle size is reduced there is a reduction of light loss by reflection and scattering and the intensity of an absorption band increases from an apparent absorptivity to its true absorptivity value. Descriptions of this relationship between particle size and absorptivity for the mineral calcite has been given by Lejeune (19) and Duyckaerts (10) and for quartz by Tuddenham (35). Other workers have used the more empirical approach of relating infrared absorptivities to sample grinding time, which is proportional to particle size. The commonly used sedimentation technique for obtaining the required particle size of the sample, while applicable to single component samples, cannot be employed with multicomponent samples (14, 35) since this procedure leads to a differential separation of the individual components. The effects of particle size reduction can vary with different minerals and can vary for absorption bands of different intensities. Kirkland (17) has pointed out that the absorptivities of bands associated with crystallinity can be more susceptible to particle size variations than those originating from functional group vibrations. These considerations necessitate a careful study of the effects of particle size on absorptivity for each band being considered for quantitative analysis. For this work the expedient method of studying absorptivity as a function of grinding time was chosen. If a strict grinding schedule is followed, particle size need only be determined on those samples ground for lengths of time necessary to produce constant absorptivity values. Thus, knowledge of particle size requirements for constant absorptivities is available with a minimum of effort. A typical example of such a grind study is shown in Figure 2 for the mineral pyrite. The data show that the apparent absorptivity becomes constant after a minimum grinding time and remains constant even with extended grinding and further particle size reduction. The minimum grinding time for a particular mineral can vary with the type of vial used and the amount of sample loaded into the vial. Grind studies on all five minerals reveal that at the minimum grind time, the mean particle size of the sample falls in the range of 4 to 13 microns. This fulfills the theoretical requirement for solid phase spectroscopy, that is, sample particle size should be less than the wavelength of the incident radiation, in order to minimize scattering, reflection, and the Christiansen effect.

While the absorptivities as determined for use in this analysis are constant, they are not necessarily maximum values. Particle size reduction of the cesium iodide matrix can cause band absorptivities to increase markedly. This effect was shown in a grind study in which preground kaolinite was added to samples of cesium iodide, also preground, but for different lengths of time. Each mixture was then hand blended to prepare a pellet according to the chosen procedure. Absorptivities for several kaolinite bands were seen to increase 30 to 50% when prepared with cesium iodide that had been ground for 20 minutes. True absorptivities could not be determined because, at a very fine particle size, cesium iodide pellets crumble. While not recommended for quantitative work, grinding samples for five minutes in a ball mill with cesium iodide is a good technique for improving the qualitative appearance of the spectrum; band resolution improves and background is considerably reduced. The relatively gentle grinding that the cesium iodide receives during the blending stage of pellet preparation reduces its particle size very little as shown by particle size determinations. Since quantitative accuracy is more a function of reproducibility rather than absolute measurement, the relatively simple and highly reproducible method of hand blending was chosen. An additional reason for selecting this method over the technique of mechanical blending in a ball mill is that the cesium iodide mixture packs in the vial and is not quantitatively recoverable.

Sample Alteration. Extensive grinding can cause polymorphic transformations or alteration of mineral composition. For example, Dachille (8) has shown that a few minutes grinding in a Wig-L-Bug with a metal vial and ball can transform calcite to the high-pressure phase of aragonite. He assigns this transformation to a pressure component in the mechanical action of the vibrator. Burns (7) also studied this calcite-aragonite transformation and found that it can occur by grinding at room temperature. Morris (27) found that vibrating for more than one minute in a stainless-steel Wig-L-Bug will cause dehydration of gypsum. Liberti (20) has reported destruction of the crystalline structure of quartz under certain grinding conditions. We have noted changes in the spectrum of kaolinite after it was subjected to severe grinding conditions. However, none of these alterations were observed by using the chosen procedure, presumably due to the periodic cooling periods during grinding and to the use of an agate grinding ball mill. Since the density of agate is about one-third the density of stainless steel, there is less mechanical stress exerted on the sample in this vial. The absorptivity values of some absorption bands began to decrease with prolonged grinding, although no qualitative spectral changes occurred. Since some form of sample alteration occurred, these bands were not selected for use in the quantitative analysis.

Particle Distribution. If Beer's law is to be followed, all absorbances must show a linear dependence on effective concentration. The concentration is considered effective because the infrared beam does not completely cover the entire pellet in the instrument. The use of sample weight as a concentration factor thus requires a high degree of uniform dispersion, or a homogeneous mixture of sample and matrix. This can be achieved if particle size is small and if blending is thorough. In the instrument used, the infrared beam covers about 50% of the pellet area. As a test of the dispersion achieved with the chosen sample preparation technique, pellets of each of the five minerals were rotated systematically through 360° with scans taken at several settings. For all positions, the band intensities were identical, indicating that dispersion is adequate, and also that there are no polarization or orientation effects.

Choice of Matrix. Several salts were tested for use as a matrix. Cesium iodide appeared to be the best choice on the basis of its superior transparency at long wavelengths. The low background at shorter wavelengths due to scattering was not objectionable since most of the useful absorption bands for minerals are found at longer wavelengths. The triple press method reduced scattering at short wavelengths, often as much as 40% over single pressing. The over-all transmission of a blank cesium iodide pellet was acceptable, as shown in Figure 1, curve (a), and therefore no pellet was used in the reference beam. Although cesium iodide is slightly hygroscopic, there was less difficulty from water adsorption than is generally experienced using the more common potassium bromide matrix. While mechanical grinding of cesium iodide intensified the water absorption bands, hand blending produced no more than 0.02 absorbance units at the 3430 cm^{-1} OH stretching frequency. This behavior of cesium iodide has a decided advantage since coal minerals often have useful OH absorption bands.

The pellet thickness must be controlled in order to prevent interference or fringe patterns. In the longer wavelength region where the requirements for parallel pellet surfaces are relaxed, these fringe patterns can become quite pronounced on thin pellets. In order to eliminate this as a potential source of quantitative error, pellets at least 0.80 mm thick were used.

Other Parameters. There are other sampling problems sometimes encountered in solid state analysis. Among these is interaction of the sample with the matrix, believed to be negligible for the minerals analyzed here. A large refractive index difference between the sample and the dispersion medium can cause a pronounced Christiansen effect, characterized by the asymmetrical shape of an absorption band, and resulting in high light scattering which can introduce errors into quantitative measurements. However, the small particle size used should minimize any error arising from this effect. Departure from Beer's law is possible, but with the base line technique for absorbance measurements and with controlled particle size, Beer's law was obeyed for concentration ranges of 0.02 to 0.2 wt-pct. One of the limitations in the quantitative analysis of minerals and inorganics is due to their inherently high band absorptivities. With intense absorption, only a very small amount of sample can be included in the pellet, so that the band will still be measurable, thus increasing weighing errors. However, reproducible results could be obtained with a microbalance and a large area of beam coverage of the pellet.

Qualitative Analysis

Since natural mineral specimens, which were used as standards in this analysis, often occur in polymorphic aggregations, it was necessary to determine the qualitative infrared spectral differences for polymorphs of each mineral. In the coal samples thus far investigated no polymorphic mixtures were encountered, although they can be expected. Table 1 lists the spectral data from this laboratory for each of the five minerals and some polymorphic forms.

Quartz. The two quartz samples used as standards, for which bands are presented in Table 1 and absorptivity data in Table 2, are both low-temperature α-quartz. This was established from differences shown in the infrared spectra of samples of polymorphs of crystalline silica in this laboratory, from literature data (21, 33, 39), and from X-ray powder data. The α-quartz form can be distinguished in the 650 to 200 cm^{-1} region from the polymorphic forms of α-tridymite and α- and β-cristobalite. Work remains to confirm the distinction of α-quartz from β-quartz and β-tridymite. The distinction of α-quartz from its crystalline polymorphs and other modifications of silica can be made by the highly unique bands at 256, 363, 388, and 688 cm^{-1}.

Calcite. The natural aggregation of calcite and its dimorph aragonite is common (3). Infrared literature data (2, 3) in the rock-salt region show that hexagonal calcite can be distinguished from orthorhombic aragonite. The data from our laboratory in Table 1 show the marked difference in their spectra and list the additional bands obtained for the region 650 to 200 cm^{-1}. Petrographic distinction between these two polymorphs is often inadequate as shown by the fact that three of our samples labeled aragonite were shown by infrared to be calcite. Adler (3) found that several specimens of aragonite and calcite differed from their museum labels.

Gypsum. For gypsum (monoclinic), it was necessary to show that the crystallographically different anhydrite (orthorhombic), often found in coal, and the hemihydrate (hexagonal, $CaSO_4 \cdot 1/2H_2O$), can be differentiated in the infrared for the preliminary qualitative analysis of the sample. Data from Morris (27) and from our laboratory, in Table 1 show that the hemihydrate has unique bands and can be differentiated from gypsum. These spectral differences were used to show that the low-temperature oxidation technique produced a conversion of gypsum to the hemihydrate. Gypsum was selected for testing in synthetic mixtures since it has been identified and analyzed in coal product samples not subjected to low-temperature ashing. Anhydrite is also readily distinguishable from gypsum. The primary difference is a splitting of the large, broad band of gypsum at 594 cm^{-1} into two sharp bands at 587 and 607 cm^{-1} for anhydrite. The 660 cm^{-1} band of

Table 1. - Infrared Absorption Bands for Minerals

Mineral	Absorption bands, cm^{-1} *
α-Quartz	256 (w), 360 (mw), 388 (mw), 452 (m), 465 (w, sh), 501 (mw), 688 (w), 772 (mw), 790 (m), 1075 (s), 1135 (w), 1160 (w)
α-Tridymite (synthetic) . .	465 (s), 500 (sh), 782 (m), 1088 (s), 1155 (sh)
α-Cristobalite**	485 (s), 515 (sh), 620 (m), 798 (m), 1104 (s), 1160 (sh), 1204 (w)
Calcite	217 (m), 337 (sh), 307 (s), 707 (m), 842 (vw), 869 (m), 1420 (s), 1600 (w), 1792 (vw)
Aragonite	205 (sh), 245 (s), 288 (sh), 692 (m), 705 (m), 836 (w), 850 (m), 1076 (w, sharp), 1450 (sh), 1464 (s), 1600 (w), 1780 (w)
Gypsum	215 (m), 298 (mw), 412 (w), 445 (w), 594 (m), 660 (m), 998 (vw), 1106 (s), 1132 (s), 1155 (s, sh), 1615 (m), 1680 (mw), 3250 (vw), 3400 (m), 3492 (sh, vw), 3550 (m)
Hemihydrate of $CaSO_4$	235 (m), 250 (sh), 412 (w), 455 (w), 590 (m), 605 (sh, w), 619 (w), 652 (m), 665 (sh, w), 1000 (mw, sharp), 1008 (vw, sh), 1090 (s), 1110 (s), 1128 (s), 1147 (s), 1613 (mw), 3552 (w), 3610 (mw)
Anhydrite	252 (m), 502 (vw), 587 (m), 606 (m), 669 (m), 875 (vw), 998 (vw), 1008 (vw), 1115 (s), 1148 (s)
Pyrite	284 (w), 340 (m), 391 (vw), 406 (s)
Marcasite	285 (w), 321 (m), 350 (m), 396 (s), 407 (s), 422 (vw)
Kaolinite	268 (m), 338 (m), 352 (vw, sh), 405 (vw, sh), 422 (m), 460 (s), 528 (s), 689 (m), 747 (w), 782 (w), 908 (s), 929 (w, sh), 1002 (s), 1026 (s), 1095 (s), 3622 (m), 3652 (w), 3670 (vw), 3698 (m)

---

* Very weak = vw; weak = w; medium = m; strong = s; shoulder = sh.

** Data from reference (21).

Table 2. - Analytical Absorption Bands and Absorptivities for Minerals

Mineral	Source	Absorption bands, cm^{-1} and absorptivities, 1/mm*
Quartz	Hot Springs, Ark. . . . . Rock crystal Ward's Natural Science Establishment, Inc.	360 (448), 388 (525), 452 (1010), 790 (589)
	Berkeley Springs, W. Va. . . Oriskany sandstone W. Va. University Geology Department	360 (430), 388 (500), 452 (970), 790 (580)
Calcite	Germany Valley, W. Va. . . Crystals W. Va. University Geology Department	307 (720), 869 (610), 1420 (2050)
Gypsum . . .	Niagara, N. Y. . . . . Crystals U. S. National Museum, No. 80022	594 (245), 660 (251)
	Washington County, Utah . . . Crystals Ward's Natural Science Establishment, Inc.	594 (246), 660 (254)
Pyrite	Park City, Utah . . . . Ward's Natural Science Establishment, Inc.	340 (190), 406 (630)
	Gilman, Eagle County, Colo. . . . . Minerals Unlimited	340 (180), 406 (640)
Kaolinite . .	Macon, Ga., Oneal Pit . . . . API Reference Clay Mineral Kaolinite No. 4 Ward's Natural Science Establishment, Inc.	338 (353), 422 (505), 460 (986), 528 (1106), 689 (338), 747 (131), 908 (617)

---

* Absorptivities in parentheses.

gypsum shifts to 669 cm^{-1} in anhydrite, and the water vibrations appearing at 1615, 1680, 3400, and 3555 cm^{-1} are unique for gypsum. Data in Table 1 also show the differences between the hemihydrate and anhydrite.

Pyrite. Both polymorphs of FeS_2, pyrite and marcasite, have been identified in coal (6, 9, 36). White (37) has presented infrared data to 400 cm^{-1} which is insufficient for differentiation between these two polymorphs. However, the infrared spectra to 200 cm^{-1} obtained on samples in this laboratory show that these two polymorphs are distinguishable in this region. Table 1 shows that, although marcasite exhibits two bands common to pyrite, there are four distinctly different bands which uniquely characterize this polymorph. Further, the band at 340 cm^{-1}, which is unique for pyrite, allows detection of pyrite in marcasite samples. These infrared differences, along with X-ray confirmation, established the phase purity of the pyrite standards selected for calibration and thus also the qualitative identification of pyrite as the observed form occurring in the coal samples studied. It was particularly important to establish by X-ray that no pyrrhotite (FeS) was present in the standard samples since this mineral has no absorption in the entire 5000 to 200 cm^{-1} region. Optical examination is also often unreliable for this mineral class since out of 15 different mineral specimens labeled marcasite, two were pyrrhotite, six were pyrite, and only seven were actually marcasite as shown by infrared analysis.

Kaolinite. Clays other than kaolinite are found in coal. Kaolinite can be identified by infrared in mixtures of clay minerals and even in mixed-layer clay minerals (29). Montmorillonite, illite, and kaolinite predominate in many coals and Angino (4) has discussed the infrared spectral differences among these out to 90 cm^{-1}. The OH region is especially useful in the qualitative identification of kaolinite. Kodama (18) states that the absorption band at 3698 cm^{-1} can distinguish kaolinite from other clay minerals down to a few weight-percent of kaolinite in total amounts of clay minerals. Lyon (22) has shown that the use of ratios for bands appearing in the OH region, along with other spectral differences, enables a unique distinction to be made among the kaolin group minerals of kaolinite, dickite, and halloysite. This literature data, and data obtained in our laboratory from a number of API reference clay minerals, were used to substantiate the identification of kaolinite in the coal low-temperature ash samples and as a guide in the selection of bands for quantitative analysis.

Quantitative Analysis

The apparent absorptivity of a band was calculated from the relationship:

$$a = \frac{A}{b\,c}$$

where a = absorptivity in units of 1/mm;
A = absorbance of the band (baseline technique);
b = pellet thickness, mm;
c = concentration, weight-percent.

The value of absorptivity is specific for a 13 mm diameter pellet.

After completion of grind studies for each mineral, bands were selected for quantitative analysis. These selections were based on both their specificity and the constancy of their absorptivities with prolonged grinding. Table 2 lists the bands selected for analysis. When it is necessary, for the sake of specificity, to use a band which does not remain constant with particle size reduction beyond the minimum grind time, the error introduced must be considered.

Only one source for kaolinite was used for the calibration data because there is extensive mineralogical data for it in the literature. The data in Table 2 are the results of duplicate grind studies that were quite reproducible. Only one source of calcite was used because of the wide variation of absorptivity values from different sources, even though their spectra were qualitatively identical and their particle sizes were the same. Therefore, calcite from the same source was used for synthetic mixtures and for calibration data in order to obtain agreement. Additional work is required to resolve this limitation by examination of these samples by other analytical techniques in order to determine the cause for such a variation.

Several synthetic mixtures, listed in Table 3, were prepared to test the accuracy of the multicomponent analysis. Preground standard mineral samples of the required particle size were used and the same technique for pellet preparation used as described for the mineral standards. The concentration ranges of the pure minerals were selected to represent the concentration ranges commonly encountered in the coal samples examined. No attempt was made to determine the limit of detectability for each mineral since this was different for different sample compositions. Figure 3 shows the infrared spectrum of synthetic mixture No. 7, which approximated the composition of a typical coal low-temperature ash as shown in Figure 1, curve (c), except for the gypsum-hemihydrate conversion. When band overlapping occurred, the required absorbance correction was obtained from the standard spectra of the interfering mineral, using the standard procedures for quantitative analysis. An expedient technique of chart overlay to obtain background and band overlapping corrections was as accurate as the more time consuming procedure of matrix solution. The agreement shown in Table 3, within an average error of 6.2% for all minerals, demonstrates the method to be satisfactory for the multicomponent mixtures investigated. It is difficult, without an independent reliable method of analysis, to determine the accuracy limits of the infrared method when applied to coal ash samples. Greater accuracy is expected with the synthetic mixtures since they were prepared under controlled conditions of particle size and contained no unknown interferences. In our work it was necessary to pregrind coal samples to speed oxidation in the low-temperature asher. This pregrinding was sufficient to achieve the required particle size reduction for an accurate quantitative analysis, as ascertained by particle size measurements on the ash. Optimum particle size was also indicated for at least the mineral kaolinite from a grind study using its bands that appear fairly well resolved in the spectrum of the total coal sample (see Fig. 1). Grind curves similar to those in Figure 2 were obtained with a relatively small increase in absorptivity before becoming constant. It is essential to conduct a grind study on any mineral mixture prior to analysis in order to establish when the required particle size reduction for each component in the mixture has been achieved. The infrared analysis should be made only after absorptivity values have become constant and particle size has been checked.

Table 3. - Analysis of Synthetic Mixtures of Minerals

Synthetic mixture no.	Kaolinite, %		Quartz, %		Gypsum, %		Calcite, %		Pyrite, %	
	Calc.	Found	Calc.	Found	Calc.	Found	Calc.	Found	Calc.	Found
1	71.86	72.70	28.14	27.10						
2	69.60	71.15	30.40	29.13						
3	53.10	43.71	23.17	19.65	23.72	20.10				
4	41.53	41.04	19.29	19.33	39.18	33.50				
5	54.63	55.18	18.51	19.68	26.85	26.98				
6	29.92	29.39	12.50	11.53	47.32	48.10	10.26	10.31		
7	35.72	31.11	24.11	20.77	31.69	30.78	8.48	10.24		
8			12.21	14.22	33.07	31.13	12.20	12.40	42.52	44.92
9			22.90	19.00	31.30	31.20	8.40	7.00	37.40	30.00
10			15.20	12.00	30.50	30.80	10.60	11.30	43.00	35.12
Average error	2.6		1.9		1.7		0.8		5.9	

A limitation of the application of infrared spectroscopy to mineral mixtures in coal is in the analysis of pyrite in the presence of high amounts of kaolinite (15). Both of the analytical bands of pyrite are overlapped considerably by kaolinite bands and amounts of pyrite as high as 20% might be undetected when kaolinite is present to the extent of 30% or greater. For this reason, no attempt was made to analyze synthetic mixtures containing both. Work is continuing to develop a satisfactory analysis for kaolinite-pyrite mixtures when kaolinite content is high.

CONCLUSIONS

This paper describes the development of a quantitative infrared multicomponent analysis for five minerals commonly occurring in coal. It shows that a successful analysis for quartz, calcite, gypsum, pyrite, and kaolinite is possible if sampling conditions are controlled. The infrared region of 650 to 200 cm^{-1} is seen to contain data that contribute to both the preliminary qualitative and the quantitative analysis of these mixtures. The accuracy of the method was evaluated with tests on synthetic mixtures. Average errors were within 6.2% for all five component minerals. Although the method was primarily applied to the analysis of unaltered mineral matter obtained from coal by use of the new technique of low-temperature ashing in an oxygen plasma, the calibration data obtained can be used in the analysis of other materials connected with the mining and utilization of coal. For example, we have determined these minerals directly in coal mine refuse samples, which often have low organic matter content. The development of the analysis revealed that infrared spectroscopy is a valuable tool for differentiating among various polymorphic mineral forms and provides a collection of high resolution standard reference spectra for naturally occurring minerals and their polymorphs to 200 cm^{-1}.

ACKNOWLEDGMENT

Special thanks are due to Edward E. Childers for assistance in obtaining infrared spectra, and to Dr. John J. Renton, Geology Department, West Virginia University, for providing X-ray data on the mineral samples.

REFERENCES

1. Adler, H. H., E. E. Bray, N. P. Stevens, J. M. Hunt, W. D. Keller, E. E. Pickett, and P. F. Kerr, Am. Petrol. Inst., Project 49, Preliminary Rept. No. 8, July 1950, 146 pp.

2. Adler, H. H., and P. F. Kerr, Am. Mineralogist 48, Nos. 1-2, 124 (1963).

3. _____. Am. Mineralogist 47, Nos. 5-6, 700 (1962).

4. Angino, E. E., Nature 204, No. 4958, 569 (1964).

5. Baker, A. W., J. Phys. Chem 61, No. 4, 450 (1957).

6. Brown, H. R., and D. J. Swaine, J. Inst. Fuel 37, No. 285, 422 (1964).

7. Burns, J. H., and M. A. Bredig, J. Chem. Phys. 25, No. 6, 1281 (1956).

8. Dachille, F., and R. Roy, Nature 186, No. 4718, 70 (1960).

9. Durie, R. A., Fuel 40, No. 5, 407 (1961).

10. Duyckaerts, G., Analyst 84, 201 (1959).

11. Friedel, R. A., and J. A. Queiser, Anal. Chem. 28, No. 1, 22 (1956).

12. Gluskoter, H. J., Fuel 44, No. 4, 285 (1965).

13. Harshaw Chemical Co., Pressed Pellet Techniques, Data Sheet 023.

14. Hunt, J. M., and D. S. Turner, Anal. Chem. 25, No. 8, 1169 (1953).

15. Karr, C., Jr., P. A. Estep, and J. J. Kovach, Chem. Ind. (London) 9, 356 (1967).

16. Kemezys, M., and G. H. Taylor, J. Inst. Fuel 37, No. 285, 389 (1964).

17. Kirkland, J. J., Anal. Chem. 27, No. 10, 1537 (1955).

18. Kodama, H., and K. Oinuma, Proc. Nat. Conf. on Clays and Clay Minerals, 11th, Canada, 236 (1962).

19. Lejeune, R., and G. Duyckaerts, Spectrochim. Acta 6, 194 (1954).

20. Liberti, A., and G. Devitofrancesco, Staub. 25, No. 4, 28 (1965).

21. Lippincott, E. R., A. VanValkenburg, C. E. Weir, and E. N. Bunting. J. Res. Natl. Bur. Std. 61, No. 1, 61 (1958).

22. Lyon, R. J. P., and W. M. Tuddenham, Nature 185, No. 4716, 835 (1960).

23. Lyon, R. J. P., W. M. Tuddenham, and C. S. Thompson, Econ. Geol. 54, 1047 (1959).

24. McDevitt, N. T., and W. L. Baun, Tech. Doc. Rept. No. RTD-TDR-63-4172, AF Materials Lab., Wright-Patterson Air Force Base, Ohio, Jan. 1964, 77 pp.

25. Miller, F. A., G. L. Carlson, F. F. Bentley, and W. H. Jones, Spectrochim. Acta 16, Nos. 1-2, 135 (1960).

26. Miller, F. A., and C. H. Wilkins, Anal. Chem. 24, No. 8, 1253 (1952).

27. Morris, R. J., Jr., Anal. Chem. 35, No. 10, 1489 (1963).

28. Nelson, J. B., Brit. Coal Util. Res. Assoc., Monthly Bull. 17, No. 2, 41 (1953).

29. Oinuma, K., and H. Hayashi, Am. Mineralogist 50, 1213 (1965).

30. Omori, K., Sci. Rept. Tohoku Univ., Third Ser. 7, No. 1, 101 (1961).

31. _____. Sci. Rept. Tohoku Univ., Third Ser. 9, No. 1, 65 (1964).

32. Sadtler Research Laboratories, High Resolution Spectra of Inorganics and Related Compounds, Vols. 1 and 2.

33. Saksena, B. D., Proc. Symp. Raman and Infrared Spectry., Nainital, India, 93 (1959).

34. Stewart, J. E., J. Res. Natl. Bur. Std. 54, No. 1, 41 (1955).

35. Tuddenham, W. M., and R. J.P. Lyon, Anal. Chem. 32, No. 12, 1630 (1960).

36. Whelan, P. F., J. Inst. Fuel 27, No. 164, 455 (1954).

37. White, W. B., and R. Roy, Am. Mineralogist 49, Nos. 11-12, 1670 (1964).

38. Yoganarasimhan, S. R., and C. N. R. Rao, Chemist-Analyst 51, 21 (1962).

39. Zarzycki, J., and F. Naudin, Ch. in Advances in Molecular Spectroscopy, Proc. Intern. Meeting on Molecular Spectry., 4th, Bologna and Rome, 1959, ed. by A. Mangini. The Macmillan Co., New York, vol. 3, 1071 (1962).

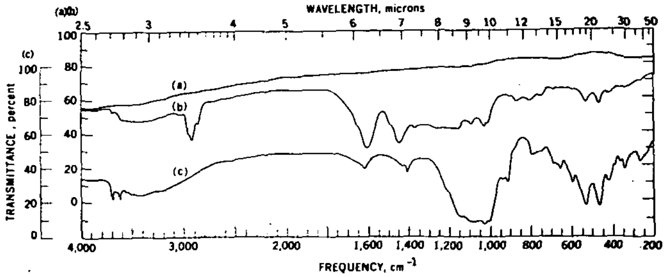

FIGURE 1. - Infrared Spectra of (a) Cesium Iodide, (b) Pittsburgh-seam Coal, and (c) Low-temperature Ash from Pittsburgh-seam Coal.

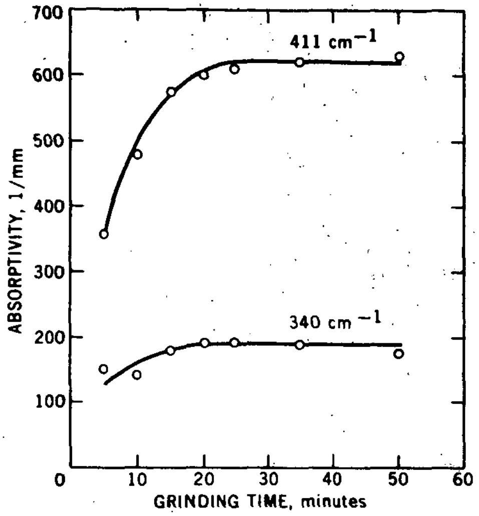

FIGURE 2. - Absorptivity as a Function of Grinding Time for Pyrite, in an Agate Vial.

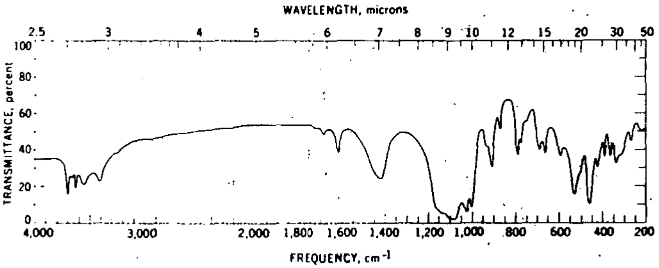

FIGURE 3. - Synthetic Mixture of Kaolinite, Calcite, Gypsum, and Quartz.

Aromatic Ring Proton Determination by Infrared Intensity Measurement in the 1650-2000 Wavenumber Region

Arthur S. Wexler

Dewey and Almy Chemical Division
W. R. Grace & Co.
Cambridge, Massachusetts 02140

The infrared absorption spectra of aromatic compounds in the 1650-2000 cm^{-1} region are well known to be characteristic of ring substitution pattern (5). The observed frequencies in benzene derivatives have been assigned to overtones and combinations of =CH out-of-plane deformations (4). The absorption in this region has been employed for the determination of total aromatics in petroleum distillates (2). Most compounds with =CH out-of-plane deformation vibrations in the 750-1000 cm^{-1} region may also be expected to exhibit absorption bands due to overtones and combination tones in the 1650-2000 cm^{-1} region and such is the case for polynuclear hydrocarbons (3) and olefinics (1). In the course of a survey of the absorption of aromatics at equimolar concentration in carbon tetrachloride, it was observed that the integrated intensity over the entire absorption band complex in the 1650-2000 cm^{-1} region appeared to be a monotonic function of number of aromatic ring protons. This observation prompted a detailed study of the relationship between integrated intensity and aromatic structure which is reported in this paper.

Experimental

All compounds were apparently of sufficient purity so as to be used as is, without purification. Spectra were obtained, where solubility permitted, at 0.5 molar concentration in carbon tetrachloride, in path lengths of 0.5 to 2 mm., with solvent compensation in the reference beam. A few samples were run "neat" in 0.1 or 0.2 mm. cell paths. Compounds of limited solubility were analyzed at a path length of 5 mm. Spectra were obtained in all cases on a Beckman IR-12 infrared spectrophotometer flushed with dry air to remove all but traces of water vapor. Spectra were run in absorbance on a 2x abscissa scale at moderately high resolving power to permit resolution of closely overlapping bands. Areas under the absorption bands were measured with a planimeter. Baselines were usually drawn parallel to the abscissa to intercept the absorption at 2000 cm^{-1}. Integrated intensities were calculated in practical units, cm^{-1} ℓ mole^{-1}, log 10 basis.

Results

Spectra in the 1650-2000 cm^{-1} region of aromatic hydrocarbons (0.5 molar, 0.5 mm path), selected to illustrate the characteristic absorption intensities as a function of ring type and substitution, are shown in Figure 1. These spectra are facsimile presentations which also can be used as a guide to determination of ring type or substitution. Obviously the total absorption varies markedly with degree of substitution. Integrated intensities for a group of aromatic hydrocarbons, selected to represent all the twelve possible classes of substituted benzenes, along with values for some dinuclear, trinuclear and condensed ring systems, are listed in Table I by individuals, and in Table II by averages for ring type. The most obvious variable appears to be the ring proton concentration, or number of =CH oscillators per ring. The relationship between integrated intensity and ring proton concentration appears to be monotonic, as shown in Figure 2. A linear relationship between intensity and ring proton concentration was observed for phenyl rings (benzene derivatives and polyphenyls), as shown in Figure 3. The plot for phenyls does not run into the origin, which suggests that some other type of vibration is making a constant contribution per phenyl ring to the total intensity in the combination band region. Polynuclear hydrocarbons fall on a line with a steeper slope, which does extrapolate to the origin. Substituted naphthalenes and dinuclear heterocyclics appear to fall on a line of intermediate slope, but there are insufficient data on this group at the present to justify a strictly linear plot. Assuming that the absorption in hexasubstituted benzenes is a constant measure of skeletal or other phenyl ring vibrations, a fairly constant intensity of about 100 (cm^{-2} ℓ $mole^{-1}$) per proton in pendent phenyl rings and 75 per proton in interior rings is obtained in the polyphenyls as shown in Table III. In the polyphenyls only the terminal phenyl rings are considered to be pendent while the remaining interior phenyl rings are assumed to contribute only combination tones of =CH oscillators in the 1650-2000 cm^{-1} region.

The effects of some polar and other ring substituents on the aromatic absorption intensity in this region are listed in Table IV. Olefinic double bonds display overtones in this region, as exemplified by the spectrum of styrene with an increased absorption at 1820 cm^{-1} compared with its brominated derivative, shown in Figure 4. The intensity per olefinic =CH oscillator is approximately equal to an aromatic =CH oscillator.

Additional bands are observed in the spectra of monosubstituted benzenes in solution in an inert solvent, as shown in Figure 5, for pure tert. butylbenzene and for a 10-fold dilution in carbon tetrachloride run at equivalent pathlengths times concentration. The two highest frequency bands split into doublets. A suggested assignment for each of these doublets (which were observed in the spectra of nearly all monosubstituted benzenes) as combinations of fundamentals is given for a few cases in Table V. At sufficiently high resolution some splitting can be observed even in undiluted compounds (dotted line of Figure 5).

Discussion

There appears to be little doubt that the integrated absorption intensity of aromatic hydrocarbons in the 1650-2000 cm^{-1} region is a monotonic function of the ring proton concentration, as depicted in Figure 2. This observation is at variance with the apparent constancy per ring, independent of degree of substitution, reported by Bomstein (2) for a number of alkylbenzenes. Bomstein's data, however, does show a significant variation of intensity with substitution. His K values for benzene/mono/di/trialkylbenzenes are in the ratio of 1.6/1.2/1.06/1.0, compared with ratios of integrated intensities in this paper of 1.7/1.35/1.15/1.0. (Differences between the two sets may reflect differences in integration range, background assumptions, types of compounds and instrument performance.) Bomstein stated that naphthalenes have different, presumably higher, K values, reflecting perhaps a higher ring proton concentration. Therefore, the apparent constancy observed by Bomstein for absorption in the 1700-2000 cm^{-1} region independent of degree of substitution holds only because his data were restricted to a relatively narrow range of ring proton concentration, perhaps 1.5 to 2 fold, compared with the 12-fold range explored in this study.

There also appears to be little doubt that the absorption due to phenyl rings is a linear function of ring proton content in both mononuclear hydrocarbons and polyphenyls, as shown in Figure 3. The intersection of this plot above zero on the ordinate can be interpreted as evidence of a background absorption of about 130 cm^{-2} ℓ $mole^{-1}$, associated with ring skeletal vibrations in pendent phenyl rings. The total 1650-2000 cm^{-2} absorption in m-quinquephenyl, for example, consists of a contribution of 260 cm^{-2} ℓ $mole^{-1}$ for the two pendent rings, plus a contribution of approximately 75 cm^{-2} ℓ $mole^{-1}$ for each ring proton, or a total intensity of 1910 cm^{-2} ℓ $mole^{-1}$, compared with an observed value of 2080. A linear plot of the 1650-2000 cm^{-1} absorption intensity against ring proton concentration which extrapolates to zero (Figure 3) was observed for polynuclear hydrocarbons and condensed ring systems, which suggests that all the intensity in this region in constrained ring systems is due to ring protons, with an average intensity per proton of about 130 cm^{-2} ℓ $mole^{-1}$. For example the integrated absorption intensity of 20-methylcholanthrene in the 1650-2000 cm^{-1} region was found to be 1168 cm^{-2} ℓ $mole^{-1}$ (Table I), equivalent to a value of 8.9 aromatic protons per molecule, compared with a formula value of 9.

Rubrene would present a complex case, since it contains 4 phenyl rings attached to a naphthacene skeleton. If the intensity relations in Table II apply to this compound (not yet measured) the lower and upper limits of numbers of aromatic protons per molecule would be estimated by infrared to be 24 to 30, compared with a formula value of 28. A reasonable expectation is the determination of aromatic protons (provided the molecular weight is known) to within ± 10% of the formula value of the infrared technique of this paper.

On the basis of integrated intensity measurements, it appears reasonable to include a band near 1620-1640 in para alkylbenzenes with the combination tones. Its inclusion on a frequency basis has already been justified by Whiffen(4).

Sharpening of peaks and splitting of bands were observed for monoalkylbenzenes and other aromatics, as depicted in Figures 1 and 5. The total 1650-2000 cm^{-1} intensity was found to be essentially constant in the range 0.5 molar to 6 molar (approximately 10 times diluted, and undiluted). In the monosubstituted benzenes the two highest frequency bands of the 1650-2000 cm^{-1} set, near 1860 and 1945 cm^{-1}, have been designated as i+h and h+j, summation tones by Whiffen (4). Under sufficiently high resolution partial splitting of one or both of these bands can be observed. More complete splitting was observed in non-interacting solvents such as hexane, carbon tetrachloride and carbon disulfide and the peaks were found to be narrower. The 1865 cm^{-1} peak of monoalkylbenzenes apparently is an i+h summation band but the three remaining peaks at 1880, 1938 and 1955 cm^{-1} appear to be, respectively, i+j, 2h and 2j bands. Little or no splitting was observed in solutions in chloroform and methylene chloride. Presumably the acidic hydrogen in these solvents (and the ring proton of undiluted aromatics) is able to complex with the π electron orbitals of the monosubstituted benzene ring in such a way as to cause the split bands to overlap and merge into broader bands.

It is possible to estimate the aromatic proton content of compounds (benzenoid and heterocyclics) from the infrared absorption intensity in the 1650-2000 cm^{-1} region using average intensities (cm^{-2} ℓ $mole^{-1}$) for each ring proton of 100 for mononuclear, 120 for dinuclear, and 130 for polynuclear hydrocarbons. The number of ring protons is then the total 1650-2000 cm^{-1} intensity divided by the appropriate unit value. As in any spectroscopic measurement, the molecular weight must be known to carry out the analysis. Interference by olefins can be handled by selective bromination or hydrogenation. The intensity of styrene (which contains a conjugated double bond) in this region was found to be equivalent to 7 protons. After bromination (cf. Figure 4) the intensity was observed to be equivalent to 5 protons, demonstrating selective disappearance of an interfering group without disturbing the ring proton contribution.

Literature Cited

(1) Bellamy, L. J., "The Infrared Spectra of Complex Molecules," Wiley, New York, 1958.
(2) Bomstein, J., Anal. Chem. 25 1770 (1953).
(3) Fuson, N. and Josien, M. L., J. Am.Chem. Soc. 78 3049 (1946).
(4) Whiffen, D. H., Spectrochim. Acta 7 253 (1955).
(5) Young, C. W., DuVall, R. B., Wright, N., Anal. Chem. 23 709 (1951).

Table I. Integrated Intensities (cm^{-2} ℓ mole^{-1}) of Aromatic Hydrocarbons in the 1650-2000 cm^{-1} Region.

Compound	Proton #	Intensity	Compound	Proton #	Intensity
Hexamethylbenzene	0	140	tert-Butylbenzene	5	525
Hexaethylbenzene	0	120	1-Phenylpentane	5	445
Pentamethylbenzene	1	180	1,1-Dimethylpropylbenzene	5	510
1,2,4,5-Tetramethylbenzene	2	350	n-Hexylbenzene	5	435
1,2,4,5-Tetraisopropylbenzene	2	310	n-Octylbenzene	5	530
2,5-Diisopropyl-p-xylene	2	300	Cyclohexylbenzene	5	455
2-Bromomesitylene	2	260	1-Phenyldodecane	5	450
1,2,3,4-Tetramethylbenzene	2	300	3-Phenyldodecane	5	510
1,2,3,5-Tetramethylbenzene	2	300	Chlorobenzene	5	457
1,2,3-Trimethylbenzene	3	300	Pyridine	5	465
1,2,4-Trimethylbenzene	3	305	2,4,6-Trimethylnaphthalene	5	560
1,2,4-Trichlorobenzene	3	360	Benzene	6	610
2,5-Dibromotoluene	3	355	1,2-Dimethylnaphthalene	6	740
1,3,5-Trimethylbenzene	3	385	1,3-Dimethylnaphthalene	6	648
1,3,5-Triisopropylbenzene	3	385	1,4-Dimethylnaphthalene	6	710
5-tert-Butyl-m-xylene	3	400	1,5-Dimethylnaphthalene	6	830
3-tert-Butyl-5-ethyltoluene	3	365	1,6-Dimethylnaphthalene	6	762
o-Ethyltoluene	4	409	2,3-Dimethylnaphthalene	6	725
o-Diethylbenzene	4	399	2,6-Dimethylnaphthalene	6	687
o-Xylene	4	406	Quinoline	7	760
o-Dichlorobenzene	4	376	iso-Quinoline	7	800
m-Ethyltoluene	4	420	1-Methylnaphthalene	7	815
m-Diethylbenzene	4	401	2-Methylnaphthalene	7	795
m-Xylene	4	412	Naphthalene	8	1030
m-Diisopropylbenzene	4	345	9,10-Dimethylanthracene	8	1130
m-Chlorotoluene	4	406	Retene	8	1000
m-Dichlorobenzene	4	439	20-Methylcholanthrene	9	1168
p-Ethyltoluene	4	425	2-Methylphenanthrene	9	1028
p-Diethylbenzene	4	415	2-Methylanthracene	9	1280
p-Xylene	4	432	9-Methylanthracene	9	1158
p-Cymene	4	452	Phenanthrene	10	1214
p-Diisopropylbenzene	4	478	Anthracene	10	1295
p-tert-Butyltoluene	4	427	Diphenylmethane	10	1100
α-Picoline	4	384	Biphenyl	10	1070
β-Picoline	4	424	Pyrene	10	1330
γ-Picoline	4	428	Chrysene	12	1600
Toluene	5	478	3,4-Benzpyrene	12	1630
Ethylbenzene	5	525	1,2-Benzanthracene	12	1430
n-Propylbenzene	5	440	Perylene	12	1900
iso-Propylbenzene	5	495	Triphenylene	12	1420
n-Butylbenzene	5	415	m-Quaterphenyl	18	1845
iso-Butylbenzene	5	490	o-Quaterphenyl	18	1575
sec-Butylbenzene	5	520	m-Quinquephenyl	22	2080

Table II. Average Intensities by Ring Type of Aromatic Hydrocarbons in the 1650-2000 cm^{-1} region.

Compound Type (and Number)		No. of Ring Protons	Total Intensity	Intensity per Ring Proton	Average
Hexa-alkylbenzene	(2)	0	130	---	
Penta-alkylbenzene	(1)	1	180	180	
Tetra-alkylbenzene	(6)	2	295	147	
Trialkylbenzene	(8)	3	360	119	104 (Mononuclear)
Dialkylbenzene	(19)[a]	4	415	104	
Monoalkylbenzene	(8)	5	485	97	
Dialkylnaphthalene	(7)	6	725	121	118 (Dinuclear)
Dinuclear	(4)[a]	7	790	113	
Polynuclear	(3)	8	1055	132	131 (Polynuclear)
Polynuclear	(4)	9	1160	129	
Polynuclear	(3)	10	1290	129	
Polynuclear	(5)	12	1610	134	
Polyphenyls	(4)	10-22	(Table I)	98	

[a] Including some heterocyclics.

Table III. Intensities of Mononuclear Aromatics and Polyphenyls in the 1650-2000 cm^{-1} Region.

Number of Ring Protons	Total Intensity	Net Intensity[a]	Intensity per Ring Proton
1	180	50	50
2	295	165	83
3	300	230	77
4	415	285	71
5	485	355	71
6	610	480	80
10	1070	810	81
18	1710	1450	81
22	2080	1825	83

[a] Net intensity equals total intensity minus a background or skeletal vibration value of 130 cm^{-2} ℓ mole^{-1} for each pendent aromatic ring.

Table IV. Intensity Effects of Polar and Olefinic Substituents on the Aromatic Absorption in the 1650-2000 cm^{-1} Region.

Substituent	Ring Proton Equivalent
Electron Donating Group	+ 1.5 to 2 protons
Chlorine	Little Change
Nitro	+ 2 protons
Side chains conjugated double bond	+ 1.5 to 2 protons
Isolated olefinic double bond	+ 1.5 to 2 protons

Table V. Frequencies of Absorption Bands of Monosubstituted Benzenes in =CH Out-of-Plane Deformation and Summation Regions.

	Average	Toluene	Chlorobenzene
		Fundamentals[a]	
f	751	728	740
g	837	844	830
i	908	895	902
h	962	966	965
j	982	982	985
		Summation Bands	
o	1742	1731	1731
g+i	1745	1739	1732
o	1797	1797	1788
g+h	1819	1810	1795
o	1865	1853	1861.5
i+h	1870	1861	1867
o	1880	1869	1882
i+j	1890	1877	1887
o	1938	1937	1941.5
2h	1924	1932	1930
o	1955	1955	1962
2j	1964	1964	1970

[a] Fundamentals from Reference 4.

o = Observed frequencies in carbon tetrachloride solution, 0.5 molar.

Captions for Figures

Figure 1. Spectra of aromatic hydrocarbons in 1650-2000 cm^{-1} region at 0.5 molar concentration in carbon tetrachloride, 0.5 mm. path length, compensated with solvent in reference beam.

Figure 2. Integrated intensities (cm^{-2} ℓ $mole^{-1}$) of aromatic hydrocarbons in the 1650-2000 cm^{-1} region as a function of ring proton concentration.

Figure 3. Integrated intensities (cm^{-2} ℓ $mole^{-1}$) of mono and polynuclear aromatic hydrocarbons in 1650-2000 cm^{-1} region as a function of ring proton concentration.
• Polynuclear
x Dinuclear
° Mononuclear and Polyphenyls

Figure 4. Spectra of styrene — and brominated derivative --- in 1650-2000 cm^{-1} region at 10% v/v in carbon tetrachloride, 1 mm. path length.

Figure 5. Spectra of tert. butylbenzene in 1650-2000 cm^{-1} region.
— undiluted, 0.1 mm. path, run at 9 cm^{-1} resolution
··· (offset) undiluted, 0.1 mm. path, run at 1.5 cm^{-1} resolution
--- 10% v/v in carbon tetrachloride, compensated, 1 mm. path, run at 1.5 cm^{-1} resolution.

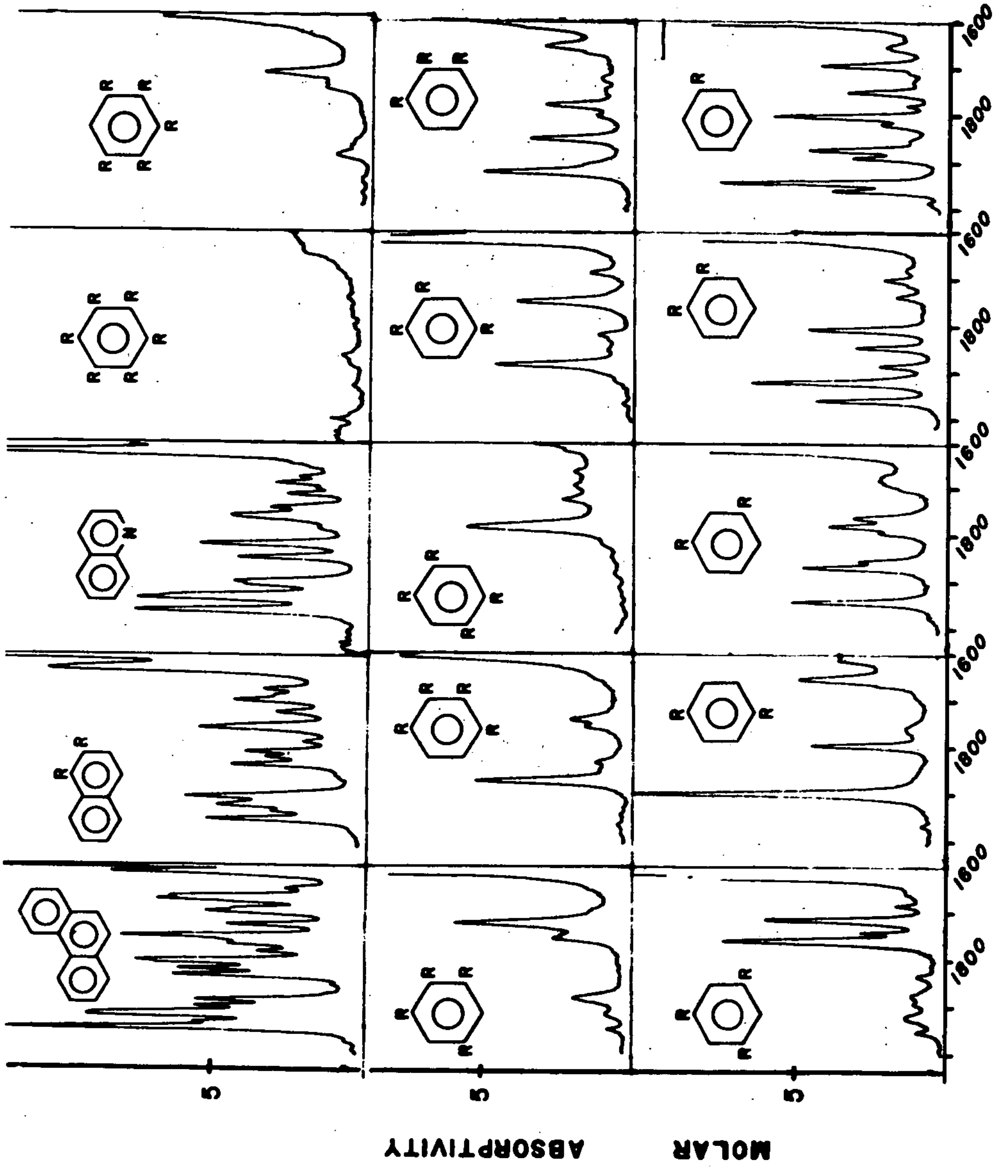
MOLAR ABSORPTIVITY
5
5
5
1600
1800
1600
1800
1600
1800
1600
1800
1600
1800
1600
R
N

Figure 1.

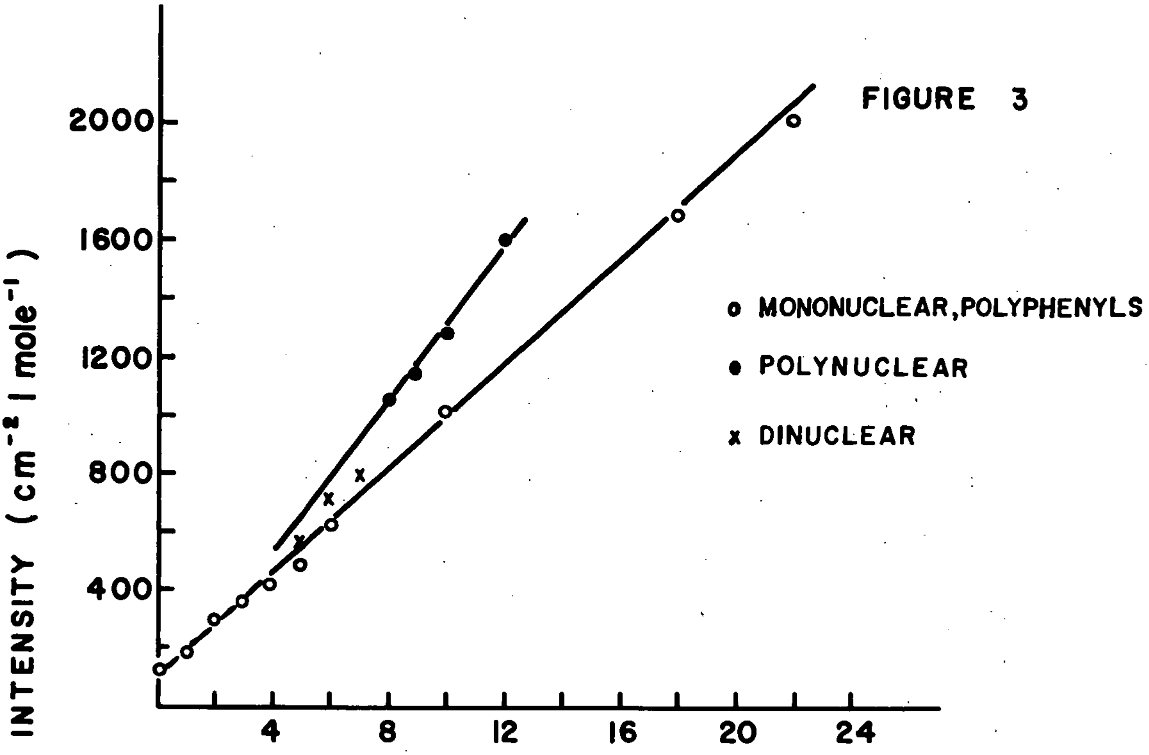

FIGURE 3

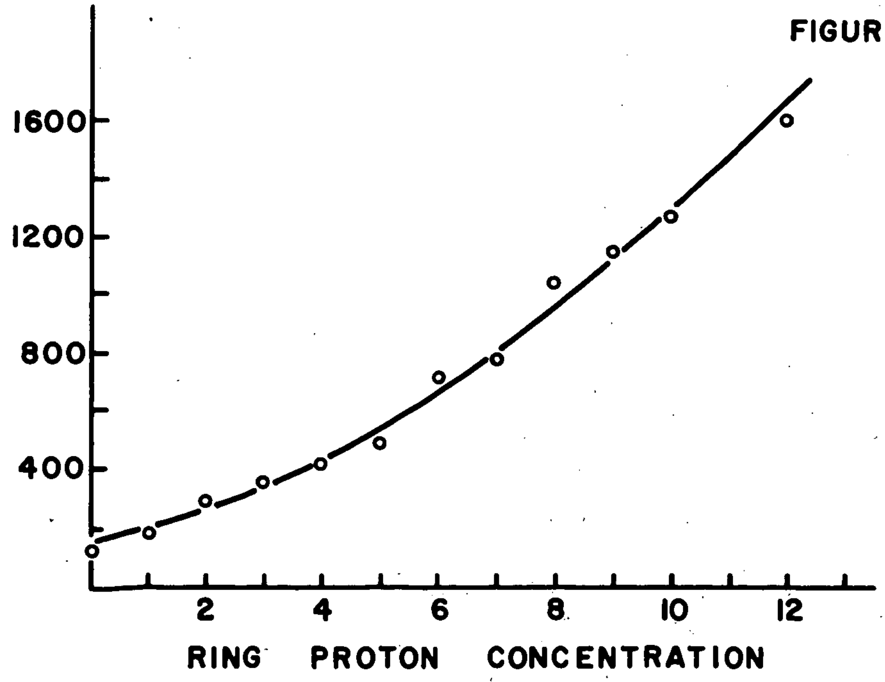

FIGURE 2

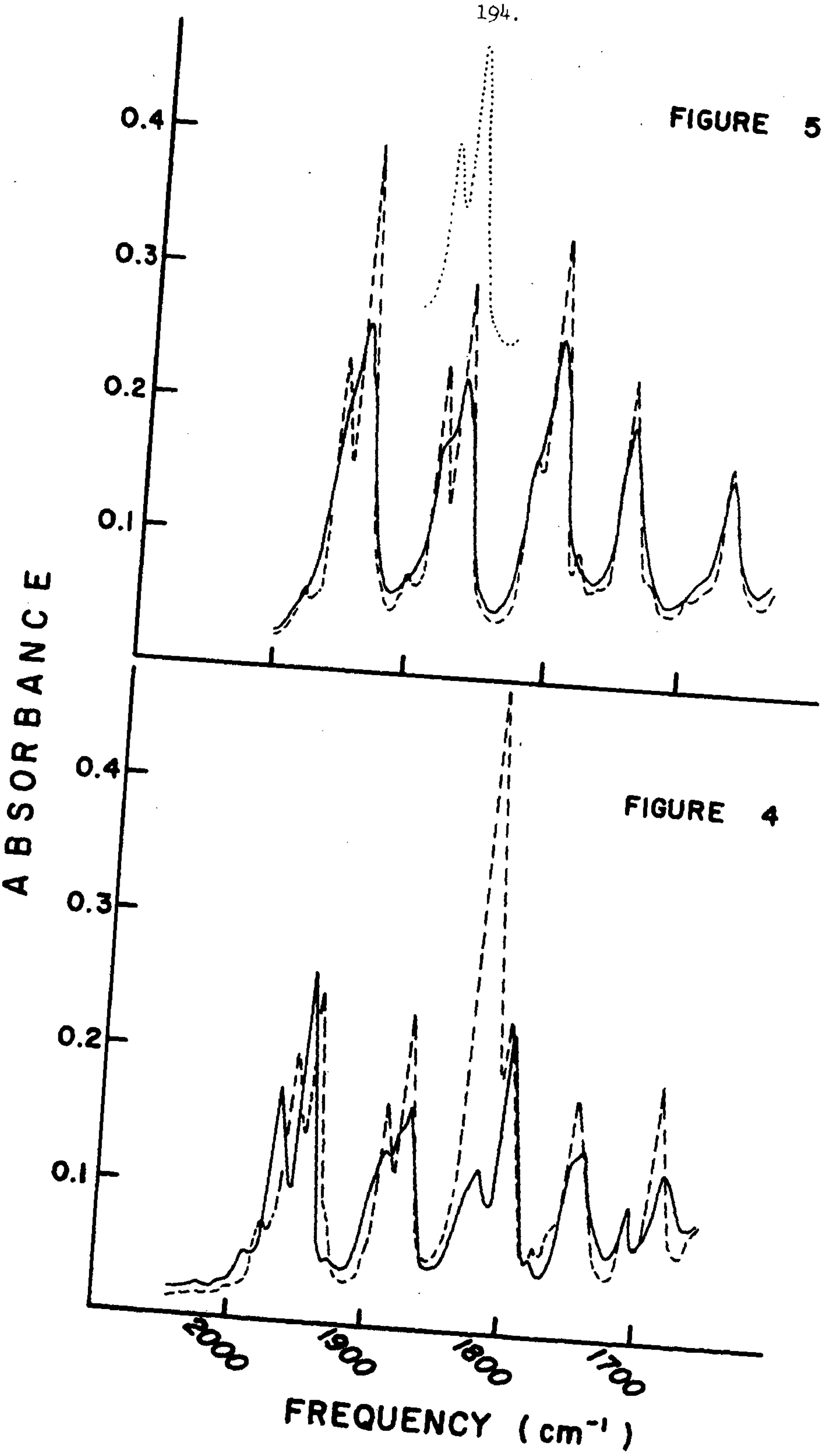

FIGURE 5

FIGURE 4

SPECTROSCOPIC STUDIES OF PHYSICO-CHEMICAL EFFECTS OF ULTRA-HIGH PRESSURES

J. W. BRASCH, R. J. JAKOBSEN, and E. JACK KAHLER

BATTELLE MEMORIAL INSTITUTE
Columbus Laboratories
505 King Avenue
Columbus, Ohio 43201

During recent years, a considerable volume of literature has appeared dealing with pressure studies. Inspite of all this work, very little is actually known of the chemical effects, on a molecular level, produced by high pressure. This lack of knowledge stems from the previous necessity of determining changes almost exclusively by postmortem examination of the pressurized material. Obviously, if no permanent phase change or reaction occurred, no pressure effect could be determined.

Battelle has pioneered in the utilization of commercially available equipment for infrared spectroscopic in situ monitoring of changes in liquids under ultra-high pressures. These techniques are now applicable to almost any liquid or solid sample, and potential applications have been shown to bridge virtually every area of physical-chemical endeavor.

It is easily demonstrated, by changes in the infrared spectrum as a sample is pressurized, that moderate pressures of 20 to 50 kilobars can produce significant, but completely reversible, effects on molecular structure. Definitive interpretation of these changes have exciting ramifications in every aspect of chemical knowledge. However, the broad spectrum of pressure studies can be grouped into three phenomenological areas:

1. Phase Behavior. Most liquid solidify under pressure, with polymorphism the rule rather than the exception (even the simple benzene molecule has at least two solid phases and we obtained a "plastic crystal" form of benzene under pressure. High-pressure, high-temperature polymorphic transitions are known for many, if not most, solids, as the eight forms of ice, five forms of amonium nitrate, or seven forms of tripalmitin. In situ measurements will reveal new phases undetectable by conventional postmortem examinations of quenched samples.

   Infrared spectroscopy has played an important role in solid-state studies. While the infrared spectrum is usually characteristic of a particular polymorphic form, it is particularly sensitive to any modification of molecular shape such as rotational isomerism, tautomerism, or conformational differences which may be encountered in high-pressure phases.

2. Intermolecular Forces. Fascinating possibilities for elucidating intermolecular interactions in condensed phases are offered by controlled variation of pressure from ambient to 100 kilobars, and of temperature from ambient to 400 C, on a sample of determinable volume. Questions of particular chemical importance which can now be approached experimentally are:

   (a) At what point do repulsive intermolecular forces exert an appreciable influence on intramolecular forces? For example, most intramolecular vibrations in condensed phases shift to higher frequencies with increasing pressure. Is this shift simply a dielectric effect related to increasing density with compression, or does it actually represent a decrease in bond length of the particular vibrating entity? While there will be a dielectric effect with compression, evidence from studies of hydrogen-bonded compounds indicates that bond lengths are definitely affected.

(b) When compressions are sufficient to result in decreased intramolecular bond lengths, is the shortened bond more, or less, chemically active? Do polar bonds behave the same as less polar bonds under similar conditions?

(c) Does order or orientation in the liquid approach the order in a corresponding solid as the density of the pressurized liquid approaches the density of that solid? Techniques developed for measuring compressibilities with photomicrographic and infrared spectroscopic data were used to show that some liquid halogenated ethanes compress to the density of the solid before solidification occurs. Also, the pressure behavior of strongly hydrogen bonded liquids indicates a higher degree of order than was previously suspected.

3. Synthesis. Novel syntheses are possible in pressurized systems. For example, we have successfully polymerized a conjugated aromatic substituted acetylenic compound by UV irradiation of a high-pressure solid phase. Reaction was not induced in either the ambient or pressurized liquid phases, nor in a low-temperature solid phase of the material.

These techniques are described and the value of in situ capabilities is demonstrated by completely revisible pressure effects which cannot be detected by post mortem examination. These techniques involve using a diamond anvil high-pressure cell fitted with a metal gasket to contain the liquid. The very small aperture of the diamond cell greatly limits the energy available to the spectrometer and requires unusual instrumental conditions to achieve reliable results. The determination of these operating conditions and their effect on spectral results is discussed. These spectral results clearly show that much more than simple close-packing of moleclues is involved at pressures of 10-100 kilobars. It is a great aid in pressure studies to be able to observe by normal optical microscopy any corresponding changes in the physical state of the sample. This is particularly true for the study of organic liquids, many of which solidify at relatively low pressures. This phenomenon has been used in the easily manipulated diamond cell to grow single crystals, quickly and easily, of many organic compounds. The powerful combination of infrared spectroscopic and optical microscopic monitoring allows some very interesting comparisons of these high-pressure single crystals with normal crystals produced by freezing.

Spectra will be shown of various ranks of coal obtained by high-pressure techniques. These spectra will be discussed both in terms of a routine sampling method for qualitative identification and in terms of new knowledge to be gained concerning the structure of coals.

ATR-PYROLYSIS SPECTRA OF COAL

Stanley E. Polchlopek
William J. Menosky
Louis G. Dalli

Barnes Engineering Company
Instrument Division
30 Commerce Road
Stamford, Connecticut 06902

Infrared spectra of coal have been prepared, historically, as might be expected, by the usual techniques. Each of these has something to recommend it and each has some disadvantage. Both mulls and alkali halide discs have exhibited excessive scattering and have provided good spectra only after long periods of grinding, often under selected solvents.

But even after a sample was prepared and its spectrum recorded, the interpretation was complicated by the presence of a large amount of carbon which contributes nothing. In fact, the presence of a large amount of highly absorbing carbon detracts from the spectrum by imposing attenuation requirements on the reference beam. In addition, the organic components have reacted with alkali halide discs and in some cases spurious water bands have been reported.

The combination of ATR and pyrolysis offers a new approach to the study of coal samples by infrared spectrophotometry. In this study a Barnes PY-2 Pyrolyzer and a Barnes ATR-4 unit were used in conjunction with a Perkin-Elmer 257 Spectrophotometer. The use of this combination of techniques simplifies sample preparation but imposes certain precautions which must be observed in interpretation.

Experimental

Two charges of 250mg each were used to prepare each spectrum. One charge was deposited on each side of an ATR-4 KRS-5 (thallous bromide-iodide crystal). After appropriate experimentation, a time of 90 seconds and 900°C was used for each charge. All of the samples were pyrolyzed in a vacuum of 0.1mm or less. Pyrolysis in a vacuum is necessary in order to eliminate open flame combustion and to minimize possible end group reactions.

Results

Six coals of varying rank were studied. These were obtained from Dr. R. A. Friedel, the symposium chairman. They are described in Table I.

TABLE I

COAL	SOURCE AREA	PERCENTAGE C
Anthracite	Reading, Pennsylvania	92.5%
Bituminous Low volatile	Pocahontas, West Virginia	91.0%
Bituminous Medium volatile	Wyoming County, West Virginia	89.0%
Bituminous High volatile B	Waltonville, Illinois	79.2%
Bituminous High volatile A	Bruceton, Pennsylvania	83.1%
Sub-bituminous	Sweetwater County, Wyoming	73.7%

One of the results of this study which was somewhat surprising is that the same time-temperature conditions could be applied to produce spectra of approximately equivalent appearance for all six of the samples studied.

Fig. 1 shows the ATR spectrum of the pyrolyzate of sub-bituminous coal. The spectrum shows the presence of phenols in large amounts. The -OH band centered at about 3225 cm^{-1}. There are shoulders on both sides of the absorption peak indicating the presence of other species of -OH or perhaps -NH.

In Fig 2, which is the pyrolyzate of high volatile A bituminous, shows clearer separation of bands in the -OH stretch region. The carbonyl region is substantially unchanged and the phenyl frequencies in the 650 to 850 cm^{-1} region have become more complex. The spectrum continues to show the presence of phenols.

The pyrolyzate of high volatile B bituminous shown in Fig. 3 shows that the amount of volatile -OH has decreased in quantity and in complexity. The phenyl frequency region from 650 to 850 cm^{-1} has become somewhat less complicated. The carbonyl region is also changed and shows fewer bands. This indicates that the very volatile components found in very low rank coals are present in decreased amounts.

The spectrum of medium volatile bituminous shown in Fig. 4 shows a pattern in the carbonyl region and in the 1400 to 1500 cm^{-1} region. The -OH stretch region remains about the same. The phenyl frequencies from 650 to 850 cm^{-1} have again become more complex. The appearance of the band at 1420 cm^{-1} may be taken to mean that there has been an increase in the aliphatic substitution of the phenyl systems.

Low volatile bituminous which has almost the same carbon content as the pyrolyzate shown in Fig. 5. The spectrum is not as intense probably because there are not as many volatiles present. The band at 1200 to 1300 cm^{-1} has almost disappeared. The 650 to 850 cm^{-1} region has become quite complex.

The spectrum of the pyrolyzate of anthracite is shown in Fig. 6. This spectrum is not related to the others. It is, in fact, simply a spectrum of tar. The same spectrum has been observed from asphalts used to black top roads and driveways. The only difference is in the size of the charge used to produce the spectrum. A charge of about 25mg of asphalt will produce the spectrum of about the same intensity as a 250mg charge of anthracite.

The spectra in this study show that a combination of ATR and pyrolysis offer a new approach to the study of coal spectra. The major benefit of the technique lies in the fact that it speeds up sample preparation.

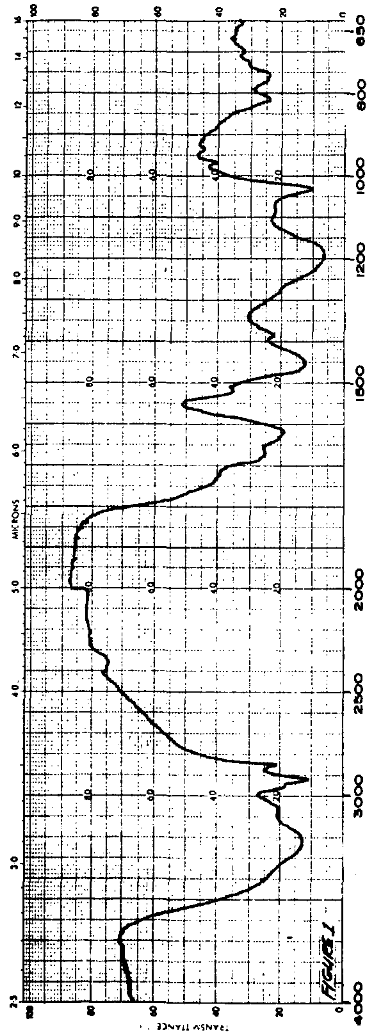

Figure 1.

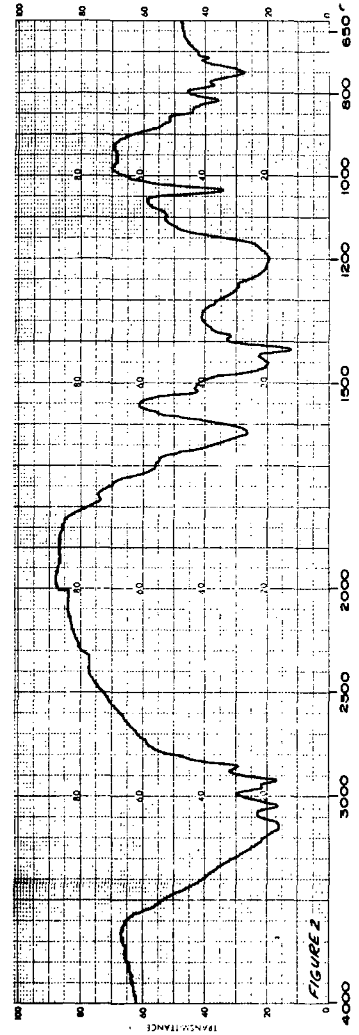

Figure 2.

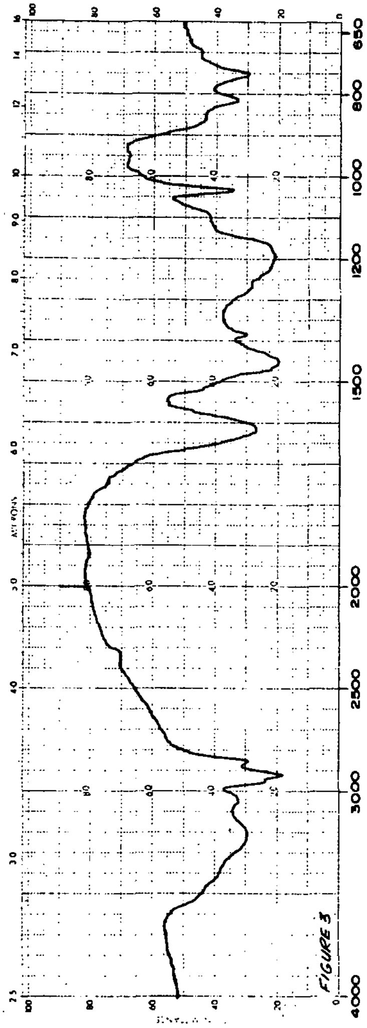

Figure 3.

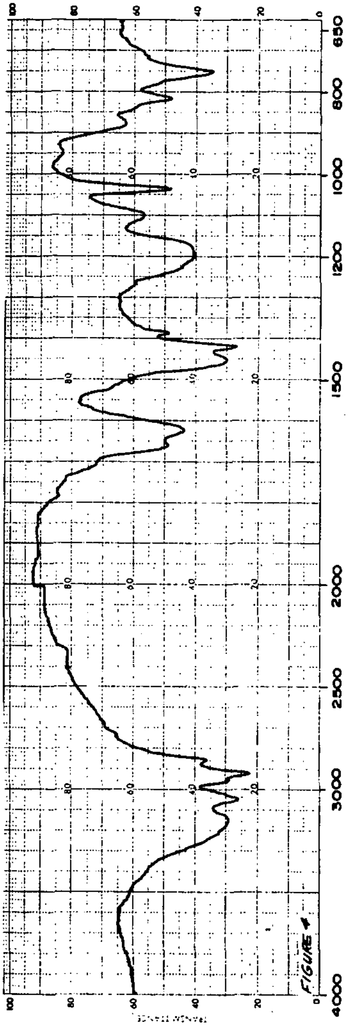

Figure 4.

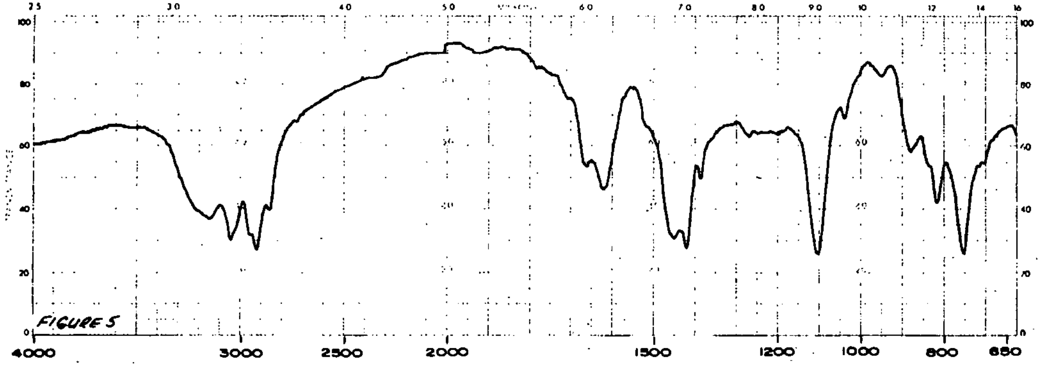

Figure 5.

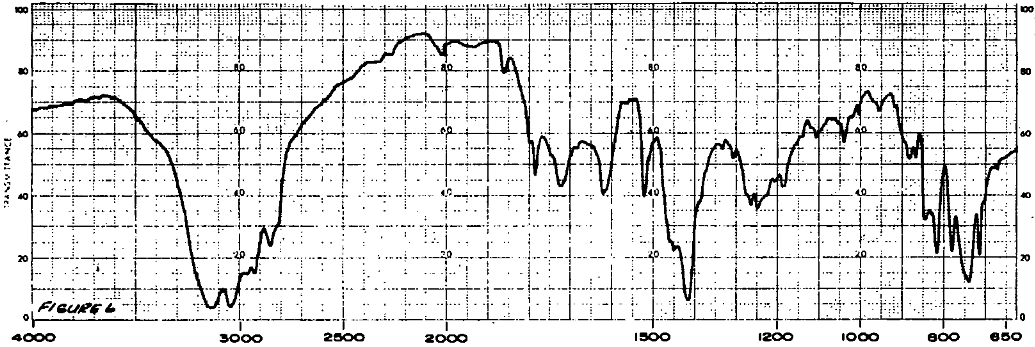

Figure 6.

THE USE OF INFRARED SPECTROSCOPY TO STUDY SURFACE GROUPS AND ADSORBED SPECIES ON CATALYSTS

By Michael R. Basila

Gulf Research & Development Company
Pittsburgh, Pennsylvania 15230

INTRODUCTION In recent years the application of spectroscopic techniques to problems in surface chemistry and catalysis has been growing at an ever-increasing rate. The most popular technique has been infrared followed by nuclear magnetic resonance and electron spin resonance.

Infrared techniques are most useful in surface functional group identification and (through the use of adsorbed molecules as probes) in studying the nature of the active sites for adsorption and reaction. In some cases it has been possible to obtain mechanistic information concerning the nature of intermediates in simple reactions such as the decomposition of formic acid over supported and unsupported metal catalysts (1).

As an illustrative example of the use of infrared techniques in studying the behavior of surface functional groups and the utilization of molecular probes to characterize active surface sites, a review of our studies of the surface of silica-alumina will be given. Here, use was made of nitrogen containing molecules -- pyridine and ammonia -- as probes to characterize the surface acid sites.

SURFACE GROUPS ON SILICA-ALUMINA In Fig. 1 the spectrum of a highly dehydrated silica-alumina (25 wt.% Al_2O_3) is given. The band at 3745 cm^{-1} is due to the OH stretching vibration in surface hydroxyl groups. The bands at 1975, 1866 and 1633 cm^{-1} are overtone and combination lattice vibrations (2). There is also a weak band at 1394 cm^{-1} which is due to an unidentified surface group, possibly a surface impurity. The 3745 cm^{-1} band has been assigned to the OH stretching vibration in hydroxyl groups attached to surface silicon atoms (2). This assignment was made on the basis of similarities in the frequency, band shape and other properties with the surface hydroxyls on silica. It has been confirmed by nuclear magnetic resonance measurements (3). The presence of a single surface hydroxyl group type is rather surprising. A number of workers (4) have observed three to five OH stretching bands due to isolated (non-hydrogen bonded) surface hydroxyl groups on alumina, while only one band at 3750 cm^{-1} is observed on silica (5). The results for silica-alumina suggest that there are no alumina-like areas on the surface or conversely, that the aluminum ions are distributed evenly throughout the lattice. We have looked at other commercial silica-aluminas ($Al_2O_3 \leqslant 25$ wt.%) and all have only a single surface hydroxyl type (attached to surface silicon atoms). Other workers have made similar observations (6a) however there have been several cases where the presence of alumina-like surface hydroxyl groups have been reported in addition to the silica-like groups (6b).

SURFACE ACID SITES Use has been made of ammonia as a molecular probe to study surface acidity on alumina and silica-alumina catalysts by a number of workers (7). Pyridine on the other hand has only been used in a few studies (8). Pyridine offers the advantage that one can distinguish unequivocably between coordinately bonded (LPY), protonated (BPY), and hydrogen bonded (HPY) adsorbed species (8). The bands that are used in making these distinctions are shown in Table I (8b).

TABLE I

BAND POSITIONS FOR COORDINATELY BONDED, PROTONATED AND HYDROGEN-BONDED PYRIDINE ADSORBED ON SILICA-ALUMINA*

Species	Type	LPY (cm^{-1})	BPY (cm^{-1})	HPY (cm^{-1})
8a	$\nu CC(N)$	1620	1638	1614
8b	$\nu CC(N)$	1577	1620	1593
19a	$\nu CC(N)$	1490	1490	1490
19b	$\nu CC(N)$	1450	1545	1438

*LPY = coordinately bonded pyridine (chemisorbed)

BPY = protonated pyridine (chemisorbed)

HPY = hydrogen bonded pyridine (physically adsorbed)

Chemisorbed NH_3 exhibits two bands that can be used to distinguish between the coordinately bonded and protonated species. The position of these bands are at 1620 (LNH_3) and 1432 cm^{-1} (NH_4^+), respectively (7, 9). However, the (physically adsorbed) hydrogen-bonded species (PNH_3) cannot be distinguished from LNH_3 which introduces some uncertainty in the estimation of Lewis/Bronsted acid site ratios (9).

Figs. 2 and 3 are spectra of pyridine and ammonia adsorbed on silica-alumina. An expression for calculating the ratio of Lewis to Bronsted acid sites on the surface of silica-alumina using the 1490 and 1450 cm^{-1} bands of LPY and BPY has been developed (10).

$$\frac{[LPY]}{[BPY]} = \frac{1.5\ A_{1450}}{A_{1490} - 0.25\ A_{1450}} \quad ; \ A = \text{peak absorbance}$$

The band at 1545 cm^{-1} cannot be used directly in conjunction with the 1450 cm^{-1} band because it has a much smaller absorption coefficient and the ratios are usually considerably greater than 1. The use of the 1490 cm^{-1} band is convenient because for LPY and BPY it has different absorption coefficients with $\varepsilon_{BPY}/\varepsilon_{LPY} = 6$ (10).

The bands at 1620 and 1432 cm^{-1} of chemisorbed ammonia can be used directly to estimate the Lewis/Bronsted acid site ratio. The relative absorption coefficients are: $\varepsilon_{1432}/\varepsilon_{1620} = 7$ (9). By these two methods it has been determined that one out of every five (NH_3, (9)) to 7 (PY, (10)) molecules that are chemisorbed are adsorbed as the protonated species for the silica-alumina which was studied comparatively. Other silica-aluminas have different Lewis/Bronsted acid site ratios (10) which is to be expected since the relative amounts of alumina and methods of preparation vary over considerable ranges.

EFFECT OF WATER ON SURFACE ACIDITY More detailed studies of the adsorption of pyridine and ammonia on silica-alumina have exposed some rather interesting behavior. When H_2O is adsorbed on chemisorbed pyridine (8) or ammonia (10) containing samples most of the LPY (LNH_3) is converted to BPY (NH_4^+) (Figs. 2b, c). However, this reaction is reversible and the spectrum returns to the original upon evacuation (Fig. 2d). During this experiment H_2O does not displace pyridine since no pyridine is removed and no band due to HPY is observed. If pyridine is added to chemisorbed H_2O, the same spectrum results but the water is removed by subsequent evacuation (8b). Hence, it appears that the H_2O molecules interact with the chemisorbed LPY and a proton transfer occurs without displacement of LPY.

It is difficult to rationalize the nature of this interaction between water and chemisorbed pyridine or ammonia. It is important to note that pyridine and water in solution do not interact to form pyridinium ion but merely engage in hydrogen bonding interactions (11). The formation of BPY therefore must result from activation of one or both of the components by the surface. The results suggest that the nitrogen containing base stays on the primary acid site and the water participates in a secondary interaction. Presumably adsorption of pyridine to form LPY occurs by an electron transfer interaction from the lone electron pair on the N atom to a trigonal surface aluminum atom leading to a surface complex of the type (I).

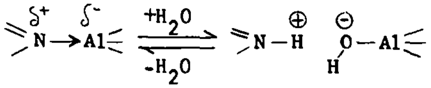

(I) (II)

In the presence of water, the electron transfer from N to surface Al may be essentially complete if a hydrogen atom from the water is transferred to the LPY and the OH radical migrates to the aluminum atom to give a complex of type (II). The same result would occur if a proton was transferred to the pyridine and the hydroxyl ion to the trigonal aluminum atom. In either case the pyridinium ion would then be held on the surface in an ion pair with ($\geqslant$AlOH)$^-$. The only difficulty with this model is that the nitrogen base is apparently strongly held during this interaction (8b) since it does not desorb upon evacuation whereas the pyridinium ion should have some surface mobility. The real situation most likely involves an equilibrium between (I) and (II), however, the data suggest that it is strongly displaced to the right since most of the LPY can be converted to BPY. It should be noted that there are no data available to indicate whether the added H_2O molecules are in a 1:1 ratio with the number of LPY molecules. If the ratio were higher, the equilibrium would be pushed toward the right.

SURFACE ACIDITY MODEL These results have led us to postulate (8b) that all of the acidic sites on silica-alumina are of the Lewis or electron acceptor type and that Bronsted type acidity results from a secondary interaction between the molecule chemisorbed on the primary Lewis type site and an adjacent SiOH group. This interaction is pictured as similar to that between water and chemisorbed LPY.

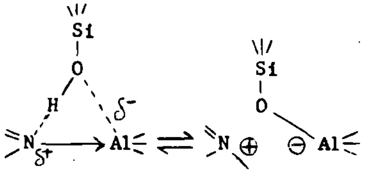

(III) (IV)

This model's chief advantage is that it allows the rationalization of extensive data in the literature which heretofore has been taken as evidence that silica-alumina has predominantly Lewis type sites or conversely predominantly Bronsted sites. It suggests that a proton is available if needed mechanistically such as to form a classical carbonium ion from an olefin, but is not necessarily involved in all acid-catalyzed reactions that proceed over silica-alumina (9).

Spectroscopic evidence supporting this model will now be considered. In Fig. 4 a plot of the concentration of chemisorbed NH_4^+ versus total ammonia adsorbed is given. As would be expected the slope decreases as the total amount of ammonia adsorbed increases. The initial slope is 0.25 which indicates that initially one out of every five ammonia molecules is chemisorbed as NH_4^+. Fig. 5 is a plot of the concentration of isolated (non-hydrogen bonded) surface hydroxyls versus the total amount of ammonia adsorbed. For analysis the smooth curve is broken into two linear segments. Note that the intersection point coincides with the point (Fig. 4) where the increase in (NH_4^+) as total ammonia adsorbed increases begins to flatten out. The inverse slope of the low coverage linear segment in Fig. 5 is 5.5 ± 0.5 and that of the high coverage linear segment is 0.98 ± 0.09. Hence, at low coverage one out of every five or six chemisorbed ammonia molecules is hydrogen bonded to a surface hydroxyl group. At high coverage every adsorbed ammonia is hydrogen bonded to a surface hydroxyl group, which is typical of the physical adsorption of ammonia on silica gel (no acidic sites). It is evident from these results that the high coverage segment corresponds to physical adsorption and the low coverage segment to chemisorption. The curvature near the transition point is a result of both processes occurring simultaneously.

According to the predictions of the model $[NH_4^+] \leqslant [OH]_{bonded}$, that is the number of chemisorbed ammonia molecules which are involved in "hydrogen-bonding" interactions with surface hydroxyl groups should be greater than or equal to the concentration of chemisorbed NH_4^+. The results in Figs. 4 and 5 (at low surface coverage) are that one in five ammonia molecules is chemisorbed as NH_4^+ and one in five or six is hydrogen bonded to a surface hydroxyl group, in good agreement with the prediction. Furthermore, it is predicted that hydroxyl groups involved in proton transfer interactions with chemisorbed ammonia molecules should not exhibit an OH stretching band, hence at low surface coverage where chemisorption predominates the intensity of the 3050 cm^{-1} band (due to the hydrogen-bonded OH stretching) should increase at a very much lower rate than at high coverage where physical adsorption predominates. This behavior is evident in Fig. 6 where the peak absorbance of the 3745 cm^{-1} band is plotted versus that of the 3050 cm^{-1} band. This evidence is not conclusive however because the OH groups in a non-proton transfer interaction with chemisorbed molecules may have a different peak frequency and absorption coefficient than those involved in a normal hydrogen-bonding interaction (9).

Additional supporting evidence for the proposed model is shown in Fig. 7. In this experiment the silica-alumina was poisoned by impregnation with potassium acetate followed by calcination. The presence of alkali metals in acidic catalysts is known to poison carbonium ion reactions (13). Fig. 7a shows that the band due to BPY at 1545 cm^{-1} is absent, hence poisoning with potassium ions eliminates Bronsted type acidity. It has been shown (8b) that the strength of the acidic sites is markedly decreased when silica-alumina is poisoned by the addition of potassium. The hydroxyl groups are little effected. When water is adsorbed on the pyridine containing surface the LPY species are converted to BPY (Fig. 7b). Hence the added potassium ions do not prevent the conversion of LPY to BPY by adsorbed water. This result is quite surprising. It eliminates the surface species ($\geqslant$AlOH)$^-$H+ as the source of inherent Bronsted acidity on a fresh silica-alumina surface. If this species were present the K+ ions would exchange with the H+ ions and render the sites completely inactive. The fact that water can still convert LPY to BPY suggests that even though the degree of activation of pyridine by the acidic site is decreased (8b) the protonation reaction can still proceed if the proton donor can get close enough.

This behavior can be rationalized in terms of our model as follows and hence is taken as indirect supporting evidence. Since the reactions of the LPY-acid site complex and the adjacent OH are geometrically fixed a decrease in the degree of activation of LPY can prevent the transfer of a proton. However, water molecules are mobile and can come in very close proximity to the complex to effect proton transfer.

SUMMARY The results discussed above demonstrate that infrared spectroscopic techniques can provide details of surface chemistry and the nature of surface functional groups. Spectroscopic techniques do not provide the panacea for all catalytic problembs, however. They sometimes raise more questions than they answer. It can be concluded that they will (and do) constitute an important tool for the catalytic chemist. They are most effective when used in conjunction with other techniques such as gravimetric adsorption measurements (used for example to obtain surface concentrations in Figs. 4 and 5) and isotope exchange techniques.

REFERENCES

1. See review by L. H. Little, "Infrared Spectra of Adsorbed Species," Academic Press, New York, N. Y., 1966, Chapter 5.

2. M. R. Basila, J. Phys. Chem., 66, 2223 (1962).

3. W. K. Hall, H. P. Leftin, F. J. Cheselske, and D. E. O'Reilly, J. Catalysis, 2, 506 (1963).

4. (a) J. P. Peri and R. B. Hannan, J. Phys. Chem., 64, 1526 (1960); (b) J. P. Peri, Ibid, 69, 211 (1965); (c) D. J. C. Yates and P. J. Lucchesi, J. Chem. Phys., 35, 243 (1961); (d) R. H. Lindquist and D. G. Rea, presented at 136th National Meeting, American Chemical Society, Sept., 1959.

5. R. S. McDonald, (a) J. Am. Chem. Soc., 79 850 (1959); (b) J. Phys. Chem., 62, 1168 (1958).

6. (a) J. B. Peri, J. Phys. Chem., 70, 3168 (1966); (b) See reference 1, Chapter 10.

7. See reference 1, Chapter 7.

8. (a) E. P. Parry, J. Catalysis, 2, 371 (1963); (b) M. R. Basila, T. R. Kantner and K. H. Rhee, J. Phys. Chem., 68, 3197 (1964).

9. M. R. Basila and T. R. Kantner, J. Phys. Chem., 71, 467 (1967).

10. M. R. Basila and T. R. Kantner, Ibid, 70, 1681 (1966).

11. A. N. Sidorv, Opt. i Spektroskopiya 8, 51 (1960).

12. A. V. Kiselev, V. I. Lygin and T. I. Titova, Zh. Fiz. Khim., 38, 2730 (1964).

13. (a) D. Stright and J. D. Danforth, J. Phys. Chem., 57, 448 (1953); (b) G. A. Mills, E. R. Boedeker, and A. G. Oblad, J. Am. Chem. Soc., 72, 1554 (1950).

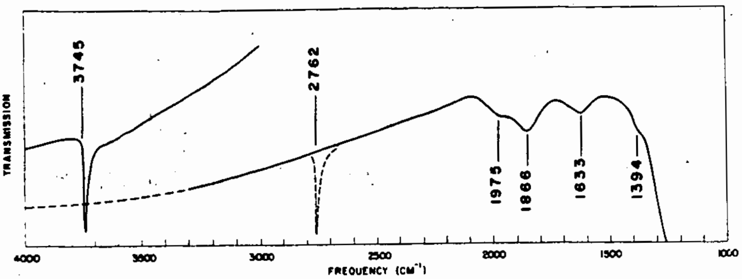

Fig. 1. Silica-alumina dehydrated at 500°C. The dashed lines indicate the spectrum of deuterated silica-alumina.

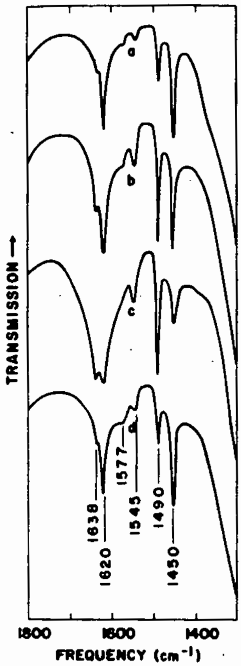

Fig. 2. Dual adsorption of pyridine and H_2O on silica-alumina. (a) SA exposed to pyridine at 17 mm. and 150°C for 1 hr. followed by evacuation at 150°C for 16 hr. (b) Exposure to H_2O at 15 mm. and 150°C for 1 hr. followed by evacuation at 150°C for 1 hr. (c) Exposure to H_2O at 15 mm. and 25°C for 1 hr. followed by evacuation for 1 hr. at 25°C.
(d) Evacuation for 16 hr. at 150°C.

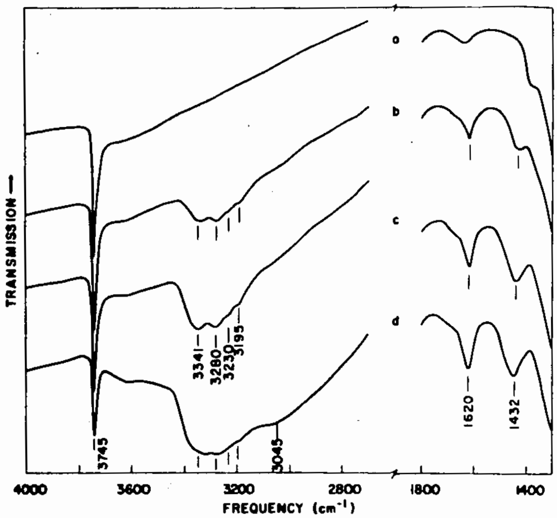

Fig. 3 (a) SA calcined 16 hours in O_2 at 500°C, evacuated 5 hours at 500°C. (b) Exposed to 10 mm NH_3 for 1 hour at 150°C, evacuated 1 hour at 150°C. (c) Subsequently exposed to 10 mm NH_3 for 1 hour at 25°C, evacuated for 1 hour at 25°C. (d) Subsequently exposed to 10 mm NH_3 for 1 hour, no evacuation. Very weak bands due to gaseous NH_3 have been subtracted.

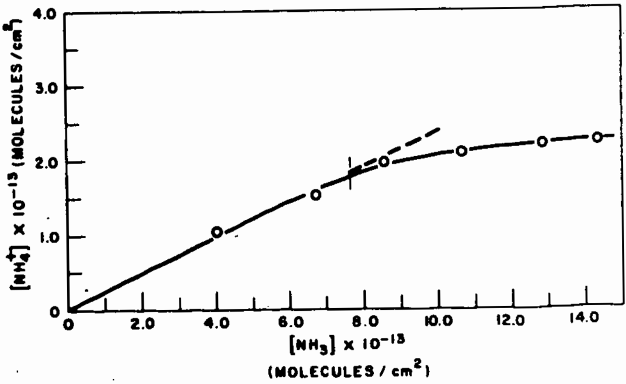

Fig. 4. A comparison of the concentrations of NH_3 and NH_4^+ adsorbed on SA as the total amount of ammonia adsorbed increases. $[NH_3]$ is the sum of $[PNH_3]$ and $[LNH_3]$. The vertical line denotes the point of straight line intersection in Fig. 5.

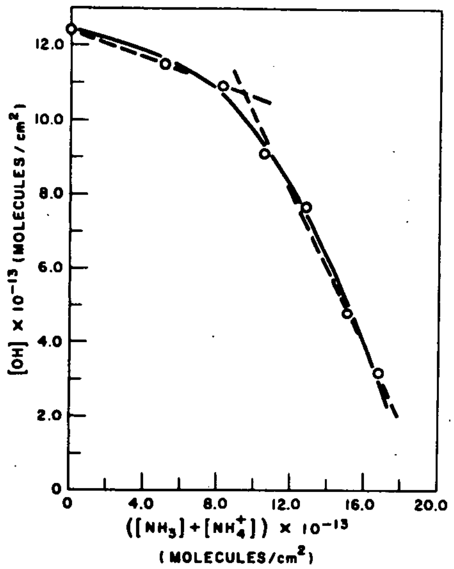

Fig. 5. The concentration of non-hydrogen bonded surface OH groups vs the total amount of ammonia adsorbed on SA. $\overline{\mathrm{NH}_3}$ is the sum of PNH_3 and LNH_3 .

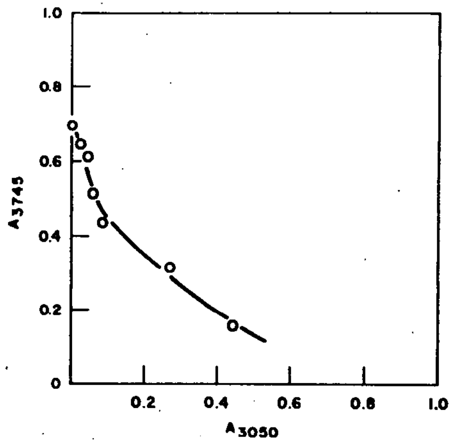

Fig. 6. A comparison of the concentrations of free and hydrogen-bonded surface OH groups as the amount of ammonia adsorbed increases. The values of A are the peak absorbancies of the characteristic bands.

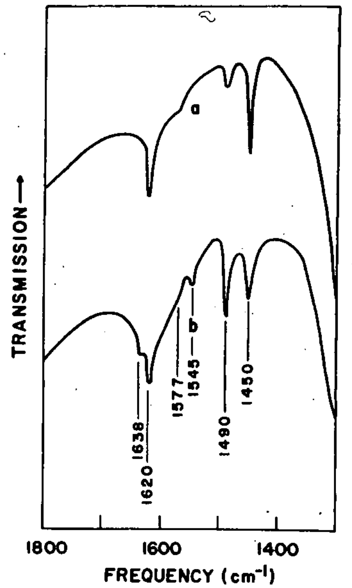

Fig. 7. Dual adsorption of pyridine and H_2O on K-poisoned silica-alumina. (a) KSA exposed to pyridine at 17 mm. and 150°C for 1 hr. followed by evacuation for 16 hr. at 150°C. (b) Exposed to H_2O at 15 mm. and 150°C for 1 hr. followed by evacuation for 1 hr. at 150°C.

SELF-ASSOCIATION OF PHENOL IN NON-POLAR SOLVENTS

Kermit B. Whetsel and J. Harold Lady

Tennessee Eastman Co., Division of Eastman Kodak Co., Kingsport, Tenn. 37660

Although the self-association of phenol has been studied by a variety of methods, our knowledge of the thermodynamics of the process is still incomplete. Thermodynamic constants for the dimerization of phenol in carbon tetrachloride solution have been reported (1, 2), but comparable data for the formation of higher multimers are not available. Furthermore, the effects of solvents on the self-association process have not been reported.

The objective of the present work was to determine thermodynamic constants for the dimer and higher multimers of phenol in carbon tetrachloride and cyclohexane solutions. The intensity of the first overtone O-H stretching band of phenol was measured as a function of concentration and temperature in both solvents and the fit of the data to a variety of self-association models tested. A method was developed for calculating the approximate absorptivity of O-H end groups in linear associated species and for taking this factor into account in the determination of formation constants. The effects of concentration, temperature, and solvent upon the fundamental O-H stretching bands of phenol were investigated briefly.

EXPERIMENTAL

Equipment and Materials. Measurements in the fundamental and first overtone regions were made with Beckman IR-9 and Cary Model 14 spectrophotometers, respectively, equipped with thermostated cell holders. Spectral slit widths were approximately 2.3 cm^{-1} in the fundamental region and 6.4 cm^{-1} in the overtone region. Spectro grade cyclohexane was used as received. Reagent grade carbon tetrachloride was dried over molecular sieve Type 5A. Reagent grade phenol was distilled and stored in a desiccator over Drierite and phosphorous pentoxide. When not being used, all solutions were stored in glass-stoppered flasksin a desiccator.

Calculations. For the self-association equilibria $nC_1 \rightleftharpoons C_n$, the following equations apply:

$$K_n = \frac{C_n}{C^n} \qquad (1)$$

$$A/l = \epsilon_1 C_1 + \epsilon_2 K_2 C_1^2 + --- + \epsilon_n K_n C_1^n = \epsilon_1 C_1 + \sum_{n=2}^{n=n} \epsilon_n K_n C_1^n \qquad (2)$$

$$C_{\mathring{A}} = C_1 + 2K_2 C_1^2 + 3K_3 C_1^3 + --- + nK_n C_1^n = C_1 + \sum_{n=2}^{n=n} nK_n C_1^n \qquad (3)$$

where A is absorbance, l is path length, C_1 is monomer concentration, $C_{\mathring{A}}$ is stoichiometric concentration, ϵ_1 is monomer absorptivity, and ϵ_n is the absorptivity of polymeric species. For the special case of $\epsilon_n = 0$, equations 2 and 3 reduce to and

$$A/1 = \epsilon_1 C_1 \tag{4}$$

$$C_A^\circ = A/1\epsilon_1 + \sum_{n=2}^{n=n} nK_n \, (A/1\epsilon_1)^n \tag{5}$$

The number of unknown parameters in Equation 5 can be reduced by imposing the restriction that the stepwise formation constants for all multimers above dimer are equal. This type of association is described by the expressions:

$$C_1 + C_{n-1} \overset{K}{\rightleftharpoons} C_n \qquad K = \frac{(C_n)}{(C_1)\,(C_{n-1})} \tag{6}$$

where K̲ is independent of n̲ when n̲ > 2. Under these conditions K_n is equal to K_2K^{n-2}, and the only unknowns in Equation 5 are K_2, K, and ϵ_1.

The values of ϵ_1 required for the solution of Equation 5 were determined by extrapolating plots of apparent absorptivity versus C_A° to infinite dilution. The formation constants were calculated using a computer and a standard least squares method for polynomials. The program used to solve the general form of Equation 5 allowed formation constants to be calculated for single multimers or any combination of multimers from dimer through octamer. The program used to solve the restricted form allowed the contribution of up to 20 species to be taken into account.

Equation 5 is not directly applicable when $\epsilon_n \neq 0$, but it can be used to determine formation constants by an iteration procedure as follows: Initial estimates of K_n are obtained by assuming than $\epsilon_n = 0$ and using Equation 5 in the normal manner. A small increment of end group absorptivity ($\Delta\,\epsilon_n = 0.05$ to 0.10) is assumed and a set of corrected A/1 values generated by using the equation

$$(A/1)_{C(1)} = (A/1)_{obs} - \Delta\,\epsilon_n \sum_{n=2}^{n=n} K_n \, (1/\epsilon_1)^n \, (A/1)_{obs}^n \tag{7}$$

This set of values is substituted into Equation 5 to obtain second estimates of K_n. The second estimates of K_n and the first set of corrected A/1 values are substituted into the right side of Equation 7 to obtain a second set of corrected A/1 values. Successive estimates of K_n and corrections of A/1 are made until the standard error of fitting Equation 5 passes through a minimum. The values of K_n giving the minimum error are taken as the best estimates of these quantities. The approximate end group absorptivity is equal to $\underline{N}(\Delta\,\epsilon_n)$, where N̲ is the number of iterations required to obtain the minimum error. The best estimate of the end group absorptivity is calculated from the equation

$$(A/1)_{obs} = (A/1)_{C(N)} + \epsilon_n \sum_{n=2}^{n=n} K_n \, (1/\epsilon_1)^n \, (A/1)_{C(N)} \tag{8}$$

where $(A/1)_{C(N)}$ is the set of corrected A/1 values which gives the minimum error in fitting Equation 5.

The iteration procedure was used only with the model involving dimerization and stepwise association constants, where $K_n = K_2K^{n-2}$. The results obtained when the method was tested with synthetic data are shown in Table I. While the method does not converge to the theoretical values, it yields values for the formation constants and ϵ_n that are within 5 and 20%, respectively, of the true values.

RESULTS

Spectral Data. Solutions of phenol above a few hundredths molar show three O-H bands in the fundamental region. The free O-H band is near 3612 cm^{-1} and the two bonded O-H bands are near 3500 and 3350 cm^{-1}. The band near 3500 cm^{-1} is normally assigned to a cyclic dimer species and the one near 3350 cm^{-1} to linear associated species. The relative intensity of the band near 3350 cm^{-1} increases with increasing concentration and decreasing temperature.

The principal feature of the first overtone spectrum is a free O-H band near 7050 cm^{-1} whose apparent absorptivity decreases as self-association occurs. Bonded O-H groups are evidenced only by a broad, weak band extending from about 7050 to 6000 cm^{-1}. The absorptivity of the monomer is approximately 50% greater in cyclohexane than in carbon tetrachloride. Self-association occurs more readily in the hydrocarbon solvent, however, and at concentrations above 0.1 or 0.2$\underline{M}$ the order of apparent absorptivities is reversed.

Model Fitting. In the initial attempts to find the best model, only the data for phenol concentrations less than 0.1$\underline{M}$ were used. Several different models gave satisfactory fits over this limited concentration range. But when the formation constants derived from these tests were applied to data for higher phenol concentrations, the agreement between calculated and observed absorbances deteriorated rapidly.

A variety of models were tested using data for phenol concentrations up to 0.65$\underline{M}$ in cyclohexane and 1.0$\underline{M}$ in carbon tetrachloride. The standard errors for the different models are shown in Table II. Several of the models which gave good fits over a limited range of concentration gave negative values for one or more constants when tested over the more extended range. The model involving a dimerization constant and equal stepwise association constants for higher multimers gave the best fit in both solvents.

In Figure 1 the fits of several different models are shown graphically. The good fit of the dimer-stepwise model and the poor fit of most of the other models are evident. These curves indicated that certain combinations of simpler models might give good fits, and subsequent calculations showed that a trimer-hexamer model did, indeed, provide a good fit. This model does not appear to be as plausible physically as the dimer-stepwise model, and it was not studied further.

Application of the end group correction to the data for the carbon tetrachloride system is illustrated by the curves in Figure 2. With the data taken at 2.5°, the minima in the standard error curves correspond to an end group absorptivity of approximately 0.3 l./mole-cm. The average value of ϵ_n determined at temperatures between 2.5 and 46° was 0.4 l./mole-cm., which is equivalent to $0.11\epsilon_1$.

When the end group correction was applied to the data for the cyclohexane system, the standard error of fit decreased at four temperatures but did not at three others. The maximum value for ϵ_n was $0.08\epsilon_1$ and the average was only $0.03\epsilon_1$. In view of these results, we do not feel that application of the correction to the data for the cyclohexane system is valid.

Thermodynamic Results. Plots of formation constants vs 1/T for dimerization and stepwise association are shown in Figure 3. The thermodynamic constants derived from the plots are summarized in Table III. The lines in Figure 3 for the carbon tetrachloride system represent data to which the end group correction was applied. In Table III the thermodynamic constants calculated for both the original and the corrected data are shown for comparison.

DISCUSSION

Coggeshall and Saier (3) found that a dimerization-stepwise association model adequately describes the effects of self-association on the fundamental O-H band of phenol in carbon tetrachloride solution. Our results obtained in the first overtone region confirm the validity of the model and show, in addition, that it is applicable to self-association in cyclohexane solution.

Our values of 0.94 and 3.25 l./mole for K_2 and K in carbon tetrachloride at 25° can be compared with values of 1.39 and 2.94 l./mole found by Coggeshall and Saier at ambient instrument temperature and with values of 0.70 and 0.83 l./mole reported by West and coworkers (1, 2) for K_2 at 25°. Our heat of dimerization of -5.03 kcal./mole is in excellent agreement with the value of -5.1 kcal./mole reported by Maguire and West (1). A more recent value of -3.6 reported by Powell and West (2) seems abnormally low. No direct comparison can be made for the heat of formation of higher multimers, but our value of -4.32 kcal./mole agrees well with an overall heat of association of -4.35 kcal./mole reported by Mecke (4). Mecke worked with relatively high concentrations of phenol, and his value is heavily weighted toward the stepwise heat of formation.

Both the dimerization constants and the stepwise formation constants are approximately twice as large in cyclohexane solution as in carbon tetrachloride solution. The heats of formation in the hydrocarbon solvent, however, are only 10 to 20% higher than those in the chlorinated solvent. Similar results have been obtained recently for a variety of hydrogen bonded complexes of phenol in these two solvents (5).

The average value of 0.4 l./mole-cm. found for the end group absorptivity in carbon tetrachloride solution is approximately 0.1 as large as the absorptivity of the free O-H group. This result indicates either that the O-H end groups interfere only slightly at the frequency where the monomer band occurs or that the concentration of end groups is much lower than one would expect on the basis of a linear association model. A low concentration of end groups could result from the formation of cyclic multimers or three dimensional aggregates. Most workers in this field have assumed that end group absorption is negligible but have recognized that the assumption might introduce major errors in the calculated formation constants. The present results show that the assumption is reasonably valid, at least in the first overtone region. Data recently presented by Bellamy and Pace (6) indicate that the end group absorptivity may be as large as $0.3\epsilon_1$ in the fundamental region.

The question of whether alcohols and phenols form linear or cyclic dimers, or both, has been discussed widely. Considerable evidence favoring the predominance of cyclic dimers has been presented, but recent work by Bellamy and Pace (6), Ibbitson and Moore (7), and Malecki (8) emphasizes the importance of linear dimers. Our thermodynamic results indicate that a significant fraction of the phenol dimer is in the linear form.

The apparent dimerization constant and heat of formation of the dimer are related to the individual values for the linear and cyclic forms as follows (9):

$$K_A = K_L + K_C \tag{10}$$

$$\Delta H_A = \frac{K_L(\Delta H_L) + K_C(\Delta H_C)}{K_A} \tag{11}$$

where the subscripts A, L, and C represent apparent, linear, and cyclic. If we assume that the heat of formation of the linear dimer is equal to the stepwise heat of formation of higher multimers, we can calculate values of ΔH_C, ΔS_C, and ΔS_L for various assumed ratios of K_L and K_C (Table IV). Making the reasonable assumption that ΔS_C is larger than ΔS_L but somewhat less than twice as large, we conclude that the ratio of K_L to K_C is at least 0.5 and possibly greater than unity.

LITERATURE CITED

1. M. M. Maguire and R. West, Spectrochim. Acta, 17, 369 (1961).
2. D. L. Powell and R. West, Spectrochim. Acta, 20, 983 (1964).
3. N. D. Coggeshall and E.L. Saier, J. Am. Chem. Soc., 73, 5414 (1951).
4. R. Mecke, Discussions Faraday Soc., 9, 161 (1950).
5. J. H. Lady and K. B. Whetsel, Unpublished results.
6. L. J. Bellamy and R. J. Pace, Spectrochim. Acta, 22, 525 (1966).
7. D. A. Ibbitson and L. F. Moore, J. Chem. Soc. (B), 1967, 76.
8. J. Malecki, J. Chem. Phys., 43, 1351 (1965).
9. L. E. Orgel and R. S. Mulliken, J. Am. Chem. Soc., 79, 4839 (1957).

TABLE I

TEST OF METHOD FOR END GROUP CORRECTION (SYNTHETIC DATA)

	Theoretical	Calculated	
		Uncorrected	Corrected
ϵ_n	1.53(0.3ϵ_1)	0	1.22(0.24ϵ_1)
K_2	2.96	3.17	2.92
K	9.97	7.05	9.45
Standard Error	0	0.0069	0.0001

TABLE II

TEST OF MODELS FOR SELF-ASSOCIATION OF PHENOL

Model	Standard Error	
	Cyclohexane[a]	CCl_4[b]
Dimer	0.058	0.061
Trimer	.035	.032
Tetramer	.019	.010
Pentamer	.009	.013
Hexamer	.009	.029
Dimer-Trimer	----[c]	----[c]
Dimer-Tetramer	----[c]	----[c]
Dimer → Tetramer	----[c]	----[c]
Dimer → Pentamer	----[c]	----[c]
Dimer → Octamer	----[c]	----[c]
Dimer-Stepwise	.004	.005

[a] Phenol concentrations up to 0.65M at 22.2°.

[b] Phenol concentrations up to 1.0M at 20.7°.

[c] Negative values for one or more constants.

TABLE III

THERMODYNAMIC CONSTANTS FOR SELF-ASSOCIATION OF PHENOL

Thermodynamic Constant	Dimer Formation	Higher Multimer Formation
	Cyclohexane Solution	
$K_{25°}$, l./mole	2.10	6.68
ΔF, kcal./mole	- 0.44	- 1.13
ΔH, kcal./mole	- 5.63±0.21	- 5.22±0.13
ΔS, cal./mole-degree	-17.4	-13.7
	CCl_4 Solution (With End Group Correction)	
$K_{25°}$, l./mole	0.94	3.25
ΔF, kcal./mole	0.04	- 0.70
ΔH, kcal./mole	- 5.03±0.27	- 4.32±0.28
ΔS, cal./mole-degree	-17.0	-12.2
	CCl_4 Solution (Without End Group Correction)	
$K_{25°}$, l./mole	1.09	2.74
ΔF, kcal./mole	- 0.05	- 0.60
ΔH, kcal./mole	- 6.08±0.21	- 4.07±0.06
ΔS, cal./mole-degree	-20.2	-11.7

TABLE IV

THERMODYNAMIC CALCULATIONS FOR PHENOL DIMERIZATION

Assumed	CCl_4[a]			Cyclohexane[b]		
K_L/K_C	$-\Delta H_C$	$-\Delta S_C$	$-\Delta S_L$	$-\Delta S_C$	$-\Delta S_C$	$-\Delta S_L$
0	5.03	17.0	∞	5.63	17.4	∞
0.1	5.10	17.4	19.3	5.73	17.9	20.9
0.5	5.40	19.0	17.0	5.85	18.9	17.9
1.0	5.74	20.8	16.0	6.05	20.2	17.4
2.0	6.44	24.0	15.4	6.48	22.4	16.9

[a] ΔH_L = -4.32 kcal./mole

[b] ΔH_L = -5.22 kcal./mole

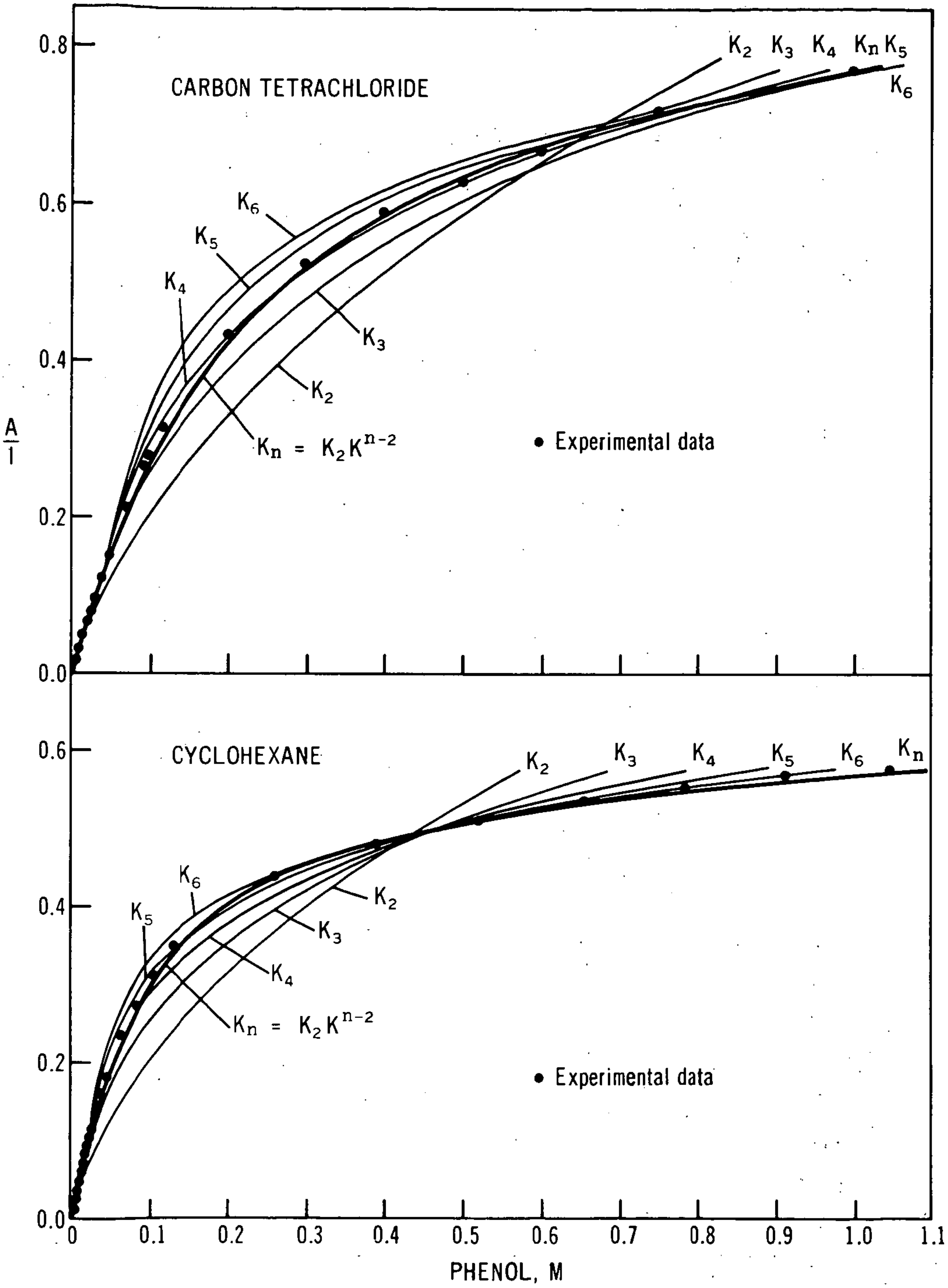

Figure 1. Fit of Experimental Data to Various Self-Association Models

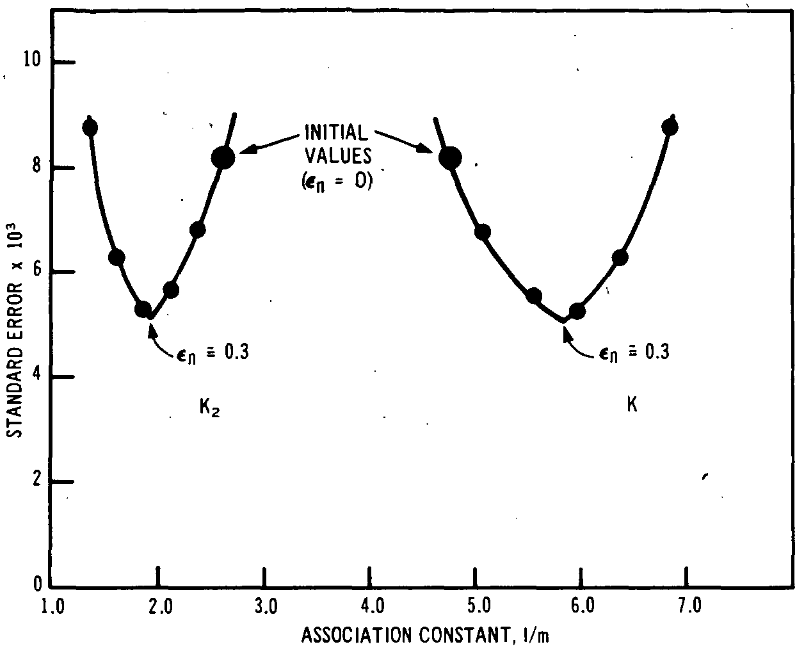

Figure 2. Correction for End Group Absorptivity (CCl_4 Solutions at 2.5°)

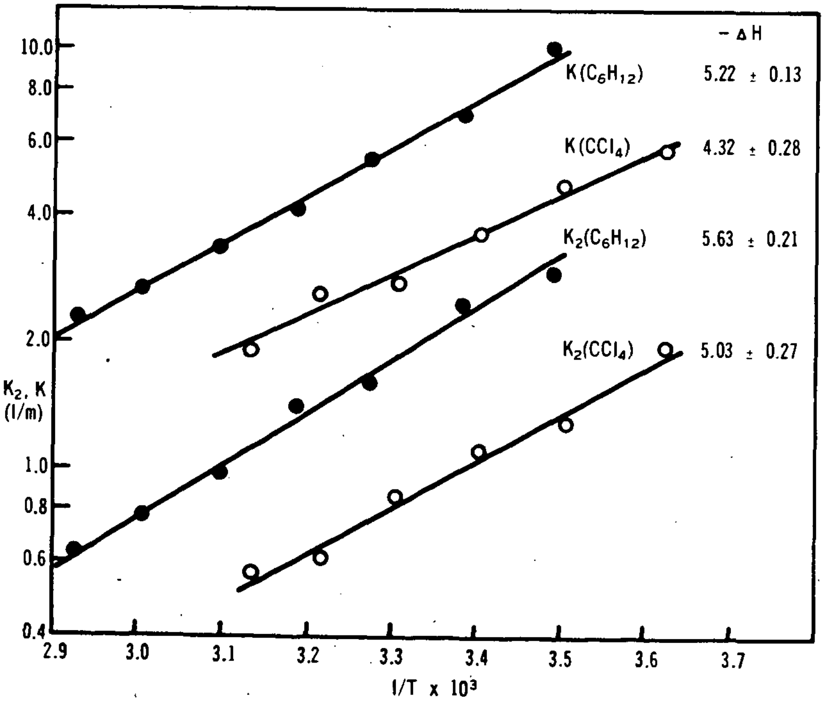

Figure 3. Enthalpies for Dimerization and Stepwise Association.

Infrared Interferometry - Emission Spectra in the Sodium Chloride Region

L. R. Cousins and K. H. Rhee

Gulf Research & Development Company
Pittsburgh, Pa.

Introduction

Spawned primarily by the space industry,(1) infrared interferometry is a relatively new technique to the practicing spectroscopist. Interferometry differs from spectrophotometry in two major areas. First, in interferometry the radiation is not dispersed into monochromatic frequencies but rather the radiation is modulated by means of a vibrating mirror. The modulation process results in an interferogram that in itself does not give very much information. However if the interferogram is fed into a wave analyzer, spectral information can be extracted. Another difference between spectrophotometry and interferometry is in the physical form of the entrance aperture. In a spectrophotometer the energy enters through narrow slits, just a few tenths of a millimeter wide. In an interferometer the energy enters through a window over an inch in diameter. Consequently, the amount of energy available to the detector of an interferometer is orders of magnitude greater than that available to the detector of a spectrophotometer.

These differences give rise to the main advantage of an interferometer, sensitivity. A secondary advantage is scanning speed. A complete interferogram can be recorded in a little over a tenth of a second although more typical scanning speeds are in the order of second.

These characteristics make the interferometer first choice for anyone interested in infrared emission.(2) Some of the possibilities of infrared emission spectroscopy are that samples can be scanned "in situ" with no need of disturbing the sample. This ability could save considerable sample handling in a process-control type of analysis or make analysis of hazardous materials more feasible. Infrared emission spectroscopy is completely non-destructive to the sample and could be used in the analysis of such things as valuable oil paintings. Interferometry can also be used to analyze samples too big for conventional spectrophotometers; for example, our atmosphere in air pollution studies. And it can be used to analyze samples too small; for example, pesticide residue on plant growth.

Experimental

The heart of the interferometer is the optical head. The head is fairly small, about 3 x 6 x 7 inches and is readily portable. The head is connected to the control panel by a ten-foot cable. The aperture is 1-1/4 inches in diameter and has a field of view of eighteen degrees. No special optics are required to get the sample's radiation to enter the optical head; you simply point the aperture at the sample. Unwanted radiation from material in the field of view can be masked out with aluminum foil. The foil being very reflective has essentially zero emissivity.

The head is also readily adapted to a mirror-type telescope making it possible to analyze samples at a remote distance. Smoke has been reportedly analyzed from stacks up to one-half mile away.(3)

Figure 1 is a diagram of the optical head. The interferometer is of the Michelson type. Radiation incident on the window passes into the optical head and strikes the beam divider. Here the radiation is split into two beams; one beam traveling to a stationary mirror and returning and the other beam traveling to a vibrating mirror and returning. Upon reaching the beam divider, the two beams unite and are reflected to the detector, a thermister bolometer. Some energy is lost exiting out through the entrance aperture.

The position of the vibrating mirror when both beams have the same path length is called the zero position. Consider for the moment that the incoming radiation is monochromatic. At the mirror's zero position, all waves will arrive at the detector in-phase giving a maximum signal. As the mirror moves infinitesimally in either direction from its zero position the relative path lengths of the two beams will change and all the waves will not arrive at the detector in-phase. Destructive cancellation will result and the detector's output will be diminished. When the mirror has moved 1/4 wavelength away from the zero position the total path difference will be 1/2 wavelength, and complete cancellation of the beam will result giving a minimum output from the detector. As the mirror continues to move away, the signal will start to increase until at mirror position 1/2 wavelength away from zero position, the retardation will be one full wavelength and all waves will be in-phase again. The detector output at this point will be a maximum equal to the first maximum. As the mirror continues to travel maxima are reached every even quarter wavelength from the zero position and minima are reached every odd quarter wavelength. The continuous output then is a sine wave. The frequency of this sine wave is related to the monochromatic input radiation by the equation:

$$f = L/T \times 1/\lambda$$

Where L is the length of the mirror's repetitive travel in microns and T is the time in seconds. Lambda is in microns. For most of our work L is 500 microns and T is one second. Thus, 2 micron radiation would give rise to a 250 cycles/sec audio sine wave. A wavelength of 16 microns would result in a 31 cycles/sec sine wave. Hence, all the frequencies in the interferogram of radiation between 2 to 16 microns can be found in the audio range below 250 cycles/sec. The length of the mirror's path also determines the resolution of the interferometer. The longer the path length the better the resolution. Our normal resolution is 20 cm^{-1}, the reciprocal of the path length.

Figure 2 shows the sawtooth nature of the mirror's travel and the resulting interferograms. Note that the return time for the mirror is very short and that the mirror's travel is very linear. The interferograms shown are not of monochromatic light.

To visualize what happens when polychromatic radiation enters the interferometer is a little more difficult. At the mirror's zero position, all the frequencies will still be in-phase and a maximum output of the detector will be obtained. However, as the mirror moves away from the zero position destructive cancellation occurs diminishing the output but not in the regular fashion of a sine wave. The result is a very sharp peak at the mirror's zero position with highly damped side bands.

One of the major drawbacks to interferometry is that it is impossible to recognize a spectrum from the interferogram; the interferogram must be filtered to obtain the spectrum. The filtering may be done in several ways. The interferogram can be fed repetitively into a variable filter or wave analyzer. The wave analyzer is set for the first audio frequency and a signal is recorded that is proportional to the amount of that frequency present in the interferogram. The wave analyzer is automatically advanced to the next audio frequency and its signal recorded. As this process is continued the spectrum is recorded.

Alternatively the interferogram may be mathematically filtered by means of the Fourier transformation. The equation for this transformation is:

$$G_{(\nu)} = \int_{0}^{\infty} I_{(x)} \cos 2\nu\pi x dx$$

where $G_{(\nu)}$ is the intensity of the spectrum

$I_{(x)}$ is the intensity of the interferogram

ν is the frequency in wave numbers

x is the path difference in cm

A rather novel way of filtering the interferogram is to transfer the data to a photographic film and place it in a laser beam. Lenses can then be used to optically perform the Fourier transformation and the image recorded on another piece of film.

Results

Figures 3a and 3b show a comparison between an absorption spectrum as recorded by a spectrophotometer and an emission spectrum derived from an interferogram. The spectra are very similar but not identical. The differences are primarily in resolution and relative intensities.

The effect of temperature on the emission spectrum of beta-hydroxyethyl acetate is shown in Figure 4. The spectrum is of course more intense at the higher temperature but otherwise they are very similar. The carbonyl band near 1700 cm^{-1} is relatively more intense in the hotter spectrum and this is consistent with the Boltzmann distribution giving the higher energy levels a greater population in the hotter sample. To obtain these spectra, the acetate was poured onto a piece of aluminum foil and then allowed to drain. The thin film that remained on the foil was sufficient to give the observed results. The foil was heated by conduction.

One of the major problems of infrared emission spectroscopy is shown in Figure 5. The subject is the emission spectrum of "Saran". The bottom spectrum is of one single layer of "Saran" and shows good band structure. However, with four layers of "Saran" all of the band structure between 800 and 1500 cm^{-1} completely disappeared and we have recorded essentially the spectrum of a black body. This phenomenon is attributed to self-absorption.

Interferograms of samples which have a temperature within a few degrees of the detector's temperature are very noisy because of the low signal level. In these cases, it is necessary to time average or co-add several hundred interferograms to obtain a satisfactory spectrum.(2)

Conclusion

An infrared interferometer covering the region 2-16 microns is seen as a potential tool for the practical spectroscopist. It does not have the universal applicability of the more conventional infrared techniques but its unique characteristics of high sensitivity, rapid scanning, and portability will certainly be used to solve specific problems that would be otherwise difficult if not impossible to solve.

---

(1) L. C. Block and A. S. Zachor, Appl. Optics 3, 209 (1964).

(2) M. J. D. Low and I. Coleman, Spectrochimica Acta 22, 369 (1966).

(3) Chemical and Engineering News 45, No. 7, 54 (1967).

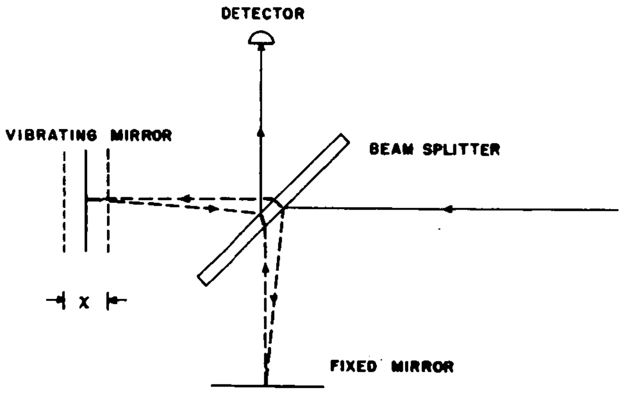
DETECTOR
VIBRATING MIRROR
BEAM SPLITTER
X
FIXED MIRROR

Figure 1. OPTICAL HEAD

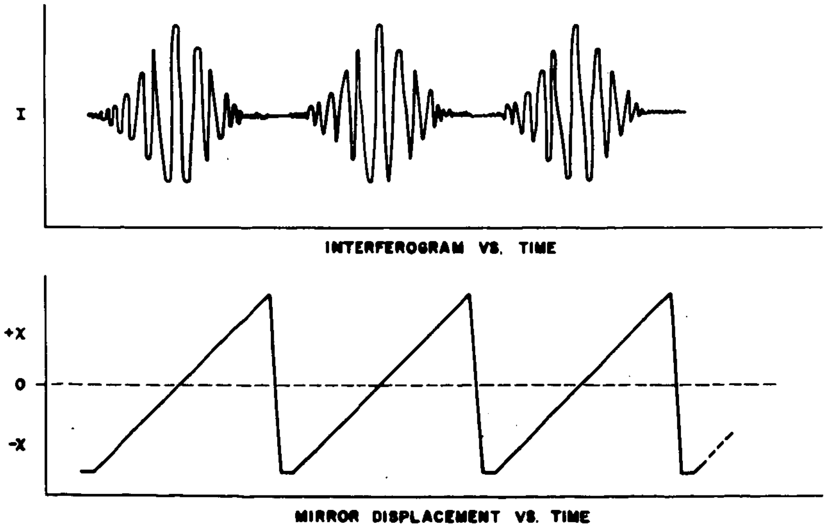

Figure 2. MIRROR TRAVEL AND RESULTING INTERFEROGRAM

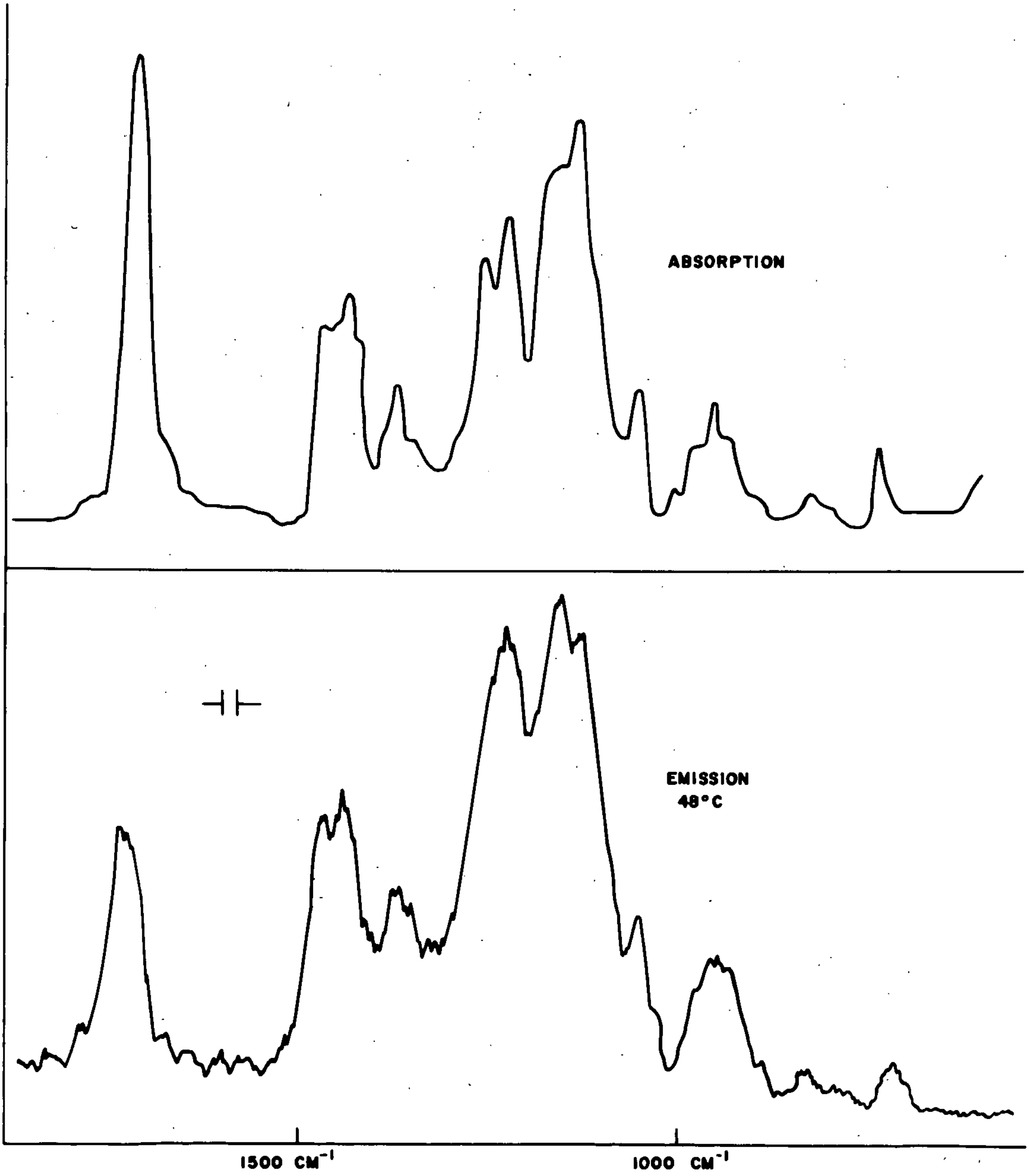

Figure 3a. and 3b. INFRARED SPECTRA OF "KRYLON"

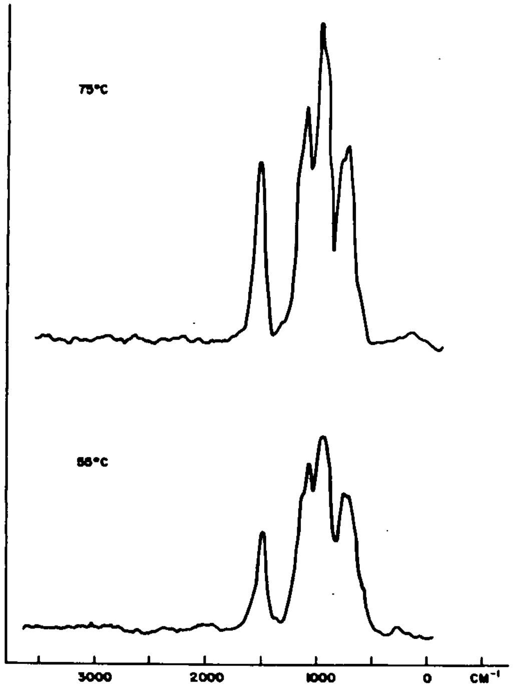

Figure 4. EMISSION SPECTRA OF β-HYDROXYETHYL ACETATE

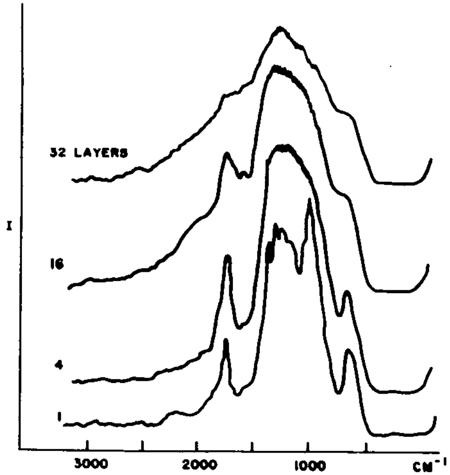

Figure 5. EMISSION SPECTRA OF "SARAN"

INFRARED CHEMICAL ANALYSIS: A NEW APPROACH

Mark M. Rochkind

Bell Telephone Laboratories, Incorporated
Murray Hill, New Jersey 07971

Utilizing an unusual low temperature sampling technique, a new approach to infrared chemical analysis which exhibits micromole sensitivities has been developed. The principal attribute of this new approach is that it offers a very general method for gas mixture analysis; a method which requires no previous knowledge of mixture composition and which entails no preanalytical separation of classes of components. Mixtures containing alkanes, alkenes, aldehydes, ketones, ethers, inorganics and aromatics may be at least qualitatively analyzed by a single step spectrophotometric procedure. Because this new approach to infrared analysis offers a very general method for determining the components of gas mixtures, it should find application in the fuel industry as a tool for kinetic and mechanistic studies of chemical combustion and as an aid in the study of combustion intermediates. This area of research is taking on increasing immediacy as we become more sensitive to the ecological menace posed by air pollution.

Sample preparation consists of diluting the gas mixture to be analyzed with a large excess (usually at least 100 fold) of nitrogen followed by condensation of the diluted gas mixture in pulsed fashion onto an infrared transmitting window previously cooled to 20°K. Using semiautomated procedures, sample preparation and deposition may be completed in less than one minute. A standard double beam spectrophotometer is used for recording the spectral data although enhanced analytical sensitivity may be obtained with modified instruments. The time required for recording a suitable spectrum varies with the problem in hand. Exhaustive analysis of an unknown mixture would, of course, require more time than would a search for some specified set of mixture components.

In the May issue of Analytical Chemistry, this technique of low temperature infrared matrix dispersion analysis is described and application of the technique to the analysis of a series of thirteen simple hydrocarbons is reported (Rochkind, M. M. (1967)). Since that writing, an additional fifty gases and volatile liquids have been examined (see, Table I), and we are now in a position to make concrete remarks regarding the analytical potential of this technique as it is applied to a broad range of chemical compounds. This will be done at the Symposium. In addition to discussing actual performance of this technique as an analytical tool, the equipment requirements will be outlined and some attention will be paid to the adaptation of automated methods with regard to sample preparation and sample deposition.

Table I. Gases and Volatile Liquids for which Standard Spectra Have Been Recorded

ALKENES

Allene
Butadiene
1-Butene
cis-Butene
trans-Butene
2,3-Dimethyl-2-Butene
Ethylene
3-Ethyl-1-Pentene
3-Ethyl-2-Pentene
Isobutylene
3-Methyl-1-Butene
2-Methyl-2-Butene
2-Methyl-1-Pentene
4-Methyl-1-Pentene
trans-4-Methyl-2-Pentene
1-Octene
1-Pentene
Propylene
2,4,4-Trimethyl-1-Pentene

ALKYNES

Acetylene
Ethyl Acetylene
Methyl Acetylene

ALDEHYDES

Acetaldehyde
Propionaldehyde

ETHERS

n-Butyl Ethyl Ether
tert-Butyl Ethyl Ether
Dimethyl Ether
Ethyl Ether
n-Propyl Ether
Vinyl Ethyl Ether

AROMATICS

Benzene

ALKANES

Butane
Cyclopropane
2,4-Dimethylpentane
Dimethyl Propane
Ethane
Heptane
Hexane
Isobutane
Isopentane
Methane
Octane
Pentane
Propane
2,2,5-Trimethylhexane
2,4,4-Trimethylpentane

KETONES

Diethyl Ketone
Dimethyl Ketone
Dipropyl Ketone
Ethyl Butyl Ketone
Ethyl Propyl Ketone
Methyl Butyl Ketone
Methyl Ethyl Ketone
Methyl Isobutyl Ketone
Methyl Pentyl Ketone
Methyl Propyl Ketone

INORGANICS

Ammonia
Carbon Monoxide
Carbonyl Sulfide
Hydrogen Sulfide
Sulfur Dioxide
Water

Different levels of sophistication may be pursued in connection with analysis of the raw spectral data. These range from hand analysis, using specially prepared tables, to strictly computer controlled analyses where the raw spectral data are digitized, transmitted over telephone lines to some centrally located computer facility and analyzed within the computer. An intermediate level of sophistication, one manifestly practical, involves transmitting via teletype a list of frequencies and approximate relative intensities to a central computer at some remote location within which analysis of the relevant data is performed. While the latter approach obviates digitization of the raw spectra, it poses the requirement that competent personnel must be present at the site of the experiment to reduce the spectral graphs to a list of meaningful frequencies and relative intensities. This level of sophistication, though less efficient on an absolute scale than a strictly computer controlled analysis, is very much easier to effect and suggests some exciting possibilities which utilize the time sharing capabilities of new generation computers. The paper to be presented will discuss this data handling problem in detail from the points of view of communications, equipment requirements, cost analysis and effectiveness. Computer controlled microfilm facilities for storing spectral data - where intelligible data need to be retained in an available state - will be discussed as well.

As pointed out in the May issue of Environmental Science and Technology, this method of infrared chemical analysis is strikingly computer oriented (Rochkind, M. M. (1967)). This is so because the sampling technique results in narrow bands (2-6 cm^{-1} bandwidths) which occur at well distributed frequencies, reproducibly from sample to distinct sample. It thus is possible to completely characterize a chemical species by a short list of frequencies (and, perhaps, relative intensities), each accurate to 1-2 cm^{-1}. This greatly simplifies the data handling and the data storing problems.

It appears as though solids may also be susceptible to the kind of matrix dispersion analysis described above for gases. A proposal for preparing samples from solid material which employs pulsed lasers and molecular beams will be considered and some possible attendant problems will be discussed. Relatively nonvolatile liquids (i.e., those having vapor pressures of less than 1 torr at room temperatures) present yet more difficult problems, but even these may be surmounted if need be.

In summary, it appears as though low temperature matrix dispersion - a technique whereby gaseous materials are sufficiently dispersed (not isolated) that in the solid state they exist in a quasi-homogeneous environment within which molecular interactions are minimized - provides a practical technique for sample preparation and permits a new approach to infrared chemical analysis. Work is currently underway to define precisely the quantitative capabilities of the method. Progress in this area will be briefly reported.

References Cited

1. Rochkind, M. M., Anal. Chem. 39, 567 (1967).

2. Rochkind, M. M., Environ. Sci. Technol. 1, 434 (1967).

Acknowledgement

The author is indebted to Robert V. Albarino who prepared gas mixtures for analysis and who recorded many of the spectral measurements.

THE ANALYSIS OF COAL WITH THE LASER-MASS SPECTROMETER

by

F. J. Vastola, A. J. Pirone, P. H. Given, and R. R. Dutcher
College of Earth and Mineral Sciences
Pennsylvania State University, University Park, Pa.

INTRODUCTION

The laser-mass spectrometer has been used to pyrolyse petrographic constituents of coal and record the mass spectrum of the pyrolysis products thus produced. The laser-mass spectrometer has been described in detail elsewhere (1,2). Essentially it consists of a small pulsed ruby laser (max. output energy 0.1 joule) whose output can be focused on the surface of a coal target located in the ionization chamber of a time-of-flight mass spectrometer. A modified microscope optical system is used to focus the laser; irradiated targets can be as small as 10 microns in diameter. Since the target to be irradiated can be viewed through the same microscope system, selected areas of the coal sample can be pyrolysed. With the 10 micron diameter limit of the irradiation zone different petrographic constituents of a coal sample can be pyrolysed in-situ and their mass spectra recorded. These spectra can be used to study the chemical composition and structure of coal or even more simply can be used as "fingerprints" to differentiate between the various heterogeneous constituents of coal.

LASER HEATING

The energy from the laser that irradiates the coal sample is not great (~0.01 cal.). However, since the energy is delivered in a short pulse and the high coherency of the laser light enables it to be focused on a small area, flux densities of 10^6 cal./sec./cm.^{2} can be established at the coal surface. These high flux densities result in extremely rapid heating rates.

It is difficult to assign a temperature to a laser pyrolysis. If one assumes that only the material vaporized was heated estimated temperatures would be about 50,000°C. This value would be decreased considerably if the heat of decomposition of the coal was taken into account. Another factor even more difficult to evaluate is the shielding of the coal surface from the laser radiation by the plume of decomposition products. The presence of high molecular weight products in the mass spectrum would seem to indicate that the bulk of the pyrolysed coal did not reach temperature much above 1000°C. The high flux output of the laser establishes large temperature gradients in the heated solid but the short pulse length restricts pyrolysis to that material in the immediate vicinity of the irradiated zone. This is demonstrated by the fact that a second laser heating of a target produces a mass spectrum characteristic of a char rather than the original material, however if the laser is fired at an area 100 microns removed from a pyrolysed crater the resulting spectrum is the same as an unheated coal.

OBTAINING THE SPECTRA

The pulse length of the laser depends upon the pumping energy, under the conditions used in this investigation a typical pulse length would be about 300 microseconds. Most of the pyrolysis of the coal sample will take place during the actual laser burst. However, pyrolysis products are still being evolved several milliseconds after the laser burst due to the finite cooling time of the coal. The TOF mass spectrometer is capable of making mass analysis of the species in the ionization chamber at 50 to 100 microsecond intervals enabling several spectra to be recorded during the pyrolysis.

The intensity of the masses recorded decreases exponentially with time. The rate of decay is not the same for all masses. In general the higher masses have the longer time constant. The distribution of decay rates cannot be accounted for by the effect of mass on pumping speed of the mass spectrometer vacuum system. A more likely explanation of the variation in decay rates of the different species is that the pyrolysis product distribution changes as the temperature of the coal decreases. For this investigation a single spectrum was recorded representing the composition one millisecond after the start of the laser burst.

THE SPECTRA

Figure 1 shows spectra obtained under similar conditions of the vitrain component of coals of several ranks. The ionization potential for all the spectra was 25 volts. The spectrum above mass 100 is magnified for ease of presentation for both the semi-anthracite and the sub-bituminous coals. With just a cursory glance one can see how easily vitrinites can be separated by the "fingerprint" technique. The general appearance of the mass spectra give some indication of the structure of the material. In the high mass region of the sub-bituminous vitrinite spectrum there are many mass peaks of about equal intensity. This tends to indicate a complex mixture of hydroaromatics and alkyl substituted aromatics. The HVA bituminous vitrinite has a much more differentiated spectrum in this region indicating more organization of structure. The semi-anthracite has a very simple mass spectrum as would be expected for a low hydrogen content, highly condensed ring system.

Figure 2 shows some comparison spectra. The high degree of similarity is seen between two HVA bituminous vitrinites from different sources. This can be contrasted to the dissimilarity between the spectrum of vitrain in sample number 1 and that of the non-vitrinitic material within 100 microns of the vitrain band edge. Although the latter two spectra have many of the same masses, differentiation can be easily accomplished by comparing selected peak ratios.

Major mass peaks can be found in the HVA spectra for the alkyl substituted benzenes and naphthalenes but the mass distributions of the spectra can not be accounted for by a mixture of stable molecules. The spectra indicate the presence of thermally produced free radicals in the pyrolysis products.

The laser-mass spectrometer is capable of differentiating between microscopic heterogeneities in coal. In order to understand the structural basis of this differentiation the behaviour of known materials under these pyrolysis conditions will have to be studied.

ACKNOWLEDGEMENT

This work was supported by a grant from the National Science Foundation.

LITERATURE CITED

1. Vastola, F. J., Pirone, A. J., Div. of Fuel Chem. preprint 151st National Meeting ACS, p. C-53, 1966.

2. Vastola, F. J., Pirone, A. J., Knox, B. E., Proceedings of the Fourteenth Annual Conference on *Mass Spectrometry* and Allied Topics, ASTM Committee E-14, p. 78, 1966.

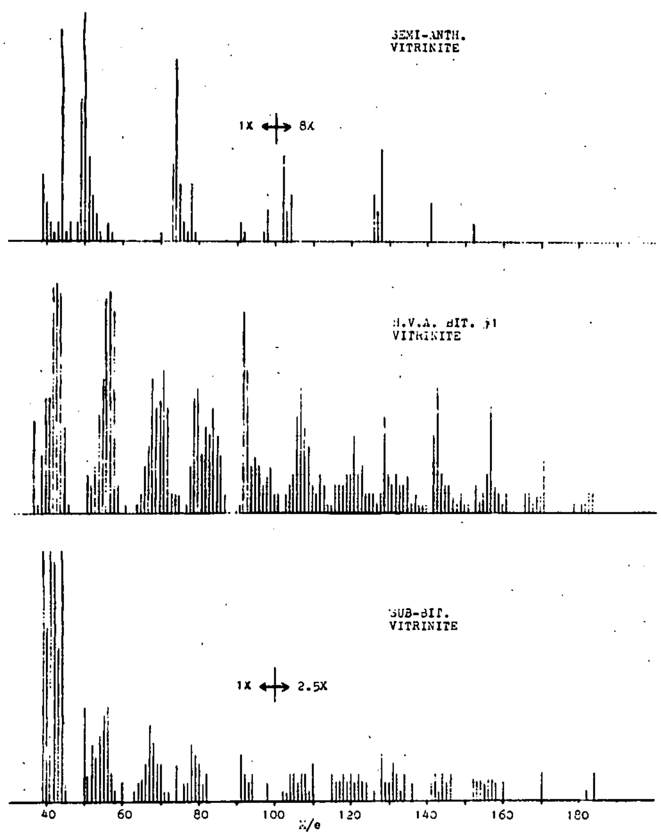

Figure 1: Mass spectra of vitrinites from selected coals.

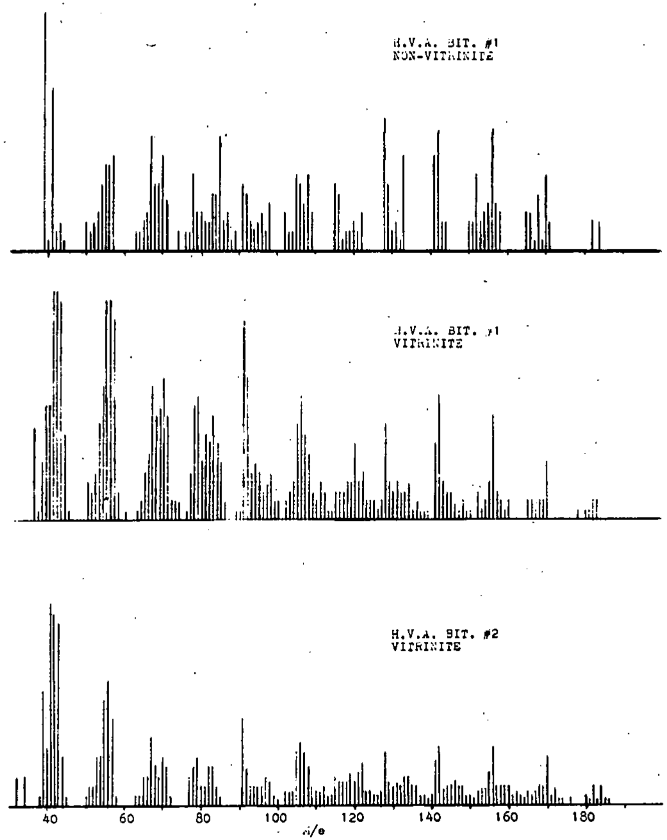

Figure 2: Mass spectra of selected components from h.v.a. bit. coals.

APPLICATIONS OF HIGH RESOLUTION MASS SPECTROMETRY IN COAL RESEARCH

A. G. Sharkey, Jr., J. L. Shultz, T. Kessler,
and R. A. Friedel

U.S. Department of the Interior, Bureau of Mines
Pittsburgh Coal Research Center, Pittsburgh, Pa.

INTRODUCTION

The Pittsburgh Coal Research Center of the Federal Bureau of Mines is attempting to determine which specific organic structures are most influential in enhancing desirable properties in commercially important fractions of coal tars such as road tar and electrode binder pitch. The current emphasis is on a survey of the types of hydrocarbon structures in coal-tar pitch detectable by high-resolution mass spectrometry. This information will provide the basis for an investigation of weathered road tar and other altered fractions of coal tar.

E. J. Greenhow and G. Sugowdz summarized the literature on pitch chemistry to 1961 by stating that less than 100 organic compounds in pitch have been isolated and identified[1]. In these investigations quantitative data were obtained for only a few of the structures identified.

In a previous investigation at our laboratory, mass spectrometric analyses were obtained for three fractions of pitch from the high-temperature carbonization of coal[2]. Semiquantitative data were reported for 34 structural types as well as carbon number distribution data for alkyl derivatives. Approximately 70 percent of the 80° to 85° C softening point pitch was investigated. An average molecular weight of approximately 250 and a value of 4.5 for the mean structural unit (number of aromatic rings per cluster) were derived from the mass spectrometric data. An aromaticity value of 0.94 (aromatic carbon/total carbon) calculated from these data is in excellent agreement with measurements by nuclear magnetic resonance.

Changes in the characteristics of road tar during weathering and in the carbonization properties of various coals following storage possibly involve alteration of certain organic constituents by reactions with oxygen, nitrogen, and sulfur. In our previous investigations of pitch by mass spectrometry only the hydrocarbon portion could be studied in detail as structures containing the heteroatoms nitrogen, oxygen, and sulfur have, in many instances, the same nominal molecular weights as hydrocarbons. Procedures commonly used to study the chemical constitution of coal-tar pitches, such as solvent fractionation, result in a separation according to molecular size but not chemical type as is required to detect changes in heteroatom concentrations.

High-resolution mass spectrometry offers a new approach to studies of species containing heteroatoms. Separation of the components is not necessary if the instrument has sufficient resolution and sensitivity. The addition of a heteroatom results in a slight change in the precise molecular weight of the species producing distinctive peaks for the various combinations of atoms.

In this preliminary study of the high-resolution mass spectrum of coal-tar pitch the investigation consisted of:

(1) Obtaining spectra by fractionating the pitch directly in the mass spectrometer ion source to effectively concentrate species in particular molecular weight ranges.

(2) Making precise mass determinations and deriving empirical formulas for components in the 150 to 320 mass range. This mass range includes components comprising approximately 70 percent by weight of the pitch.

(3) Showing that many of the high molecular weight species detected for the first time could arise from the condensation of radicals.

EXPERIMENTAL PROCEDURE

A Consolidated Electrodynamics Corp. Model 21-110B double focusing mass spectrometer was used for this study of a Koppers 80° to 85° C softening point pitch. A direct insertion probe was used to introduce the pitch into the region of ionization for the fractionation experiment. The mass spectrum and the weight of the sample vaporized were determined at the following probe temperatures: 100°, 175°, 250°, 290°, and 325° C.

A conventional umbrella-type glass introduction system was used for the precise mass study.[3]

Mass measurements on standards were accurate to ± .003 amu. The peak matching technique with perfluorokerosene as a standard was used for all mass assignments. For most of the high-resolution determinations, the instrument was operated with a resolving power of approximately 1 part in 8 to 10 thousand and with an inlet and source temperature of 300° C. The resolution was high enough to permit accurate mass assignments to approximately mass 300 and represented a compromise between sensitivity and desired resolving power. The resolving power required at mass 300 for complete separation of several of the mass doublets of interest is shown in table 1; however, complete separation is not generally required for precise mass assignments. In many instances 50 percent of the theoretical resolving power is adequate.

RESULTS AND DISCUSSION OF RESULTS

A. Mass Spectra of Pitch Fractionated in Mass Spectrometer.

Data obtained for the fractional distillation of the 80°-85° C softening point pitch in the mass spectrometer ion source are shown in table 2. Fractionation of the sample by increasing the temperature of the direct introduction probe was effective in concentrating species in a limited molecular weight range. Precise mass determinations, made as a second part of this investigation, substantiated structural assignments to about molecular weight 350.

At a probe temperature of 100° C 25.5 percent of the pitch sample was vaporized. Masses 178 and 202 are the most intense peaks in this spectrum, indicating anthracene and/or phenanthrene and 4-ring peri-condensed structures such as pyrene distill preferentially at these temperature-pressure conditions. Species with molecular weights as high as 420 were detected. When the probe temperature was increased to 175° C an additional 22.4 percent of the pitch vaporized. The molecular weight of the species showing maximum intensity increased to 252, corresponding to a 5-ring, peri-condensed aromatic structure(s); the molecular weight range of the spectrum increased to mass 526. At 250° C an additional 20.1 percent of the pitch distilled. The mass with maximum intensity was

Table 1.- Major mass doublets in mass spectrum of coal-tar pitch

Doublet	ΔM (amu)	Resolution required to separate doublet at mass 300
C_2H_8-S	.0906	3,300
CH_4-O	.0364	8,200
CH_2-N	.0126	24,000
$C^{12}H$-C^{13}	.0045	67,000

Table 2.- Fractional distillation of Koppers 80°-85° C softening point pitch in mass spectrometer ion source

Probe temperature, °C	Distillate, weight percent		Mass spectrum	
	Cumulative	Fractional	Mass with Max. intensity	Maximum mol. wt.
100	25.5	25.5	178-202	420
175	47.9	22.4	252	526+[a]
250	68.0	20.1	228	550+[a]
290	68.0[b]	-	326	620+[a]
325	68.0	-	326	570+[a]

---

a. Accurate mass numbers could not be assigned to trace peaks appearing at higher molecular weights.

b. No change in weight of residue detectable at probe temperatures > 250° C.

Table 3.- Mass assignments for several perfluorokerosene (PFK) and polynuclear hydrocarbon peaks

Experimental	Calculated (amu)	ΔM	P.P.M.	
204.9888	204.9896	.0008	4	(P.F.K.)
218.9856	218.9852	.0004	2	do
230.9856	230.9847	.0009	4	do
242.9856	242.9855	.0001	0.4	do
254.9856	254.9854	.0002	0.8	do
268.9824	268.9810	.0014	5	do
280.9824	280.9811	.0013	5	do
202.0776	202.0783	.0007	4	4-ring, peri-condensed
228.0937	228.0939	.0002	1	4-ring, cata-condensed

228, corresponding to a 4-ring, cata-condensed aromatic hydrocarbon, and the molecular weight range of the spectrum increased to mass 550. At higher probe temperatures, 290° and 325° C, the spectra indicated that the average molecular weight and ring size of the components continued to increase. The mass with maximum intensity occurred at 326 at temperatures of 290° and 325° C. The spectra indicated components with molecular weights higher than 620. There was no weight change detectable at probe temperatures greater than 250° C. Thus, the spectra obtained at 290° and 325° C represent only a very small portion of the pitch. The total amount of pitch vaporized was 68 weight percent of the charge. This value agrees well with the 70 percent vaporization obtained in our previous studies of the same pitch.[2] The mass spectra obtained at probe temperatures greater than 100° C contained trace peaks whose masses could not be assigned; these ions indicated molecular weights up to about 800.

The increased molecular weight range of the material vaporized at higher probe temperatures is illustrated in figures 1 and 2. These figures, based on low-ionizing voltage mass spectra, were plotted at the University of Pittsburgh Computer Center using a program obtained through the courtesy of the Graduate School of Public Health at the University. The trace ions up to approximately mass 800, which could not be effectively reproduced in these figures, correspond in molecular weight to structures containing at least 12 aromatic rings.

B. Precise Mass Assignments.

Table 3 lists precise mass values obtained by the peak matching technique for several peaks in the perfluorokerosene marker spectrum and for the molecular ions of 4-ring peri- and cata-condensed aromatic hydrocarbons. These data show that mass assignments can be made to within a few parts per million by this technique.

Empirical formulas were derived from the measured masses in the 150 to 319 range of the 80°-85° C coal-tar pitch. Species having from 12 to 28 carbon atoms were observed. A total of 273 peaks were indicated, many resulting from doublets and triplets at nominal masses. In addition to the hydrocarbon species, the precise masses indicated the presence of at least 10 structural types containing oxygen, 9 containing sulfur, and 10 containing nitrogen. Measured and calculated masses showed agreement in general from a few tenths to 3 millimass units. Nineteen of these masses represent structural types not previously reported for coal tar.[4]

The nominal molecular weight and atomic species for each of the components detected is shown in figures 3 and 4. The ability of the instrument to resolve complex mixtures is illustrated at mass 212 where empirical formulas were obtained for structures containing carbon-hydrogen, carbon-hydrogen-oxygen, and carbon-hydrogen-sulfur, all having the same nominal molecular weight.

Table 4 gives the formulas for 13 new high molecular weight species detected in the high-resolution mass spectrum of pitch. The formulas were derived from the observed precise masses. The particular structural type(s) cannot be identified as many isomeric variants are possible for each formula. Also shown are formulas and structures of several compounds containing (C,H), (C,H,O), (C,H,N), and (C,H,S) previously identified in coal tar.[4] The last two columns of table 4 illustrate how the high molecular weight species, with molecular formulas determined in this investigation, can arise from condensation reactions.[5] The addition of C_4H_4 or C_6H_5 radicals to radicals from previously identified structures will produce the molecular formulas shown.

Table 4.- Formation of high molecular weight components by condensation of radicals

Previously identified[a/]		High molecular weight components detected this investigation					
			Precise mass (amu)			Possible origin of component	
Compound	m/e (amu)	Formula	Observed	Theoretical	Δ	Radical from original structure	Addition required[b/]
Benzo[kl]xanthene	218.0732	$C_{20}H_{12}O$ $C_{24}H_{14}O$	268.0894 318.1052	268.0888 318.1045	.0006 .0007	$C_{16}H_8O$ $C_{16}H_6O$	C_4H_4 $2(C_4H_4)$
Naphtho[2,1,8,7-klmn]xanthene	242.0732	$C_{22}H_{12}O$	292.0880	292.0888	.0008	$C_{18}H_8O$	C_4H_4
Benzo[b]naphtho-[2,1-d]thiophene	234.0503	$C_{20}H_{12}S$	284.0657	284.0660	.0003	$C_{16}H_8S$	C_4H_4
Dibenzo[b,def]-chrysene	302.1095	$C_{28}H_{16}$	352.1161	352.1252	.0091	$C_{24}H_{12}$	C_4H_4
5H-Benzo[b]-carbazole	217.0891	$C_{20}H_{13}N$ $C_{24}H_{15}N$	267.1079 317.1250	267.1048 317.1204	.0031 .0046	$C_{16}H_9N$ $C_{16}H_7N$	C_4H_4 $2(C_4H_4)$
4H-Benzo[def]-carbazole	191.0735	$C_{22}H_{13}N$	291.1077	291.1048	.0029	$C_{14}H_5N$	$2(C_4H_4)$
Acridine	179.0735	$C_{21}H_{13}N$	279.1086	279.1048	.0038	$C_{13}H_5N$	$2(C_4H_4)$
Phenanthrene	178.0783	$C_{20}H_{14}$	254.1056	254.1095	.0039	$C_{14}H_9$	C_6H_5
Chrysene	228.0939	$C_{24}H_{16}$	304.1205	304.1252	.0047	$C_{18}H_{11}$	C_6H_5
Benzo[ghi]perylene	276.0939	$C_{26}H_{14}$	326.1116	326.1095	.0021	$C_{22}H_{10}$	C_4H_4
Coronene	300.0939	$C_{28}H_{14}$	350.1122	350.1095	.0027	$C_{24}H_{10}$	C_4H_4

[a/] Listed in "Properties of Compounds in Coal-Carbonization Products," ref. 4.

[b/] M/e of added radical: C_4H_4 - 52; C_6H_5 - 77.

CONCLUSIONS

Approximately three times the number of components reported in previous investigations of coal-tar pitch by other techniques were detected in this study. While the identification of particular structural types is not possible, the precise masses indicate the atomic species present. This study shows that high-resolution mass spectrometry provides a means of detecting changes in either the concentration or composition of organic compounds in fractions of coal tar following exposure to various atmospheres. Such information should lead to a better understanding of the properties of road tars and other commercially important fractions of coal tar.

References

1. Greenhow, E. J., and Sugowdz, G. Coal Research in C.S.I.R.O., Australia, No. 15, Nov. 1961, pp. 10-19.

2. Shultz, J. L., Friedel, R. A., and Sharkey, A. G. Jr. Fuel, 44, No. 1, Jan. 1965, pp. 55-61.

3. Lumpkin, H. E., and Taylor, G. R. A Solids Inlet System for a Mass Spectrometer. Anal. Chem., 33, 1961, pp. 476-477.

4. Anderson, H. C., and Wu, W. R. K. Bureau of Mines Bull. No. 606, 1963, 834 pp.

5. Sharkey, A. G., Jr., Shultz, J. L., and Friedel, R. A. Carbon, 4, 1966, pp. 365-374.

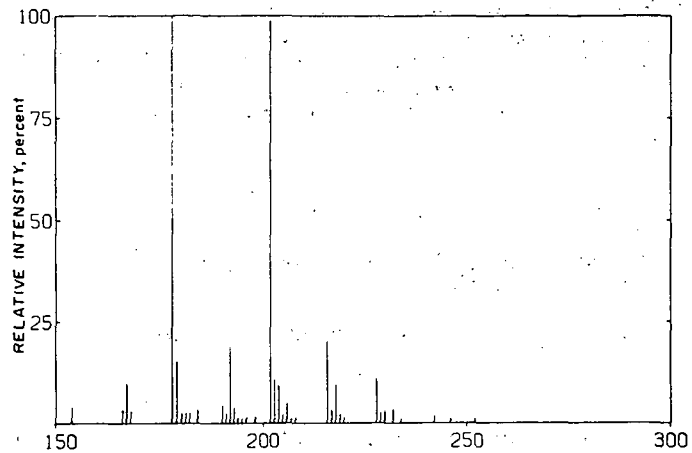

Figure I.—Mass spectrum of 80°-85°C softening point pitch fractionated at 100°C in spectrometer.

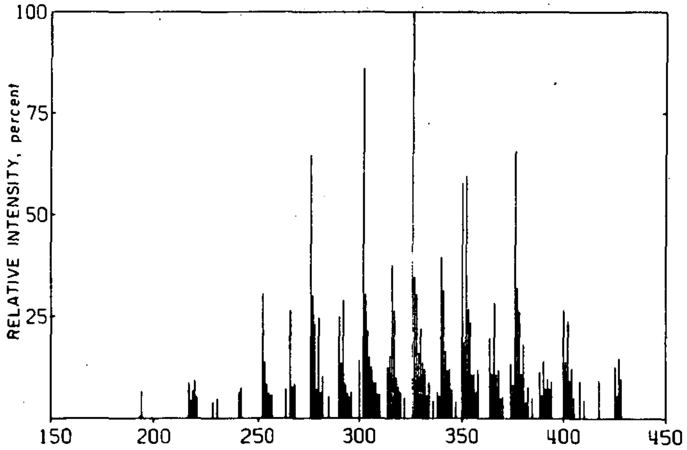

Figure 2.—Mass spectrum of 80°-85°C softening point pitch fractionated at 325°C in spectrometer.

L-9546-A

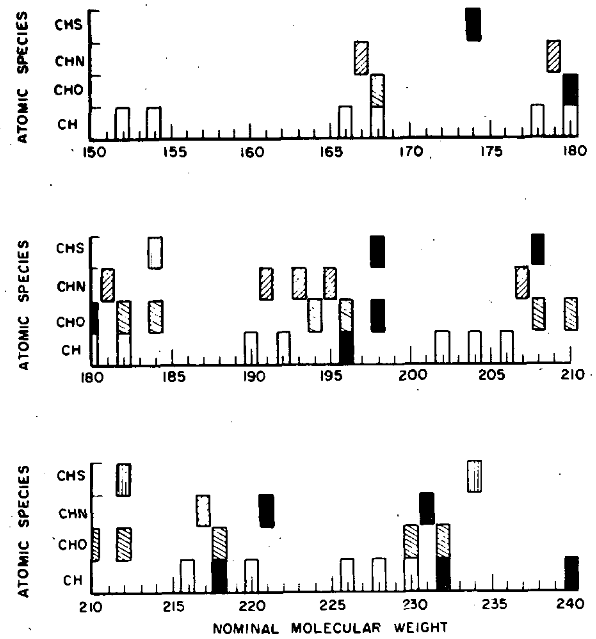

Molecular weight of and atomic species in components observed in 80° – 85 °C pitch by high-resolution mass spectrometry. Mass range 150–240

Figure 3.

L-9942

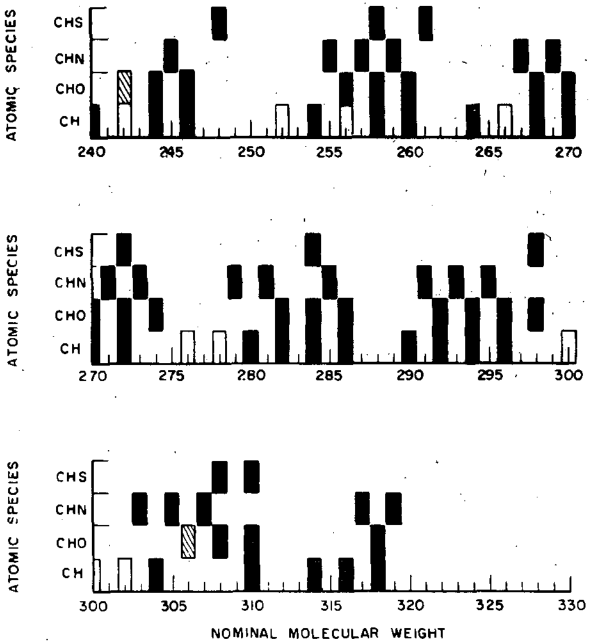

Molecular weight of and atomic species in components observed in 80° – 85 °C pitch by high-resolution mass spectrometry. Mass range 240-319.

Figure 4.

L-9943

FIELD IONIZATION MASS SPECTROMETRY - STRUCTURE CORRELATIONS FOR HYDROCARBONS

Graham G. Wanless

Esso Research and Engineering Co.
Analytical Research Division
P. O. Box 121
Linden, New Jersey

ABSTRACT

Field ionization is a preferred way of looking at molecules and mixtures thereof. Ionization is accomplished by electron abstraction in an electrostatic field of very steep gradient, of the order of 10^8 volts/cm. In contrast to spectra from electron impact, these spectra possess much greater parent ion abundances and relatively fewer fragment ions. This result facilitates analysis of unknown mixtures greatly.

Because the spectra are simpler, greater use can be made of the metastable ions for structural interpretation. An unexpected result is the fact that there is a close correlation between kind and abundance of field ionization primary metastable ions and compound structure. A more complete study of branched hydrocarbons (showing these structure correlations) will be presented than that published recently (Anal. Chem. 39, No. 1, 2-13, Jan. 1967).

The present state of development will be described. Principal problems are (a) to increase signal strength, (b) to develop improved field ion anode devices, and (c) to improve repeatability of successive spectra. How the signal averaging computer can convert the present-quality spectra to precision field-ion mass spectra will be demonstrated with examples.

NUCLEAR MAGNETIC RESONANCE STUDIES OF HYDROGEN BONDING

Norman C. Li

Duquesne University, Pittsburgh, Pennsylvania

Hydrogen bonding is a very significant type of interaction, and is of widespread occurrence. According to Pimentel and McClellan[1], a hydrogen bond exists between a functional group A-H and an atom or a group of atoms D in the same or a different molecule when there is evidence of bond formation, and when the bond linking A-H and D involves the hydrogen atom already bonded to A. Infrared method, based mainly on intensity measurements of the band assigned to the monomeric species, has been used extensively in the determination of equilibrium constants of hydrogen-bonded systems. It offers the advantages that different hydrogen-bonded complexes can be distinguished, and that relatively low concentrations can be used. For very weak complexes however, the infrared method has not proved to be a sufficiently sensitive probe of the quantitative aspects of hydrogen bonding. High resolution nuclear magnetic resonance (nmr) scores easily in providing a sensitive measure of interaction, because it permits the measurements of frequencies which can be done very accurately, rather than intensities which are more subject to uncertainty. This paper describes several ways in which nmr is used to obtain equilibrium constants and thermodynamic functions of various hydrogen-bonded systems. In addition, an application of hydrogen-bonding data to the determination of the preferred form of a beta-diketone is given.

It is well known that the formation of hydrogen bonds usually shifts the nmr signals to lower field, except in certain cases involving aromatic molecules or electron donors in which unusual magnetic anisotropic effects are present [2,3]. Virtually all hydrogen bonds are broken and re-formed at a sufficiently fast rate, so that separate resonances for both hydrogen-bonded and nonhydrogen-bonded states in the same medium are not observed. Consequently, the observed frequency v will correspond to the average of the characteristic frequencies of the complexed and uncomplexed protons (v_c, v_f), weighted according to the equilibrium fraction in each form (X_c, X_f):

$$v = X_f v_f + X_c v_c \qquad (1)$$

For an equilibrium between a monomeric hydrogen donor, A-H, and an electron-donor, D, to form a 1:1 complex C, the following equation may be derived[4] when the concentration of the electron-donor is much greater than that of C:

$$\frac{1}{v - v_f} = \frac{1}{K(v_c - v_f)}\,\frac{1}{d} + \frac{1}{v_c - v_f} \qquad (2)$$

In eq. 2, v is the measured nmr frequency of the hydrogen-bonding proton at a concentration $\underline{d}$ of D, v_f is the frequency of monomeric A-H proton signal at $\underline{d} = 0$, and K is the association constant

$$K = \frac{(C)}{(A\text{-}H)d} \qquad (3)$$

It is interesting to note that this equation is of the same form as one used for treatment of ultraviolet spectral data on 1:1 complexes,

$$\frac{1}{E-E_f} = \frac{1}{K(E_c-E_f)}\,\frac{1}{d} + \frac{1}{E_c-E_f} \qquad (4)$$

where the E's are molar extinction coefficients[5]. For the treatment of infrared spectral data for 1:1 complexes, the following equation can be derived

$$\frac{1}{E_f-E} = \frac{1}{K\,E_f}\,\frac{1}{d} + \frac{1}{E_f} \qquad (5)$$

if intensity measurements are made on the band assigned to the monomeric and uncomplexed species and if complexed species do not absorb radiation at the same frequency, so that $E_c = 0$.

Benzenethiol complexes. Mathur,et al.[4], report nmr studies of hydrogen bonding of benzenethiol with N,N-dimethylformamide (DMF), tributyl phosphate (TBP), pyridine, N-methylpyrazole, and benzene to serve as models of bonding of -SH to the carbonyl oxygen, phosphoryl oxygen, organic nitrogen bases, and an aromatic π electron system, respectively. Table I lists the results obtained.

Table I
Thermodynamic data for benzenethiol bonding to electron-donors

Electron donor	v_c-v_f (ppm)	K_{26° l./mole	$-\Delta H$ kcal./mole
Pyridine	1.2	0.22	2.4
N-methylpyrazole	1.5	.14	2.1
TBP	1.8	.43	2.0
DMF	2.2	.24	1.8
Benzene	-2.5	.039	0.5

The extent of hydrogen-bonding in these systems, as measured by the equilibrium constants and enthalpy changes, is much smaller than that for the same electron donors interacting with phenol. For example, the values of K for phenol-pyridine and phenol-DMF are 77 and 64 l./mole, respectively [6,7]. These suffice to show the weakness of -SH hydrogen bonding relative to -OH. It is only because of the fairly large association shift, v_c-v_f, and the precision of nmr frequency measurements, that the thermodynamic functions of -SH bonding systems can be obtained. In benzene the ring current effect dominates the sign and magnitude of (v_c-v_f). As shown in Table I, benzene behaves as π-electron donor and hence capable of forming weak hydrogen bond with benzenethiol.

2-Propanol complexes. When 2-propanol is used as the hydrogen donor, eq. 2 has to be modified since self-association of the alcohol occurs, and this may affect the equilibrium involving its complex formation with D. Takahashi and Li[8] have derived the following modified equation

$$\frac{1}{v-v'} = \frac{1}{K(v_c-v')}\,\frac{1}{dx} + \frac{1}{v_c-v'} \qquad (6)$$

in which x is the fraction of 2-propanol in the form of monomer at a concentration of alcohol which is not hydrogen-bonded to D (assuming the alcohol to be a mixture of monomeric and polymeric species), and v' is the weighted average OH frequency of the 2-propanol which is not hydrogen-bonded to D. Table II lists the results obtained with N-methylacetamide and N,N-dimethylacetamide as electron donors.

Table II: Thermodynamic data for 2-propanol bonding to acetamides

Temp., °C	K, l./mole	v_c, ppm
	(A) N-methylacetamide	
36	3.61	5.00
24	5.02	5.17
14	6.01	5.23
0	8.94	5.35
	(B) N,N-dimethylacetamide	
40	2.23	4.20
29	2.56	4.30
21	2.88	4.33

Muller and Reiter[9] suggest that the nmr frequency of the complexed species depends quite strongly on the degree of excitation of the hydrogen-bond-stretching vibrational mode. They reason that because this is an unusually low-frequency motion, several excited states are significantly populated even at temperatures as low as 200°K, and their calculations show a temperature dependence of v_c. The data of Table II on the values of v_c at different temperatures do indicate that v_c increases slightly with decrease in temperature. This is not in agreement with the assumption of several authors[4,10-12] that the hydrogen bond shifts do not vary with temperature.

Amine complexes. Takahashi and Li[13] report nmr studies of hydrogen bonding between the amino protons of t-butylamine and aniline, and several electron donors, in chloroform medium. CCl_4 cannot be used because of its reaction with amine. When $CHCl_3$ is used as the solvent, eq. 2 has to be modified since the proton in $CHCl_3$ also acts as a hydrogen donor to the electron donor. The modified equation is

$$\frac{1}{v-v_f} = \frac{1}{K(v_c-v_f)} \cdot \frac{1+K_s(S)}{d} + \frac{1}{v_c-v_f} \qquad (7)$$

where K and K_s are equilibrium constants of the reactions

Amine + D = amine...D	K
Cl_3CH + D = Cl_3CH...D	K_s

and (S), d are the total concentrations of $CHCl_3$ and D, respectively. The experiments were carried out so that (S) is much greater than d and d much greater than the total concentration of the amine. From eq. 7, a plot of $1/(v-v_f)$ vs. $(1+K_s(S))/d$ therefore should yield a straight line, from which K can be determined. The value of K_s is determined in separate experiments by measuring the nmr frequency of the chloroform proton signal in CCl_4 solutions containing 0.05M $CHCl_3$ and various amounts of the electron donor.

The hydrogen-bonding of N-methylacetamide (NMA) to the amines may be represented by the equation

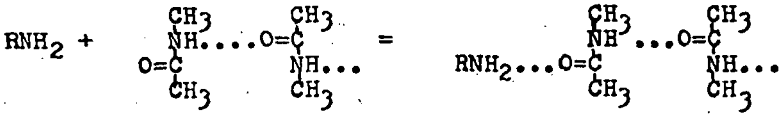

$$RNH_2 + \begin{array}{l}\quad CH_3 \qquad CH_3\\ \quad NH\cdots O=C\\ O=C \qquad\; NH\cdots\\ \quad CH_3 \qquad CH_3\end{array} = RNH_2\cdots\begin{array}{l}\quad CH_3 \qquad CH_3\\ \quad NH\cdots O=C\\ O=C \qquad\; NH\cdots\\ \quad CH_3 \qquad CH_3\end{array} \qquad (8)$$

The values of v_c-v_f for NMA bonding to the amines are independent of temperature between -19 and 36°. This means that in this system,the hydrogen-bond shift is temperature independent and that the self-association of NMA does not interfere with its bonding with the amines. The relative hydrogen-donor strength of $-NH_2$, -OH, and -SH may be obtained by noting that the association constant for aniline bonding to NMA (K = 58 at 36°) is smaller than for phenol bonding to NMA (K = 105 at 30°) and larger than for benzenethiol bonding to NMA (K = 0.13 at 37°).

Water complexes. Takahashi and Li[14] and Ting,et al.[15], report nmr studies of water as hydrogen donor to tetrahydrofuran, acetone, N,N-dimethylacetamide, N,N-dimethylformamide and dimethyl sulfoxide. In their experiments water is the hydrogen donor at low concentrations (mole fraction in the range of X_w= 0.003 to 0.02), in the presence of an electron donor (mole fraction in the range X_d = 0.5 to 0.99), and cyclohexane as an inert solvent. Since water is not soluble in the inert solvent, the presence of an appreciable excess concentration of D is necessary. In the region of low water content,linear plots of the nmr frequency of the water protons vs. the mole fraction of water,at a given value of X_d, are obtained. The extrapolation of the water proton frequency to zero water concentration is easily made, and in the limit of X_w = 0,only two species are considered: the 1:1 complex, $OH_2\ldots D$, and the 1:2 complex, $OH_2.D_2$. The two species are considered to be in equilibrium according to the relation

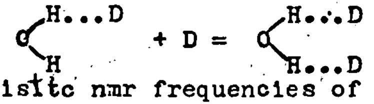

$$O\begin{array}{l}H\cdots D\\ H\end{array} + D = O\begin{array}{l}H\cdots D\\ H\cdots D\end{array} \qquad (9)$$

The characteristic nmr frequencies of the 1:1 and 1:2 complexes are designated v_{11} and v_{12}, respectively, and the following equation is derived

$$\frac{1}{v_o-v_{11}} = \frac{1}{K(v_{12}-v_{11})}\cdot\frac{1}{X_d} + \frac{1}{v_{12}-v_{11}} \qquad (10)$$

In eq. 10, v_o is the extrapolated frequency of the water protons at zero water concentration and K is equilibrium constant of eq. 9. The authors assume that $(v_{12}-v_{11})$ is approximately independent of temperature and draw plots of $1/(v_o-v_{11})$ vs. $1/X_d$. The correct v_{11} is taken to be the value which makes the plots at different temperatures come to a common intercept. From the plots and eq. 10, the values of K and v_{12} are obtained.

Equilibrium constants and enthalpy changes for water bonding to N,N-dimethylformamide (DMF) are larger than the corresponding values for water-N,N-dimethylacetamide (DMA). This order is surprising, since DMF is a weaker electron-donor than DMA towards phenol. It may be that the CH proton in DMF functions as a weak hydrogen donor to the oxygen of water, the protons of which are bonded to other DMF molecules. This would result in a greater hydrogen-donor strength of water toward DMF than toward DMA.

It is of interest to note that Muller and Simon[16] determine proton chemical shifts for dilute solutions of water in mixtures of dioxane and carbon tetrachloride. When the mole fraction of water is below 1.5×10^{-3}, self-association of water is negligible, and the authors treat the data assuming that there are three solute species, free water, a 1:1 water-dioxane complex, and a 1:2 complex. The characteristic frequencies of the complexes appear to be independent of temperature in the range 11-70°, in accordance with the assumption made by Takahashi and Li[14] and Ting, et al.[15]

β-Diketone complexes. Pukanic, et al.[17], report nmr studies of hydrogen bonding between β-diketones- thenoyltrifluoroacetone, hexafluoroacetylacetone, and trifluoroacetylacetone- and several neutral organophosphorus compounds- tributyl phosphate, diethyl ethyl phosphonate, and tri-n-octyl phosphine oxide. Of the three diketones studied, hexafluoroacetylacetone gives the most stable complex with a given phosphorus compound and this is as expected, since it has two electron-withdrawing CF_3 groups in the same molecule. Its greater hydrogen-donor strength is in line with its greater acid strength (pK_a of hexafluoroacetylacetone, thenoyltrifluoroacetone and trifluoroacetylacetone = 4.35, 5.70 and 6.40, respectively). With a given diketone, the equilibrium constant of hydrogen bond formation with the phosphorus compounds increases in the order tributyl phosphate, diethyl ethyl phosphonate, and tri-n-phosphine oxide and is in line with the relative basicity of the phosphorus compounds.

Pukanic, et al.[17], gives an example of the application of hydrogen bonding data to the determination of the preferred enol form of thenoyltrifluoroacetone (HTTA). In CCl_4 as solvent, two possible enol structures (I and II) can be postulated

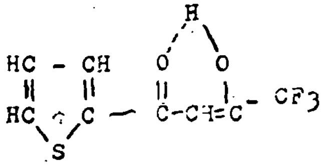

I

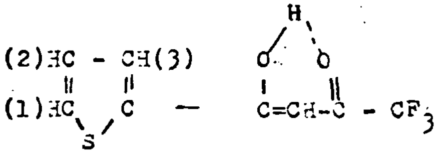

II

Intermolecular hydrogen bonding between HTTA molecules is negligible because HTTA remains monomeric and the nmr frequencies remain constant over wide range of HTTA concentrations in CCl_4 at constant temperature and in the absence of a second solute. In the presence of tributyl phosphate up to 1M, the fluorine-19 nmr resonance remains the same as in the absence of it. Under the same conditions, with hexafluoroacetylacetone in place of HTTA, the fluorine-19 signal moves upfield by 0.25 ppm. The data show that the preferred enol form of HTTA is II, rather than I, because tributyl phosphate would bond with HTTA through the enolic -COH. If the preferred enol form of HTTA were I, then the presence of tributyl phosphate should have affected the fluorine frequency, as it does with hexafluoroacetylacetone. Since no effect was observed with HTTA, the conclusion is that the preferred enol form is II, where the fluorine atoms are farther away from the hydrogen-bonding site.

Current studies. Dr. S. Nishimura and Mr. C.H.Ke in our Laboratory are carrying out nmr studies with water and chloroform bonding to organophosphorus compounds and several amines. At the Symposium in September I hope to include a discussion of their important results.

References

1 G.C.Pimentel and A.L.McClellan, "The Hydrogen Bond", W.H.Freeman and Co., San Francisco, Calif., 1960.

2 J.A.Pople, W.G.Schneider, and H.J.Bernstein, "High Resolution Nuclear Magnetic Resonance", McGraw-Hill Book Co., New York, 1959.

3 D.P.Eyman and R.S.Drago, J.Am.Chem.Soc., 88, 1617 (1966).

4 R. Mathur, E.D.Becker, R.B.Bradley, and N.C.Li, J.Phys.Chem., 67, 2190 (1963).

5 H.Baba and S.Suzuki, J.Chem.Phys., 35, 1118 (1961).

6 A.K.Chandra and S. Banerjee, J.Phys.Chem., 66, 952 (1962).

7 M.D.Joesten and R.S.Drago, J.Am.Chem.Soc., 84, 2696 (1962).

8 F.Takahashi and N.C.Li, J.Phys.Chem., 68, 2136 (1964).

9 N.Muller and R.C.Reiter, J.Chem. Phys., 42, 3265 (1965).

10 E.D.Becker, Spectrochim. Acta, 17, 436 (1961).

11 C.M.Huggins, G.C.Pimentel and J.N.Shoolery, J.Chem.Phys., 23, 1244 (1955).

12 J.C.Davis, Jr., K.S.Pitzer, and C.N.R.Rao, J.Phys.Chem., 64, 1744 (1960).

13 F. Takahashi and N.C.Li, J.Phys.Chem., 69, 2950 (1965).

14 F.Takahashi and N.C.Li, J.Am.Chem.Soc., 88, 1117 (1966).

15 S.F.Ting, S.M.Wang and N.C.Li, Can.J.Chem., 45, 425 (1967).

16 N.Muller and P.Simon, J.Phys.Chem., 71, 568 (1967).

17 G. Pukanic, N.C.Li, W.S.Brey, Jr., and G.B.Savitsky, J.Phys. Chem., 70, 2899 (1966).

THE POTENTIAL OF C^{13} NMR IN COAL RESEARCH

H. L. Retcofsky and R. A. Friedel

U.S. Department of the Interior, Bureau of Mines
Pittsburgh Coal Research Center, Pittsburgh, Pa.

SUMMARY

Current carbon-13 nuclear magnetic resonance (C^{13} NMR) studies of coal, coal derivatives, and related materials are presented and discussed. Broadline and pulsed NMR techniques have been applied to a few solid materials isotopically enriched in carbon-13, while high-resolution NMR studies of a wide variety of pure compounds and several coal derivatives have been carried out. The former techniques are used to derive spectral second moments and nuclear magnetic relaxation times. High-resolution C^{13} NMR is potentially a powerful tool for the direct quantitative determination of the aromaticity (f_a) of soluble products from coal. Values of f_a for light oils from coal and lignite and for a carbon disulfide extract of coal have been estimated from their C^{13} NMR spectra.

INTRODUCTION

Since the first published report of successful NMR measurements of the hydrogen distribution in a coal derivative[1] and the first determination of a high-resolution spectrum of a coal extract[2], proton magnetic resonance spectrometry has been used by many authors[3] to aid in the elucidation of the structure of coal. Brown and Ladner[4] developed a method for applying the hydrogen distribution data to the analysis of carbon structure, with particular emphasis on estimating three important structural parameters: f_a, the aromaticity; σ, the degree of aromatic substitution; and H_{aru}/C_{ar}, an indication of the size of the condensed aromatic ring system. C^{13} NMR offers a method by which f_a can be measured directly and realistic limiting values can be placed on the latter two parameters.

Broadline NMR, first observed for the protons in coal by Newman, Pratt, and Richards[5], is a means of determining second moments and may for very simple molecules give information on hydrogen-hydrogen distances. Values of various parameters for the mean structural units in coals have been estimated from experimentally determined second moments.[3] C^{13} NMR has been detected in natural abundance for only a few solid substances; the principal investigators being Lauterbur[6] and Davis and Kurland[7]. Observation of the C^{13} resonance in graphite has been reported by Abragam[8] using the method of Overhauser dynamic polarization. An attempt to find the C^{13} resonance in synthetic diamond proved unsuccessful[9]. Solid state C^{13} NMR studies of C^{13} enriched materials may give information on carbon-carbon or carbon-hydrogen bond distances[10].

No measurements of relaxation times for nuclei in coal have been reported in the literature to date and C^{13} nuclear relaxation times have been reported for only two substances containing naturally occurring carbon-13[11]. Preliminary measurements of proton relaxation times in a bituminous coal and C^{13} relaxation times in a few isotopically enriched materials were carried out under Bureau supervision during the course of this investigation.

EXPERIMENTAL

The high-resolution C^{13} NMR spectra obtained during the course of this investigation were of two types. Rapid passage dispersion mode C^{13} spectra were obtained using a Varian Associates V-4300C high-resolution NMR spectrometer operating at 15.085 MHz. These spectra exhibit asymmetric peaks, do not have a continuous baseline, and peak shapes and intensities are dependent upon the direction of magnetic field sweep. Thus, spectra are presented in pairs with the spectrum obtained while sweeping the applied magnetic field from low to high values being at the top of each figure. Quantitative estimates of f_a were determined by the method of Friedel and Retcofsky[12]. Time-averaged absorption mode C^{13} spectra were kindly provided by E. G. Cummins of Perkin-Elmer, Ltd., and were obtained using an R-10 spectrometer. Values of f_a were determined directly from electronic integration of the spectra.

Broadline C^{13} NMR spectra were also obtained on the Varian instrument mentioned above. The modulation and detection systems used for the broadline studies were components of a Varian V-4500 electron paramagnetic resonance spectrometer.

C^{13} magnetic relaxation times were measured from oscillographic recordings of free induction decay curves (for T_2) and of the NMR signal amplitude following 180°-90° pulse sequences (for T_1). This work was generously performed for us by NMR Specialties, Inc., using their PS-60-A pulsed spectrometer system.

RESULTS AND DISCUSSION

High-Resolution Studies

Rapid passage dispersion mode spectra of neutral oils from coal and lignite are shown in figures 1 and 2 respectively. The signal-to-noise ratio, although not high and certainly an important limiting factor in accurate determinations of f_a, is remarkably good considering the low natural abundance of C^{13}, and the complexity of the coal derivatives. The higher aromaticity of the oil from high-temperature cracking of the coal carbonization product is readily apparent from the spectra. Aromaticities for three neutral oils were estimated using the calibration procedures reported previously. The results are given in the table below and compared with f_a's estimated from proton NMR data by the Brown and Ladner[4] method. Spectra of a CS_2 extract of coal (representing 3% to 5% of the whole coal) are shown in figure 3. The signal-to-noise ratio here is considerably worse due to the presence of a large amount of the CS_2 solvent. The f_a value determined from C^{13} NMR is 0.6.

Aromaticities of Neutral Oils

Source	C/H	f_a H^1	f_a C^{13}
800° C cracking of a high-temperature coal carbonization product	1.05	0.83	0.78
700° C cracking of a low-temperature coal carbonization product	0.86	0.68	0.70
Distillation of a lignite carbonization product	0.64	0.38	0.39

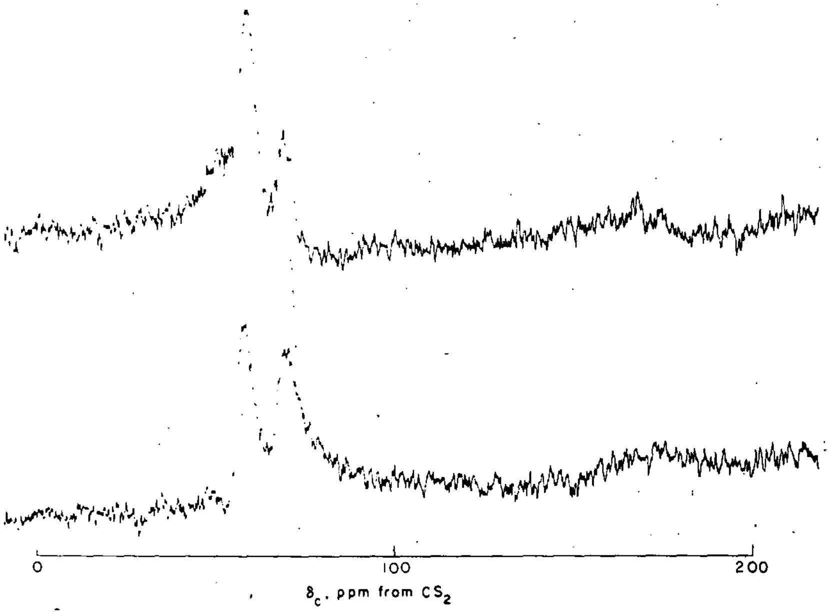

Figure 1. C^{13} magnetic resonance spectra of neutral oil from 800°C cracking of condensed tar from High Splint Coal.

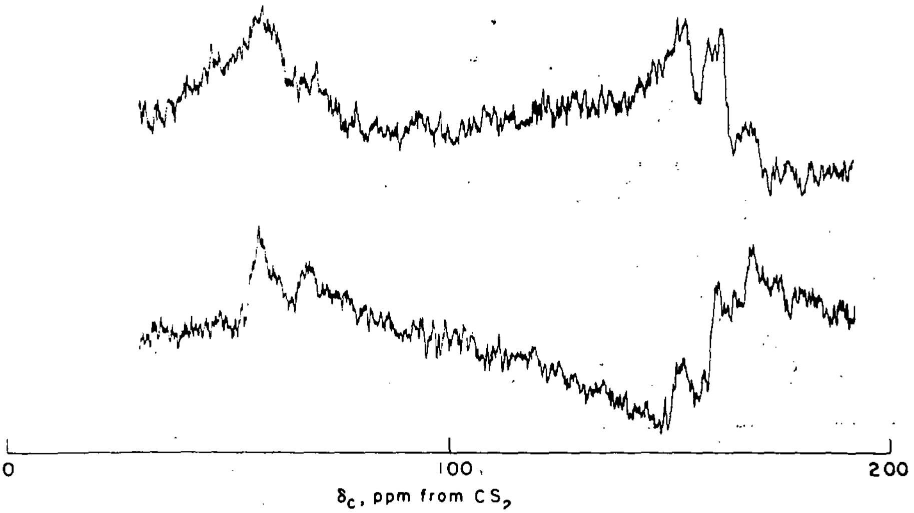

Figure 2. C^{13} magnetic resonance spectra of neutral oil from distillation of Sandow Lignite Tar.

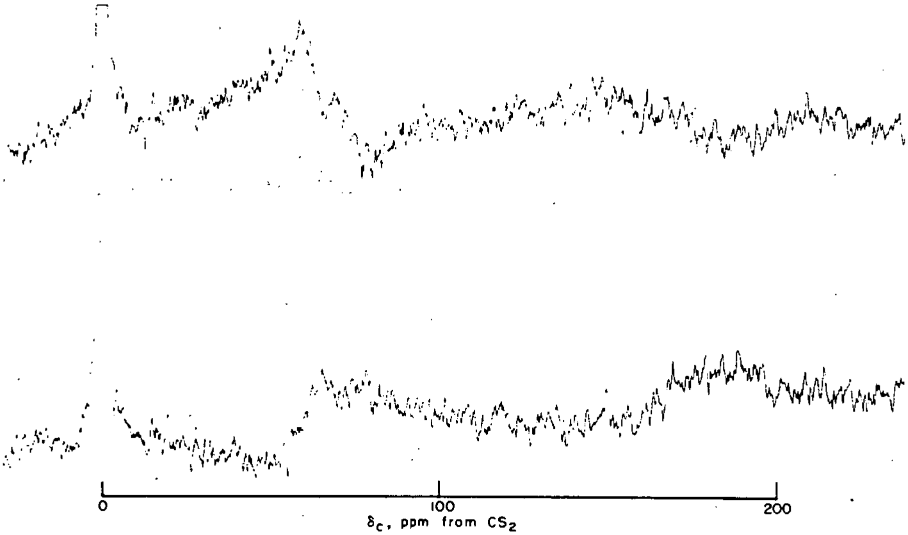

Figure 3. C^{13} magnetic resonance spectra of carbon disulfide extract of Pittsburgh Seam Vitrain.

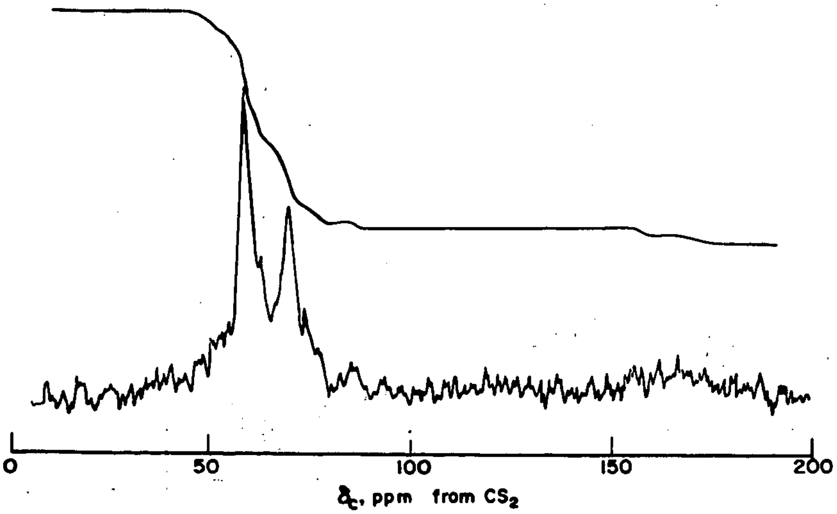

Figure 4. Absorption mode C^{13} magnetic resonance spectrum of coal tar.

The disadvantages in trying to obtain quantitative values of f_a from rapid passage dispersion mode C^{13} spectra are obvious from figures 1 and 2 and have been indicated in the foregoing discussion. Nevertheless it must be remembered that this is the first direct method for determining this heretofore very elusive structural parameter. With the advent of the time-averaging computer and its successful application in NMR experiments, the time is now here that highly precise and reasonably accurate f_a values can be obtained from absorption mode C^{13} NMR spectra. That is, spectra can be obtained under conditions similar to those used in proton NMR. Such a spectrum obtained from nearly 1,000 scans of the C^{13} spectral region is shown in figure 4 for the CS_2-soluble material of coal tar. The f_a value can be gotten directly from the integral reproduced along with the spectrum. The potential of this technique in coal structure research is an exciting one and will be pursued in our laboratory.

Broadline NMR

The C^{13} NMR spectrum of an isotopically enriched amorphous carbon produced by the 1000° C reduction of $C^{13}O_2$ is shown in figure 5. The spectrum shown is handdrawn using 6 actual spectra as guides. Isotopic enrichment is around 55 percent. The peak to peak linewidth is 5.2 gauss and the second moment was measured to be 6.0 guass^2. The spectral linewidth of the carbon can be compared to that found for barium carbonate (around 1.0 gauss) in which dipole-dipole interactions are essentially negligible and the width is determined primarily by the chemical shift anisotropy[6] of the carbonate anion.

Pulsed NMR

The C^{13} enriched carbon was also examined by pulsed NMR techniques. Room temperature measurements of the spin-lattice relaxation time (T_1) and the spin-spin relaxation time (T_2) yielded the values 360 milliseconds and 80 microseconds respectively. The free precession decay curve is shown in figure 6. One important conclusion that can be made from these measurements is that the transmitter power level used for obtaining the broadline NMR spectrum was low enough to avoid saturation. Thus true line shapes are observed. T_1 and T_2 were found to be 27 seconds and 13 seconds respectively for the carbonyl carbon in 55% C^{13} enriched liquid acetic acid. In contrast the proton relaxation times in an 84% carbon coal are 50 microseconds (T_1) and 9 microseconds (T_2).

CONCLUSIONS

The carbon-13 NMR results described here illustrate the first application of the technique to coal derivatives. The potential of the techniques described is nearly unlimited and possibly much more information than that described here will be obtained. For example, C^{13} has been shown to be a very useful tool for the characterization of carbonyl groups. Such groups are thought to be present in coal. The most recent experimental techniques involve the use of time averaging computers, instruments which are at this time beginning to appear on the work bench of many industrial, government, and academic research laboratories. The main disadvantage to C^{13} NMR spectroscopy is the long times involved in the accumulation of spectral data. Thus, although it may not become as widely applied as NMR of other nuclei such as H^1 and F^{19}, the information obtained from C^{13} NMR may be much, much more important.

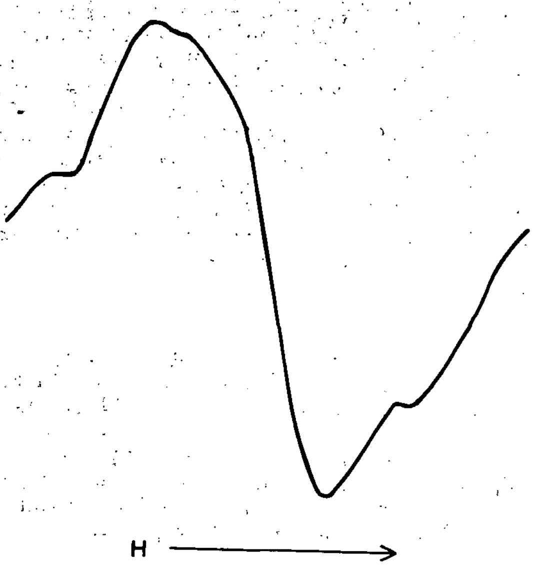

Figure 5. C^{13} magnetic resonance spectrum of amorphous carbon. (55% enriched in carbon-13)

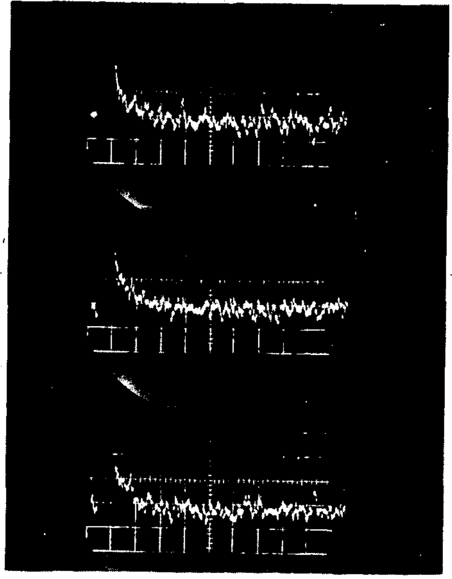

Figure 6. Free induction decay curves for amorphous carbon.

References

1. Friedel, R. A. Absorption Spectra and Magnetic Resonance Spectra of Asphaltene. J. Chem. Phys., v. 31, No. 1, pp. 280-281, July 1959.

2. Friedel, R. A., and H. Retcofsky. Spectral Studies of Coal. Paper presented at Fifth Carbon Conference, Pennsylvania State University, University Park, Pa., June 19-23, 1961.

3. For a review and leading references see:
Tschamler, H. and E. DeRuiter, Physical Properties of Coals, Chap. 2 in "Chemistry of Coal Utilization," Supl. vol. ed. H. H. Lowry, John Wiley And Sons, New York, 1963, pp. 35-118.

4. Brown, J. K., and W. R. Ladner. A Study of the Hydrogen Distribution in Coal-like Materials by High-Resolution Nuclear Magnetic Resonance Spectroscopy. II. A Comparison with Infra-red Measurement and the Conversion to Carbon Structure. Fuel, v. 39, pp. 87-96, 1960.

5 Newman, P. C., L. Pratt, and R. E. Richards. Proton Magnetic Resonance Spectra of Coals. Nature, v. 175, p. 645, 1955.

6. Lauterbur, P. C. Anisotropy of the C^{13} Chemical Shift in Calcite. Phys. Rev. Letters, v. 1, No. 9, pp. 343-344, 1958.

7. Davis, D. G., and R. J. Kurland. Carbon-13 NMR of Paramagnetic Iron-Group Cyanides. J. Chem. Phys., v. 46, pp. 388-390, 1967.

8. Abragam, A., A. Landesman, and J. Winter. Effet Overhauser dans les Charbons et graphite. Comptes Rendus, v. 247, 1852-1853, 1958.

9. Lauterbur, P. C. Private communication.

10. Slichter, C. P., Principles of Magnetic Resonance with Examples from Solid State Physics. Harper and Row, New York, p. 61, 1963.

11. McConnell, H. M., and C. H. Holm. Anisotropic Chemical Shielding and Nuclear Magnetic Relaxation in Liquids. J. Chem. Phys., v. 25, p. 1289, 1956.

12. Friedel, R. A., and H. L. Retcofsky. Quantitative Application of C^{13} Nuclear Magnetic Resonance: C^{13} NMR Signals in Coal Derivatives and Petroleum. Chem. and Ind. 1966, pp. 455-456.

Spin Echo Nuclear Magnetic Resonance Studies of Fast Chemical Reactions

T. Alger, H. S. Gutowsky and R. L. Vold

University of Illinois, Urbana, Illinois

Since the original work of Gutowsky, McCall and Slichter[1] in 1953 high resolution nuclear magnetic resonance has developed into a useful tool for studying fast chemical reactions in liquids. These reactions occur in systems at dynamic equilibrium and involve rapid, reversible transfer of nuclear spins between magnetically non-equivalent environments. For example, intermolecular hydroxyl proton transfer in ethanol,[2] ring inversion in cyclohexane,[3] and hindered internal rotation in N,N-dimethylacetamide[4] have all been studied by high resolution NMR methods. Useful reviews of such studies have been made by Lowenstein and Connor[5] and by Johnson.[6]

If the rate at which spins transfer between non-equivalent magnetic environments or "sites" is less than the difference between the resonant frequencies of the sites, separate resonance lines are observed in the spectrum. For faster exchange rates, the spins experience an average resonant frequency, and the resolved lines are collapsed; one or more lines are observed at the average resonant frequencies. By analysis of the details of the lineshape at various temperatures, it is possible to obtain the temperature dependence of the exchange rate constant.

High resolution NMR has been used for many years to measure exchange rates; it is the purpose of this paper to discuss the recently developed spin echo method, which depends on measuring the spin-spin or transverse relaxation rate. The transverse relaxation rate is measured most conveniently by the Carr Purcell method (see Fig. 1). The weak, continuous, oscillating magnetic field of high resolution NMR is replaced by a much stronger oscillating field which is turned on only in short bursts or pulses with duration of a few microseconds. The first pulse, applied at time zero, instantaneously tips the nuclear magnetization into a plane perpendicular to the constant magnetic field (xy plane). The magnetization, as viewed in a coordinate system rotating at the average larmor frequency, dephases because the constant field is not perfectly homogeneous and spins in different parts of the sample precess at different rates. The rest of the pulses, applied at times τ, 3τ, 5τ, etc., flip the magnetization by 180°, and cause the magnetization to refocus and form spin echoes at times 2τ, 4τ, 6τ etc. The decay of the envelope of echo maxima is independent of magnetic field inhomogeneity, and its time constant defines the transverse relaxation time.

It is reasonable that transfers of spins between different sites should affect the relaxation rate as well as the high resolution lineshape. Spins in magnetically non-equivalent sites precess at different rates around the constant magnetic field, and since individual spin transfers occur at random times, their macroscopic effect is to cause an additional dephasing of the magnetization; a faster relaxation rate. The amount of dephasing which occurs depends on the exchange rate (average time which a spin spends precessing in one site or the other), on the chemical shift between the sites (difference in precessional frequency), and on the spacing of the 180° refocussing pulses. The latter parameter affects the amount of dephasing because it determines the length of time in which the spins can dephase before being refocussed.

The dependence of observed relaxation rate upon rf pulse spacing forms the basis of the spin echo method of determining exchange rates. For exchange rates which are less than the chemical shift, the observed relaxation rate attains a limiting value at long pulse spacings which depends on the rate constant for exchange but not the chemical shift. At short pulse spacings, the observed relaxation rate approaches another limit which is independent of the chemical exchange rate. At intermediate pulse spacings, the relaxation rate is somewhere between these limiting values. By analysis of the dependence of relaxation rate upon pulse spacing, it is possible to obtain values for the rate constant, chemical shift, and relaxation rate in absence of exchange.

Figure 2 shows some relaxation curves, or graphs of relaxation rate versus inverse pulse spacing, obtained by Allerhand and Gutowsky[7] for N,N-dimethyltrichloroacetamide. In this molecule the rate process is hindered rotation around the C-N bond, which exchanges the non-equivalent methyl groups. At low temperatures the relaxation rate depends strongly upon pulse spacing, but at higher temperatures the relaxation rate appears to become independent of pulse spacing. This behavior is due to the fact that at higher temperatures the exchange rate is larger, and it is not possible in practice to reduce the pulse spacing sufficiently to prevent dephasing.

For simple systems such as N,N-dimethyltrichloroacetamide the spin echo method appears to be superior to high resolution NMR methods of measuring exchange rates. A larger temperature range is experimentally accessible since exchange contributions comparable to the true "natural linewidth" (without inhomogeneity broadening) can be measured. In addition, analysis of the relaxation curves usually yields values for the chemical shift at each temperature as well as the rate constant. This is important because an undetected and uncorrected temperature dependence of the chemical shift can result in large errors, particularly in the entropy of activation.[8]

These advantages of the spin echo method make its extension to more complicated systems a potentially useful theory. To date, it is possible in principle to calculate spin echo amplitudes for an arbitrarily complicated spin system, including homo- and heteronuclear spin coupling as well as chemical exchange processes.[9] In practice even large computers require two or three minutes to calculate relaxation curves for systems witn about twelve lines in their spectra; this appears to be the current practical limit of complexity.

Ethanes which have been substituted with four or five chlorine or bromine atoms provide a quite stringent test of the spin echo method. There are relatively high barriers to internal rotation about the C-C bond in these molecules,[10] and for unsymmetrically substituted molecules there are three different rotational isomers, each of which may involve spin coupling. The effect of homonuclear spin coupling is to introduce strong modulation of the echo train, and it is then not feasible to define a transverse relaxation rate (see Fig. 3). Heteronuclear spin coupling is usually not observable in Carr Purcell spin echo experiments unless the coupled nuclei are involved in an exchange process. Even in this case the heteronuclear spin coupling does not produce modulations, it contributes to the effective chemical shifts of the exchanging nuclei[9] (see Fig. 4).

In 1,1-difluoro-1,2-dibromodichloroethane, there are two possible exchange processes: between the rotamer with bromine atoms in a trans conformation and either of the d,ℓ pair of "gauche" rotamers, and between the two gauche rotamers. Homonuclear spin coupling between fluorines in the gauche rotamers is observable because the two fluorines are non-equivalent in this case. The low temperature spin echo trains therefore show characteristic modulation patterns[11] (see Fig. 3). In agreement with theory, the details of the modulation depend on the rf pulse spacing.

At temperatures above about -60°C the modulation disappears and the echo trains become exponential. This is because the chemical exchange is sufficiently rapid to "average out" effects of coupling. A high resolution NMR spectrum at this temperature would show a single, broad featureless line. The apparent relaxation rate depends upon rf pulse spacing up to about -20°C, and the dependence can be analysed to yield values of the free energy barrier for gauche trans internal rotation (11.0 kcal/mole) and for gauche-gauche internal rotation (12.0 kcal/mole).

For 1-fluoro-1,1,2,2-tetrachloroethane, only one exchange process is observable by magnetic resonance: the interchange of the rotamer with hydrogen and fluorine in a trans conformation with either of the magnetically equivalent "gauche rotamers". It is easy to show that for spin echo experiments, the observed echo trains should be a sum of two contributions, each corresponding to a two site exchange process.[12] The two processes occur at the same rate but with different effective chemical shifts, given by the true proton chemical shift between gauche and trans rotamers, plus or minus one half the difference of the heteronuclear coupling constants for each rotamer. At the field strengths used (corresponding to proton resonance at 26.8 and 17.7 MHz) the chemical shift is small, and the two effective chemical shifts are equal, and independent of field strength (see Fig. 4). In this compound the free energy barrier for interconversion of the gauche and trans rotamers was found to be about 8.7 kcal/mole. It is less than the barriers found in CF_2BrCCl_2Br because in the former compound the activated complex involves eclipse of smaller atoms than in the latter.

References

[1] H. S. Gutowsky, D. W. McCall, and C. P. Slichter, J. Chem. Phys. 21, 279 (1953).

[2] J. T. Arnold, Phys. Rev. 102, 136 (1956).

[3] F. A. L. Anet, M. Ahmad, and L. D. Hall, Proc. Chem. Soc. (London) p. 145 (1964).

[4] M. T. Rogers and J. C. Woodbrey, J. Phys. Chem. 66, 540 (1962).

[5] A. Lowenstein and T. M. Connor, Ber. Bunsenges. Physik. Chem. 67, 280 (1963).

[6] C. S. Johnson, Jr., Advances in Magnetic Resonance 1, 33 (1965).

[7] A. Allerhand and H. S. Gutowsky, J. Chem. Phys. 41, 2115 (1964).

[8] A. Allerhand, H. S. Gutowsky, J. Jonas and R. Meinzer, J. Am. Chem. Soc. 88, 3185 (1966).

[9] H. S. Gutowsky, R. L. Vold and E. J. Wells, J. Chem. Phys. 43, 4107 (1965).

[10] R. A. Newmark and C. H. Sederholm, J. Chem. Phys. 43, 602 (1965).

[11] R. L. Vold and H. S. Gutowsky, J. Chem. Phys. (submitted)

[12] T. Alger, H. S. Gutowsky and R. L. Vold, (to be published).

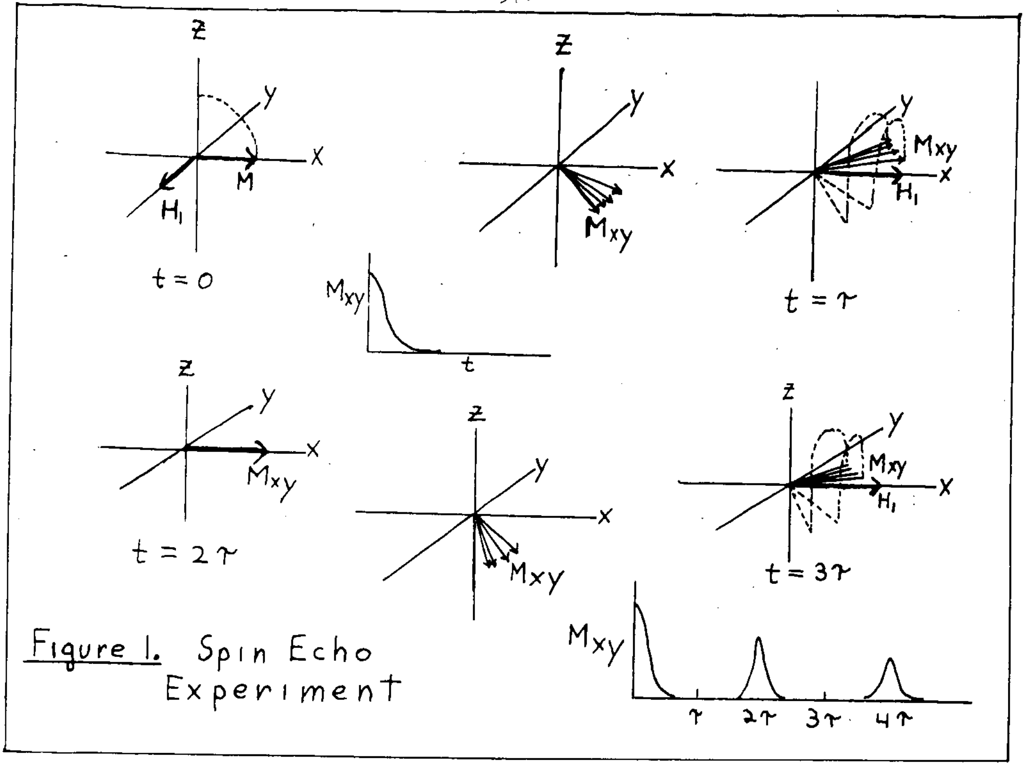
z
y
x
M
H₁
t = 0
z
y
x
Mxy
Mxy
t
z
y
Mxy
x
H₁
t = τ
z
y
x
Mxy
t = 2τ
z
y
x
Mxy
z
y
Mxy
x
H₁
t = 3τ
Mxy
τ
2τ
3τ
4τ

Figure 1. Spin Echo Experiment

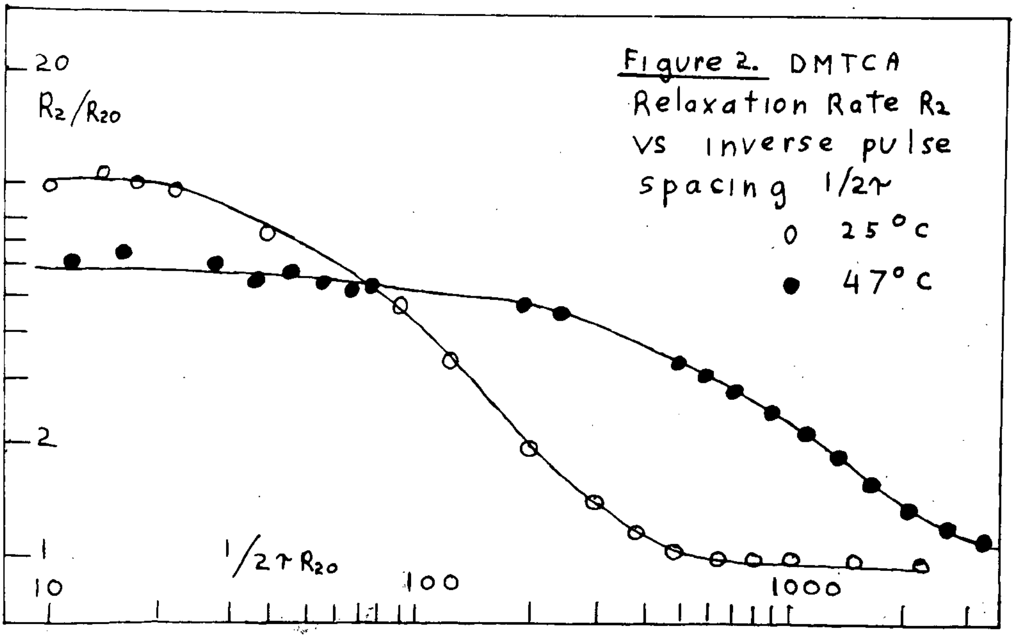

Figure 2. DMTCA Relaxation Rate R_2 vs inverse pulse spacing $1/2\tau$

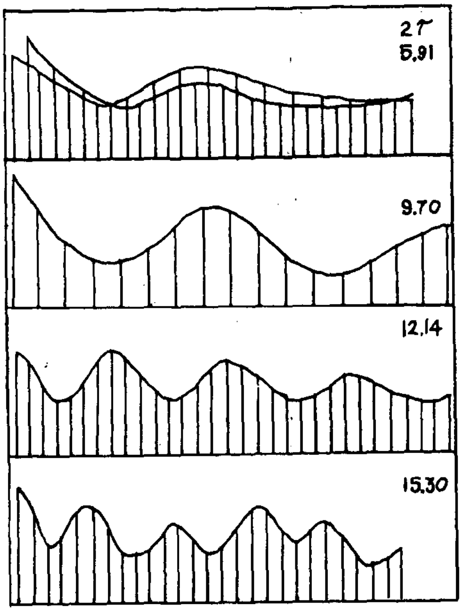

Figure 3. Fluorine spin echoes from CF_2BrCCl_2Br at -100°C and 25.27 MHz. The vertical lines represent echo amplitudes plotted on an arbitrary scale, and for each echo train the spacing between the lines is the rf pulse spacing, given in milliseconds above each echo train. The solid curves define characteristic modulation patterns for each pulse spacing.

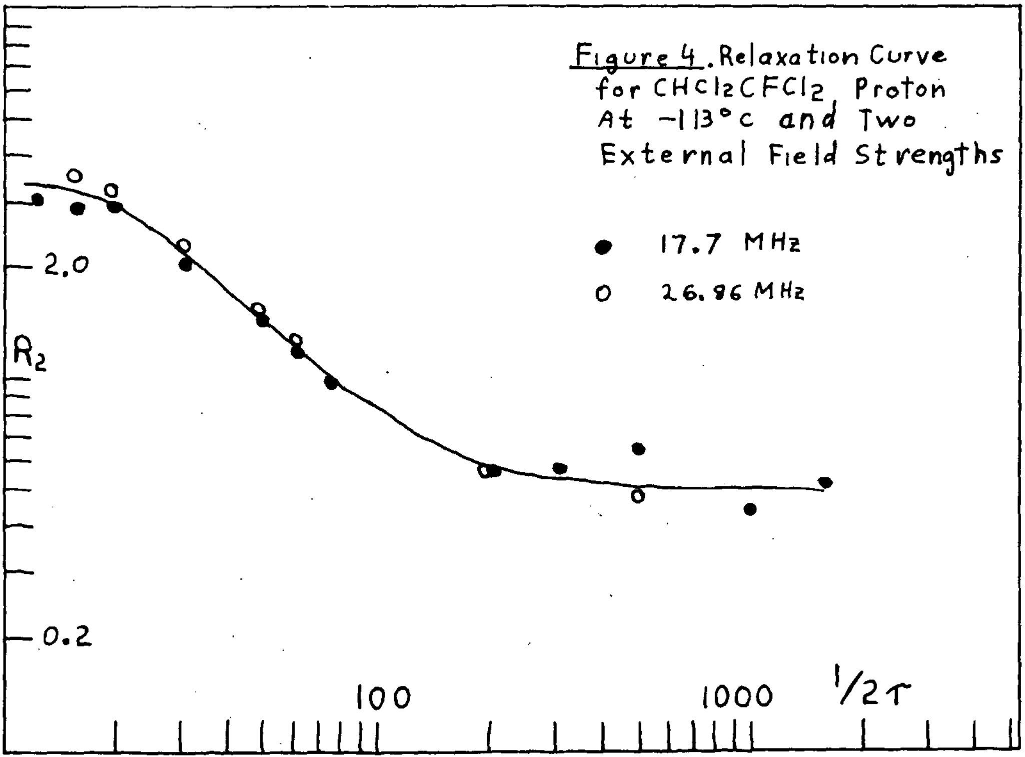

Figure 4. Relaxation Curve for $CHCl_2CFCl_2$ Proton At -113°C and Two External Field Strengths

SOME SPECTRAL OBSERVATIONS ON TWO COKING LIGNITES

R.M. Elofson and K.F. Schulz
Research Council of Alberta
Edmonton, Alberta

INTRODUCTION

Berkowitz[1] and Berkowitz and Schein[2] first drew attention to the abnormal properties of a hard black lignite from the Sharigh region of Pakistan. These properties included a low heat of wetting of about 5 Cal./g. in methanol, a low inherent moisture content of 1.7%, and caking properties corresponding to a free swelling index of 5 to 5 1/2. Since these properties occurred in a coal with a carbon content of about 75% (daf) they were considered atypical and were attributed in part to unusual tectonic conditions occurring in the early stages of the formation of the coal. These were postulated to be of such a nature as to produce the low pore volume characteristic of the British medium volatile bituminous coals. Subsequently Kreulen[3] examined another lignite from Rasa in Istria (Yugoslavia), and noted a high swelling index of 9, a low inherent moisture content, and a high sulfur content of 11.0%, again with a low carbon content of 74.8%. Kreulen drew attention to the fact that if the carbon and sulfur contents are added together the result, about 86%, is equal to the carbon content of "normal" high swelling coals.

Both of these coals, together with a number of Alberta coals, have been examined in our laboratories by means of infrared spectroscopy and electron spin resonance techniques. In the case of the lignites another property of coking coals, the formation of chloroform-soluble material upon shock heating to about 400°C[4], has also been examined. Analyses of these coals on a dry-ash-free basis are presented in Table I.

RESULTS

Infrared spectra were prepared using the potassium-bromide pellet technique and the absorption patterns for the various coals are presented in Figure 1 for the long wavelength region. These spectra show that both the Rasa and the Sharigh lignites have the three characteristic bands[5,6] near 740, 810, and 870 cm.$^{-1}$ normally associated with coals with carbon contents of greater than 85%. Moreover, the pattern is stronger for the strongly swelling Rasa coal, FSI 9, than for the Sharigh coal, FSI 5.0 - 5.5.

These three bands have been associated with out-of-plane deformation vibrations of one, two, and four adjacent aromatic CH groups respectively[7]. The absence of these absorptions in normal lignites and subbituminous coals is an indication that in these materials the aromatic lamellae are heavily substituted and crosslinked. As a result, heating does not produce plasticity and related swelling. In bituminous coals the aromatic systems are less substituted and crosslinked as indicated by the presence of the three infrared absorption bands. Heating therefore results in the development of the plasticity behavior of coking coals. In the coking lignites the presence of these bands indicates that despite their low carbon content, the aromatic lamellae are sufficiently free of crosslinking to produce a product that is thermoplastic. In other words, the various ring systems can decompose in such a manner as to produce lamellae that, upon heating, can move about relative to each other. It should be noted that these bands are strong in anthracites as well but because of the growth of the lamellae[8] the attractive forces between lamellae are too strong to allow movement so that there is no thermoplasticity.

Closely related to the aromatic substitution pattern of bituminous coals as an indication of mobile lamellae is the development of considerable chloroform-soluble material upon shock heating these coals to the vicinity of 400°C. Again, the lack of crosslinking in the bituminous coal and the resultant need to break fewer bonds to produce thermoplastic polymers is indicated. Application of this test to the Sharigh and Rasa lignites produced the results shown in Figure 2. For comparison results are also shown for a subbituminous coal (Drumheller) and for a normal coking coal (Michel). It is readily seen that the coking lignites resemble the normal coking coal and not the subbituminous coal of comparable carbon content to the lignites. The peak in the plot of chloroform extractibles for the Rasa coal is much broader and occurs at a lower temperature than those of the other coals. It is apparent that the low molecular weight thermally produced material, which presumably acts as a plasticizing agent, produced in these lignites is similar to that from normal bituminous coal. This confirms the lack of crosslinking in these lignites in agreement with the infrared results.

The e.s.r. signals of the two lignites in question and of a number of Alberta coals were measured using a Varian Model 4500 electron paramagnetic resonance spectrometer fitted with 100 KC modulation. About 10 mg. of dry coal was placed in a glass tube and evacuated to 10^{-4} mm. for 1 hour. Measurement of the e.s.r. signals produced the results shown in Table II. The number of spins observed in the coking lignites is in the lower range observed for coals of comparable carbon contents[9] and much below that observed for normal coking coals. Accurate measurements of the g-values obtained by using a dual sample cavity showed that the three higher rank coals (Luscar, Michel, and Canmore) had g-values close to 2.0031 and the three lower rank coals (Wabamun, Drumheller, and Lethbridge) had g-values of 2.0036 to 2.0037. The coking lignites again resembled the low rank coals in having high g-values. The signals for the Pakistan lignite and two of the bituminous coals are distinctive in having dual peaks, Figure 3. The weak narrow signal is reversibly suppressed by the presence of oxygen. The g-values of the narrow signals in all cases was close to 2.0030 regardless of the position of the main signal. Since signals sensitive to oxygen are characteristic of material heated to temperatures in excess of 500°C these results suggest that charred material from local heating or very severe tectonic conditions might have been the source of the narrow signals.

DISCUSSION

The infrared spectra and shock heating experiments show quite definitely that the chemical structures of the coking lignites are responsible for the swelling properties of the two coals. Basically this is because the degree of crosslinking of the aromatic lamellae as indicated by the infrared absorption bonds is quite low. Lack of polar functional groups accounts in part for the low moisture content and the so-called "liquid" structure and resulting low porosity accounts for the low heat of wetting.

The problem remains of deciding whether the lignites have these properties because of unusual starting material – both coals are high in sulfur – or because of unusual tectonic conditions or both.

The e.s.r. results which include low numbers of spins and high g-values are similar to the results for the low rank coals and in contrast to the results for the high rank coals. However, shifts in g-value of this magnitude result chiefly from atomic spin orbit coupling of atoms such as oxygen[10]. Thus the g-values of the coking lignites may be high simply because the free radicals are associated with moieties containing sulfur which cause an even larger g shift than oxygen atoms[11]. The narrow signal present in the Sharigh lignite may be indicative of severe tectonic conditions to which we know the Luscar and Michel coals were subjected.

The lack of substitution of the aromatic lamellae indicated by the infrared results suggests that breaking of weak sulfide bridges is not responsible for thermoplasticity. This is in agreement with the findings of Iyengar et.al.[12] who found no sulfide linkages in Sharigh lignite by oxidation studies. This indicates that sulfur seems to be to quite a large extent in the heterocyclic aromatic donor or quinonoid acceptor structures the interaction of which is responsible for the free radical signals[13]. This suggestion is in agreement with the finding of Kavcic of 70% of the S in Rasa coal occurring in ring structures[14].

The low number of spins in the coking lignites compared with normal bituminous coals may be a result of the sulfur content. That is sulfur may be a poorer donor compared to carbon or a weaker acceptor compared to oxygen and charge transfer complexes are as a result weaker. This point is supported by the light color of the Rasa coal.

On balance the infrared and e.s.r. evidence suggests that these lignites were subjected to fairly severe tectonic conditions. Because of the unusual constitution of the starting material, a low carbon content resulted but with the aromatic structures resembling a normal bituminous coal as revealed by the infrared evidence.

REFERENCES

1. N. Berkowitz, Fuel 29, 138 (1950).
2. N. Berkowitz and H.G. Schein, Fuel 31, 19 (1952).
3. D.J.W. Kreulen, Fuel 31, 462 (1952).
4. I.G.C. Dryden and K.S. Pankhurst, Fuel 34, 363 (1955).
5. R.R. Gordon, W.N. Adams and G.I. Jenkins, Nature 170, 317 (1952).
6. J.K. Brown and P.B. Hirsch, Nature 175, 229 (1955).
7. H.L. McMurray and V. Thornton, Anal. Chem. 24, 318 (1952).
8. P.B. Hirsch, Proc. Roy. Soc. (London), A-226, 143 (1954).
9. J. Smidt and D.W. van Krevelen, Fuel 38, 355 (1959).
10. M.S. Blois, H.W. Brown and J.E. Maling, in Free Radicals in Biological Systems by M.S. Blois et.al. Academic Press, New York, 1961, pp. 117.
11. K.F. Schulz and R.M. Elofson, presented at 49th Conference, Can. Institute of Chem., Saskatoon, June 1966.
12. M.S. Iyengar, S. Guha and M.L. Bera, Fuel 39, 235 (1960).

13. R.M. Elofson and K.F. Schulz, Amer. Chem. Soc., Div. Fuel Chem., Preprints 11 (2) 513 (1967).

14. R. Kavcic Bull. Sci. Conseil Acad. RPF, Yugoslav. 2 12 (1954) C.A. 49 5809 (1955).

TABLE I

Analyses of Coals

Coal	% - d.a.f.			
	C	H	N	S
Rasa	75.0	5.71	1.7	11.22
Sharigh	75.80	6.08	1.7	4.15
Wabamun	75.9	4.7	-	0.1
Drumheller	75.9	5.1	2.0	0.6
Lethbridge	79.7	5.6	2.5	0.9
Michel	89.1	5.2	1.4	0.4
Luscar	90.6	5.0	1.3	0.2
Canmore	91.5	4.4	1.9	0.6

TABLE II

E.S.R. Spectra of Coals

Coal	g-value (in vacuo)	spins/g. (in vacuo)	width (oersted)
Rasa	2.00395	3.8×10^{18}	6.9
Sharigh	2.00381 Broad 2.00288 Narrow	4.3×10^{18} 4×10^{16}	7.9 1.0
Wabamun	2.00372	1.1×10^{19}	7.1
Drumheller	2.00360	7.5×10^{18}	6.3
Lethbridge	2.00370	1.8×10^{19}	7.5
Michel	2.00304 Broad 2.00285 Narrow	1.5×10^{19} 2.2×10^{17}	6.5 0.8
Luscar	2.00310 Broad 2.00310 Narrow	1.1×10^{19} 2.4×10^{17}	4.7 0.5
Canmore	2.00317	1.6×10^{19}	4.7

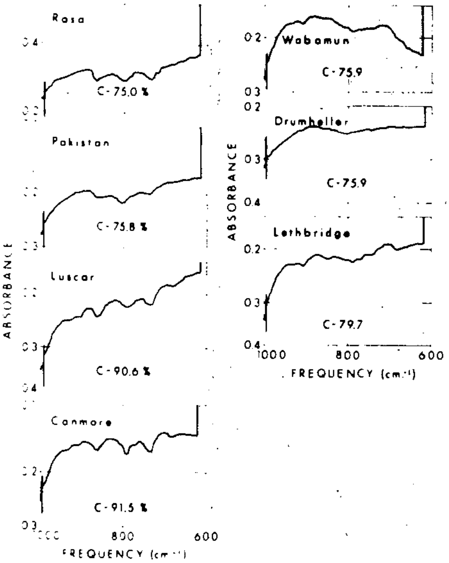

Fig. 1. Infrared spectra of coals in the region of 1000 - 600 cm.$^{-1}$ (0.2% in KBr).

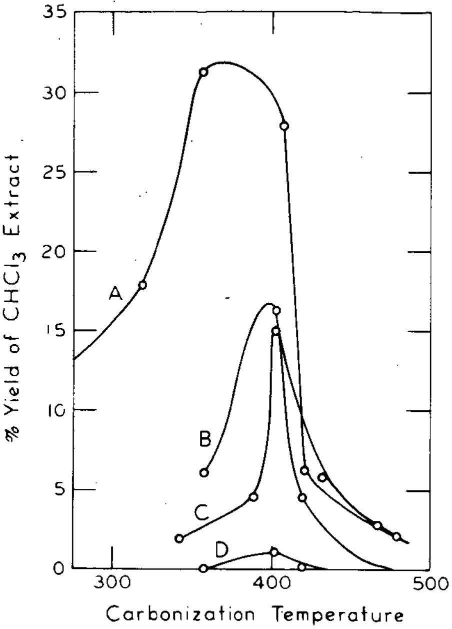

Fig. 2. Yield of chloroform - soluble material as a function of temperature of shock heating of coal.
(A) Rasa; (B) Sharigh; (C) Michel, B.C.; (D) Drumheller, Alberta.

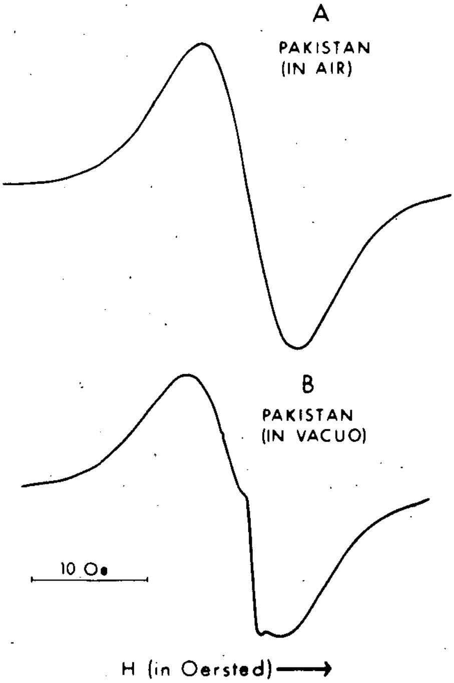

Fig. 3. Electron spin resonance spectra of Sharigh lignite.
(A) spectrum from the sample in air;
(B) spectrum from the sample in vacuo.

ELECTRON SPIN RESONANCE OF PETROLEUM ASPHALTICS

By

Teh Fu Yen, Edmund C. Tynan and George B. Vaughan
Mellon Institute, Pittsburgh, Pa. 15213

and

Laurence J. Boucher
Chemistry Department, Carnegie Institute of Technology

Introduction

A considerable body of information about the Electron Spin Resonance (ESR) properties of petroleum asphaltenes has developed during the past few years. Among the basic parameters obtained by ESR measurements are N_g, the number of unpaired spins per gram of material; $|A|$, the electron-nuclear spin coupling constant; and g, the effective Landé g-factor for the unpaired electron spins. A review of what is already known, and the addition of new data may both clarify the present state of understanding of asphaltene ESR and stimulate further research in this area. The ESR studies briefly considered here may be divided into two parts: (1) measurements of the free radical absorption, and (2) measurements of the ESR absorptions due to naturally occurring vanadium and synthetic vanadium chelates.

Nature of Free Radical

The asphaltic fraction of petroleum has been found to yield a single ESR resonance near a g-value of 2.00(1,2,3). For most asphaltics the line shape is between Lorentzian and Gaussian. The inhomogeneous broadening characteristics indicate that, in addition to dipolar interactions, the magnetic electron interacts with hydrogen or other nuclei to produce multiplet line structures. The apparent absence of fine structures in the radical absorption appears to be the result of a superposition of many such multiplets. The g-values of most asphaltics fall in the narrow range of 2.0027-2.0036. The differences between measured g-values and the g-value of a free electron (g_e), $|g - g_e|$, are shown in Fig. 1 for six native asphaltenes and a variety of other types of free radicals. It may be deduced that the unpaired spins in asphaltene do not appear to belong to the semiquinone or the radical ion families. However, they are close to neutral radicals, in contrast to the radicals in coals and L-forms of carbons which are semiquinones(1).

Intensity measurements are usually troublesome, but when properly done with suitable modulation amplitude and correct power levels (not causing saturation), the spin concentration, N_g, can be used as a basis for differentiating or classifying different asphaltic samples. Figure 2 displays the N_g data for 11 native asphaltenes from different sources: 2 native gilsonite asphaltenes, 3 refinery asphaltenes, 5 heat-treated asphaltenes(4), 3 carbenes, 4 cokes and one lithium-reduced asphaltene. Aromaticity, f_a, as obtained from x-ray analysis(5) for these materials is apparently linearly related to log N_g. These data indicate that the free radical sites of these materials are associated with the aromatic moities of the asphaltic skeleton. Present findings confirm the previous observation(1) that different families of carbonaceous substances, e.g., asphaltenes, resins(6), coals, and carbons, show a characteristic slope and intercept when their f_a values are plotted against log N_g.

No effects on N_g were observed due to the action of light, oxygen or solvents; however, these factors do affect the spin-lattice relaxation time(7). The free radical species of asphaltics are stable, in contrast to coal hydrogenation asphaltene(8). Further, it was found(1) that the color intensity of asphaltics, i.e., the integrated intensity obtained by absorption spectrometry over the 600-800 mμ region also increases with the ESR intensity (Fig. 3). These data indicate that the free radical is stabilized by the resonance of the delocalized π-system in the asphaltic structure.

Vanadium Unpaired Spin

Most asphaltics contain vanadium in concentrations ranging from 6000 to less than 1 ppm. Common valence states of vanadium are +2, +3, +4, and +5. The +5 state is diamagnetic. The +3 state, although paramagnetic, is usually not observable by ESR due to internal electric field effects. Both the +2 and the +4 states can, however, be detected at room temperature. In contrast to oxovanadium (IV), V^{+2} is unstable and easily oxidized. The +4 state requires a non-cubic field for ESR observability, and this is fulfilled by the oxovanadium (IV) VO^{+2} type complexes(9). The vanadium 51 nucleus (~100% abundance) has a nuclear spin 7/2, and so a magnetic electron coupled to it can exhibit an absorption spectrum of either 8 symmetric lines (isotropic case), or 8 unsymmetric lines (anisotropic case: 8 parallel and 8 perpendicular features in the first derivative of the spectrum).

For native asphaltenes in general a 16-feature anisotropic spectrum has been observed for this d^1 system in either solid form or in solution in non-polar organic solvents (Fig. 4). Assignment of the absorption lines is in general agreement with the assignment for the axial symmetry case as described previously by O'Reilly(10). The line positions have been carefully examined in a second derivative format(11), and with multi-amplitude recordings (Fig. 5). The line positions of the vanadium resonance for nine different asphaltenes have recently been measured and are shown in Fig. 6. When compared with a sample of vanadyl etioporphyrin I, whose line positions are also shown in Fig. 6, a number of additional lines are observed for the asphaltenes. Whether the additional lines represent other paramagnetic species or other structural environments for the vanadium in the asphaltene samples is still unknown. However, such a difference is useful in qualitatively differentiating asphaltenes from different sources.

Another empirical criterion for differentiating among asphaltenes is obtained by measuring the spacings of the $g_{\parallel}$ features: $2_{\parallel} - 1_{\parallel}$ and $8_{\parallel} - 7_{\parallel}$. Tentatively, two parameters can be derived (Table I); one is the $A_{\parallel}$ value which is the average spacing of the parallel features, and the other is the difference of the spacings, Δ, representing a second-order effect arising because of the dependence of the spectrum on the strength of the external magnetic field. The real meaning of the latter quantity has not yet been fully explored, but it is thought to represent deviations from axial symmetry. It appears that all asphaltenes studied here have axial symmetry except for the samples from Bachaquero (CY), Baxterville (GS), and Wafra A-1. Since both the $A_{\parallel}$ and Δ values of Bachaquero (CY) asphaltene differ from those of Wafra A-1 asphaltene, it might be expected that there would be a structural difference between the two asphaltenes. Analysis of the anisotropic spectrum of the asphltenes to yield complete values of $g_{\perp}$, $g_{\parallel}$ and $A_{\perp}$, $A_{\parallel}$ is hindered by overlapping line structures and the difficulty of converting the spectrum into an isotropic one.

Conversion of an anisotropic spectrum ("bound") of the vanadium in asphaltene into an isotropic spectrum ("free") can be effected by dissolving the asphaltenes in a polar solvent such as benzyl n-butyl ether, tetrahydrofuran or diphenylmethane and heating at an elevated temperature(12). Such a conversion is reversible. From the relative intensities of the isotropic and anisotropic spectra taken at different temperatures, the disassociation energy can be obtained. For a given asphaltene, identical energy values have been observed regardless of the solvent system. The energy values of three asphaltenes are given in Table II. These results suggest that the observed "bound" vanadium is associated with the asphaltene molecule, probably with the aromatic portion. The fact that this "associated" or "bound" type of vanadium becomes disassociated is further supported by dilution studies in a given solvent system. In dilute solutions (~0.4 Wt. %) a nearly isotropic "free" type of spectrum was observed. In solvents with differing basicities the vanadium-containing asphaltene usually shows some indications, though small, of the isotropic vanadium ESR absorptions even at room temperature. The relative effectiveness of solvents for producing the "free" vanadium species may be ranked as follows: diphenylmethane < benzyl n-butylether < 1-ethylnaphthalene < benzene < nitrobenzene < pyridine < tetrahydrofuran.

Nitrogen Superhyperfine Splittings (s.h.f.)

The literature indicates no nitrogen s.h.f. for the oxovanadium (IV) in a quadridentate nitrogen ligand except for the case of vanadyl tetraphenylporphin in chloroform or carbon disulfide "glass" reported by Lee(13). We have been able to observe nitrogen s.h.f. for vanadyl phthalocyanine doped at a concentration of 2000 ppm into either a condensation polymer of anthracene or of phenanthrene, or a gilsonite asphaltene (natural vanadium content < 1 ppm). Figure 7 shows the 9-line pattern of nitrogen s.h.f. structures superimposed on the vanadium No. $4_\perp$ line for vanadyl phthalocyanine doped into a polymer made from anthracene and formaldehyde. For four equivalent nitrogen nuclei the relative intensities of the nine lines are expected to be 1, 4, 10, 16, 19, 16, 10, 4, 1. The intensity distribution patterns of the nitrogen lines for vanadyl phthalocyanine either in anthracene polymer or in the gilsonite asphaltene drop off rapidly for the outer nitrogen lines, but in general retain the bell shape. However, when 2000 ppm vanadium in the form of vanadyl etioporphyrin I was doped into gilsonite asphaltene or an aromatic medium such as perylene, there were no nitrogen s.h.f. structures observed. On the other hand, there is indication that there may be nitrogen splittings in the petroporphyrins (vanadium) of native asphaltene. The repeated scan of the No. $2_\perp$ region in a second derivative format for Bachaquero (VX) asphaltene is given in Fig. 8. In addition to the line shown, fine structure suggestive of nitrogen lines appears in the overlapping region of the Nos. $4_\perp$ and $4_{\parallel}$ features. Typical poorly resolved nitrogen lines superimposed on a vanadium line are illustrated in Fig. 9. The coupling constant observed for both the vanadyl phthalocyanine and petroporphyrin (vanadium) is $A_\perp^N = 2.6$ G. This value agrees with the nitrogen splitting observed for the vanadyl tetraphenylporphin in chloroform or carbon disulfide, $A_{\parallel}^N \simeq 2.9$ G., $A_\perp^N \simeq 2.8$ G.(13). Roberts, Koski and Caughey(14) attribute the appearance of the nitrogen s.h.f. to a configuration interaction rather than to covalent bonding. At present it seems that the added aromaticity in the macrocycle does possibly bring out the nitrogen s.h.f. It may be that the π-electron system provides excitation for configuration interaction. The slight nitrogen s.h.f. found in asphaltene may indicate that there are minor constituents of the macrocycles in the form of benz-substituted porphins. Such structures have been demonstrated by mass spectrometry to be present in asphaltenes, e.g., the proposed β,β-benzoporphin(15).

Models for Non-porphyrin Vanadium

"Non-porphyrin" is used here to indicate any quadridentate macrocycle which does not belong to the alkyl- or cycloalkano-porphins (Etio and DPEP series), e.g., the rhodoporphyrin(15,16), mixed quaterenes, etc. Two classes of non-porphyrin vanadium were synthesized and characterized by ESR. The first class is vanadyl complexes of the meso-aromatic ring-substituted porphins. This series consists of vanadyl complexes of tetraphenylporphyrin (TPP), tetra-1-naphthylporphin (T1NP), and tetra-4-biphenylporphin (T4BP). The anisotropic scans of the vanadyl derivative of T1NP and T4BP are similar to that of vanadyl TPP. Each of these compounds is a 4 nitrogen ligand system.

The second class is the vanadyl complexes of β-ketoimines, i.e., quadridentate having 2 nitrogen and 2 oxygen donor atoms. This series consists of vanadyl complexes of bisacetylacetone-ethylenediimine (Acen), bisacetylacetonepropylenediimine (Acpn), bisbenzoylacetone-ethylenediimine (Bzen) and bisbenzoylacetonepropylenediimine (Bzpn). The g-values and vanadium nuclear coupling constants for some of the non-porphyrin vanadium model compounds are tabulated in Table III. One of the qualitative features of the vanadium spectra of β-ketoimines is that the Nos. $4_{\perp}$ and $4_{\parallel}$ lines are resolved in contrast to the case of etioporphyrin I.

A plot of A_o vs. g_o (the isotropic coupling constant and g-value respectively) for a variety of vanadyl square-planar complexes, both porphyrin and non-porphyrin, is useful to characterize the particular types of ligands (Fig. 10). Samples at the upper left are those containing ligands which delocalize the unpaired vanadium spins, and these are characterized by low A_o value and a g_o value approaching that of the free electron, $g_e = 2.0023$. Samples at the lower right corner usually have ligands of an electronegative nature, and these are characterized by high A_o values and low g_o values. The average values from the resulting three groups of vanadyl complexes are shown from left to right as: 4 nitrogen type (porphins), 2 nitrogen, 2 oxygen type (β-ketoimines), and the 4 oxygen type (acetylacetonates). It can be predicted that the 3 nitrogen, 1 oxygen type and the 1 nitrogen, 3 oxygen type ligands will also fall into the nearly straight line relationship. The data for asphaltenes (Bachaquero, VX; Boscan, VY) included in the plot were obtained from a polar solution at elevated temperatures. The relative location of these two points falls in the region typical of the 4 nitrogen donor system. It is hoped that by using this plot non-porphyrin types of vanadium chelates contained in asphaltenes may be readily identified.

ACKNOWLEDGMENT

This work was sponsored by Gulf Research & Development Company as part of the research program of the Multiple Fellowship on Petroleum.

REFERENCES

(1) T. F. Yen, J. G. Erdman, and A. J. Saraceno, Anal. Chem., 34, 694 (1962).

(2) T. F. Yen, J. G. Erdman, and A. J. Saraceno, Bitumen, Terre, Asphalte, Peche, 15, 141 (1964).

(3) J. Q. Adams, K. H. Altgelt, R. L. LeTourneau, and L. P. Lindeman, ACS, Div. Petroleum Chem., Preprints, 11 (2) B140 (1966).

(4) J. G. Erdman, and J. P. Dickie, ACS, Div. Petroleum Chem., Preprints, 9 (2) B69 (1964).

(5) T. F. Yen, and J. G. Erdman, in "Encyclopedia of X-Rays and Gamma Rays" (G. L. Clark, Ed.), Reinhold Publishing Company, New York, 1963, pp. 65-68.

(6) R. A. Gardner, H. F. Hardman, A. L. Jones, and R. B. Williams, J. Chem. Eng. Data, 4, 155 (1959). In this reference, the term "petrolene" is used rather than resin. These petroleum fractions were thermal diffusion cuts, prepared by Gardner and coworkers from the pentane soluble fraction of an 85 to 100 penetration asphalt derived from a blend of Illinois and Oklahoma crudes by oxidation of a 200 penetration vacuum distillation residuum.

(7) A. J. Saraceno and N. D. Coggeshall, J. Chem. Phys., 34, 260 (1961).

(8) R. A. Friedel, J. Chem. Phys., 31, 280 (1959).

(9) A. J. Saraceno, D. T. Fanale, and N. D. Coggeshall, Anal. Chem., 33, 500 (1961).

(10) D. E. O'Reilly, J. Chem. Phys., 29, 1188 (1958).

(11) C. L. Wolfe, E. C. Tynan, and T. F. Yen, Pittsburgh Conference on Analytical Chemistry and Applied Spectroscopy, Paper No. 54, March, 1967.

(12) E. C. Tynan, and T. F. Yen, ACS, Div. Petroleum Chem., Preprints, 12 (2) A89 (1967).

(13) S. K. Lee, M. S. Thesis, UCLA (1964); cf. D. Kivelson and S. K. Lee, J. Chem. Phys., 41, 1896 (1964).

(14) E. M. Roberts, W. S. Koski, and W. S. Caughey, J. Chem. Phys., 34, 591 (1961).

(15) E. W. Baker, T. F. Yen, J. P. Dickie, R. E. Rhodes, and L. F. Clark, J. Am. Chem. Soc., 87, July 5 issue (1967).

(16) M. F. Millson, D. S. Montgomery, and S. R. Brown, Geochim. Cosmochim. Acta, 30, 207 (1966).

(17) L. J. Boucher, E. C. Tynan, and T. F. Yen, to be published.

TABLE I

Empirical Parameters from Anisotropic Spectra

Petroporphyrin Sample	$A_{\parallel}$ (G)	Δ' (G)
Boscan (SR)*, Venezuela	176	4.6
Boscan (VY)*, Venezuela	172	4.0
Baxterville, Mississippi	171	-2.6
Taparito, Venezuela	172	3.6
Bachaquero (CY)**, Venezuela	170	0
Wafra A-1, Neutral Zone	179	12
Wafra 17, Neutral Zone	174	3.1
Bachaquero (VX)**, Venezuela	173	2.1
Mara, Venezuela	172	4.6
VO Etio I (castor oil)	175	11
VO Etio I (in gilsonite)	171	6.7
VO Etio I (toluene)	175	9.3
VO Acac (in gilsonite)	188	0.5
VO Acen (THF)	183	14
VO Bzpn (THF)	179	8.8
VO Bzpn (toluene)	181	8.3

---

* Boscan (SR) collected in 1959; Boscan (VY) collected in 1962 upper and lower Boscan sand.

** Bachaquero (CY), Maracaibo; Bachaquero (VX), Well Largo.

TABLE II

Activation Energy of Association for Vanadium in Asphaltenes

Asphaltene	V Content (ppm)	Dissociation Energy (kcal)
Bachaquero (VX)	2700	14.3
Boscan (VY)	4700	10.0
Gilsonite (CB) doped*	2700	10.4

* with vanadyl etioporphyrin I.

TABLE III

Vanadium Nuclear Hyperfine Splittings and g-Values for Non-porphyrin Model Compounds

Vanadyl Complex*	A_o**	g_o	$A_{\parallel}$**	$A_{\perp}$**	$g_{\parallel}$	$g_{\perp}$
Acen	101.7	1.974	182.5	61.3	1.957	1.982
Acpn	102.5	1.974	183.8	60.4	1.945	1.999
Bzen	102.4	1.975	183.3	62.0	1.952	1.986
Bzpn	103.4	1.975	182.5	63.9	1.953	1.986

* in THF.

** in Gauss.

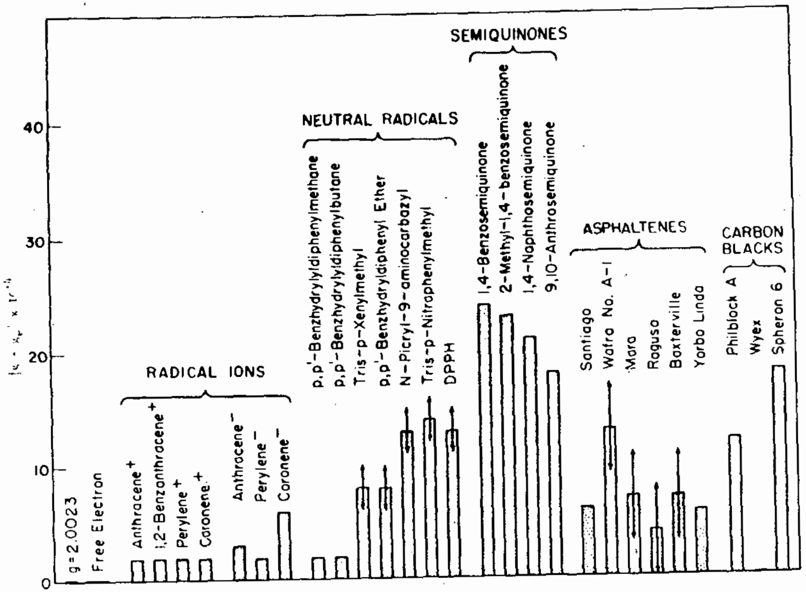

FIGURE 1: Landé g-Values of Petroleum Asphaltenes and Other Radical-Containing Substances.

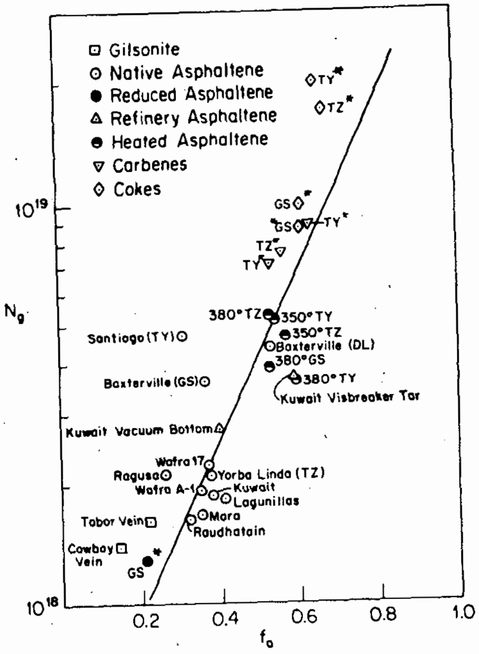

FIGURE 2: Dependence of Spin Concentration on Aromaticity.

(* A fraction from the corresponding asphaltene.)

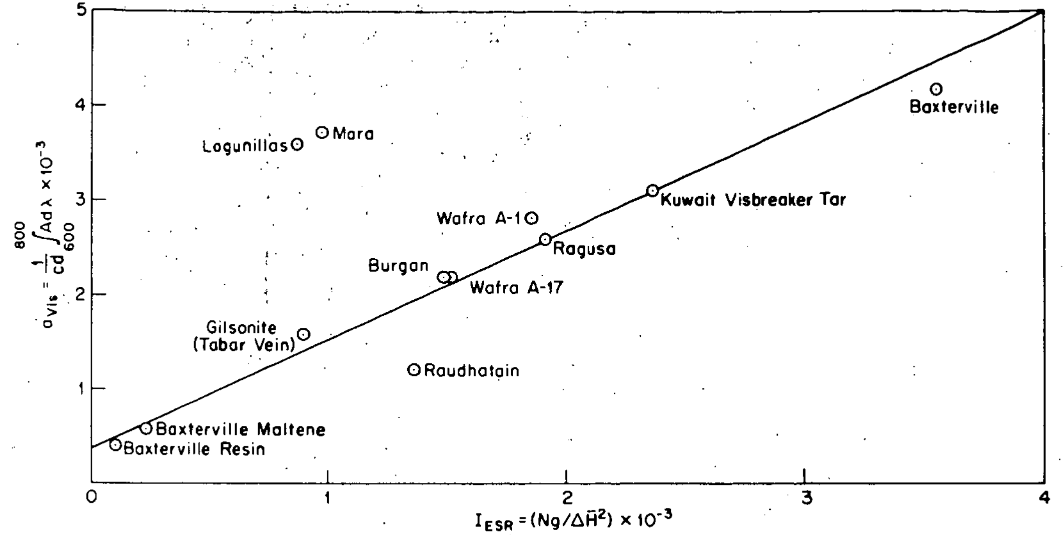

FIGURE 3: Integrated Visible Spectral Absorptivity vs. ESR Free Radical Absorption Intensity.

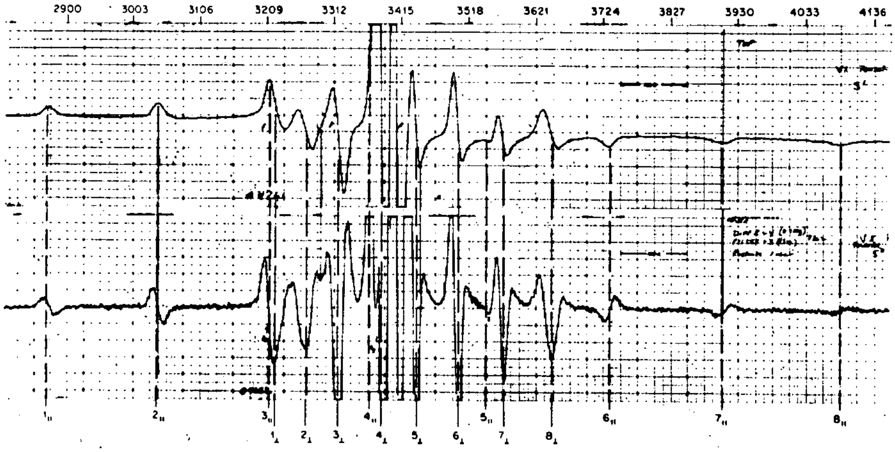

FIGURE 4: Vanadium Anisotropic Spectra of a Bachaquero (VX) Asphaltene
(Upper, First Derivative Format; Lower, Second Derivative Format).

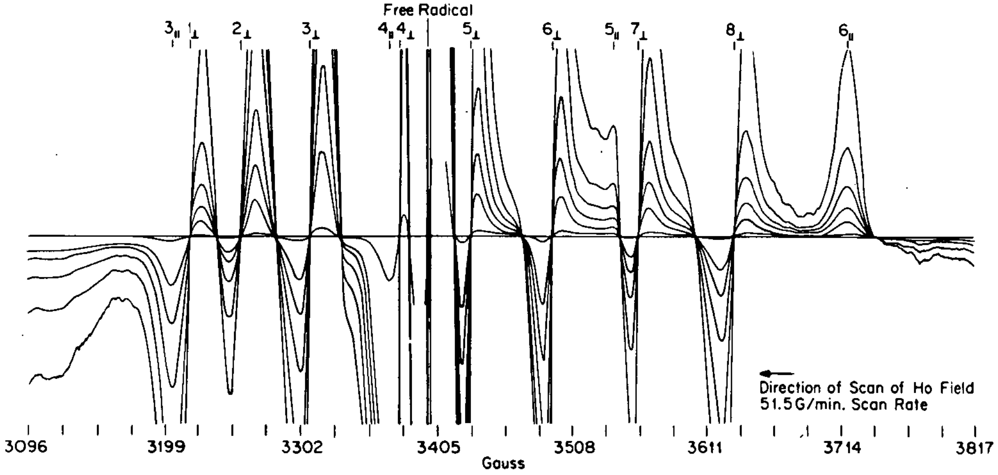

FIGURE 5: Central Portion of an Anisotropic Vanadium Spectrum from a Multi-amplitude Recording

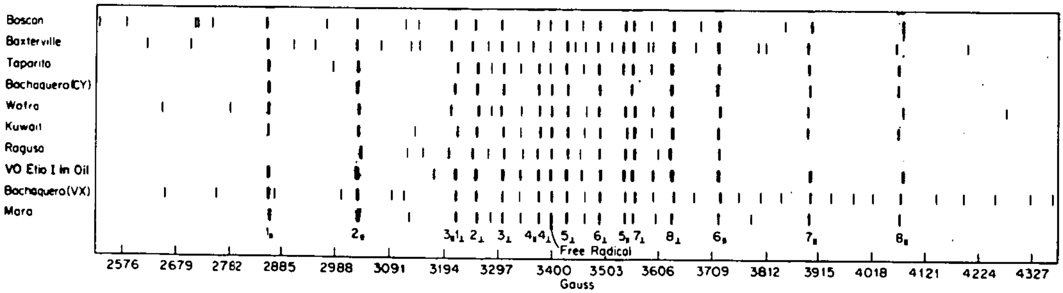

FIGURE 6: Field Positions of ESR Spectra of Native Asphaltenes

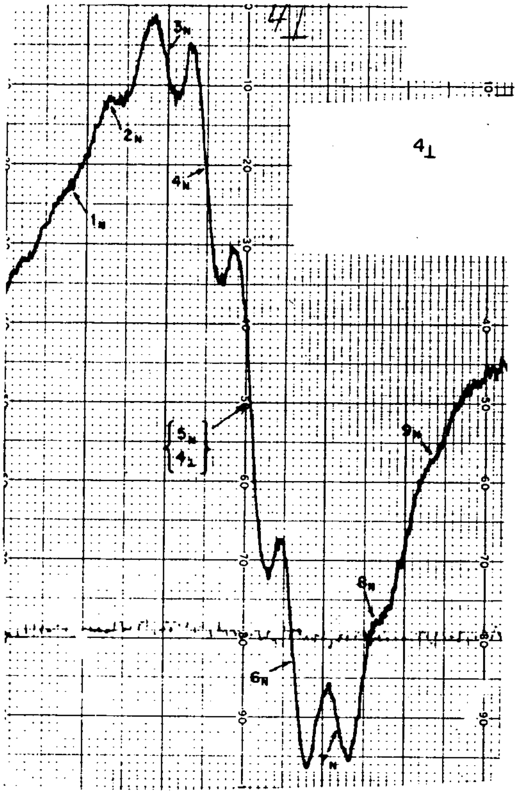

FIGURE 7: Nitrogen s.h.f. Structures of Vanadyl Phthalocyanine-Doped Anthracene Polymer

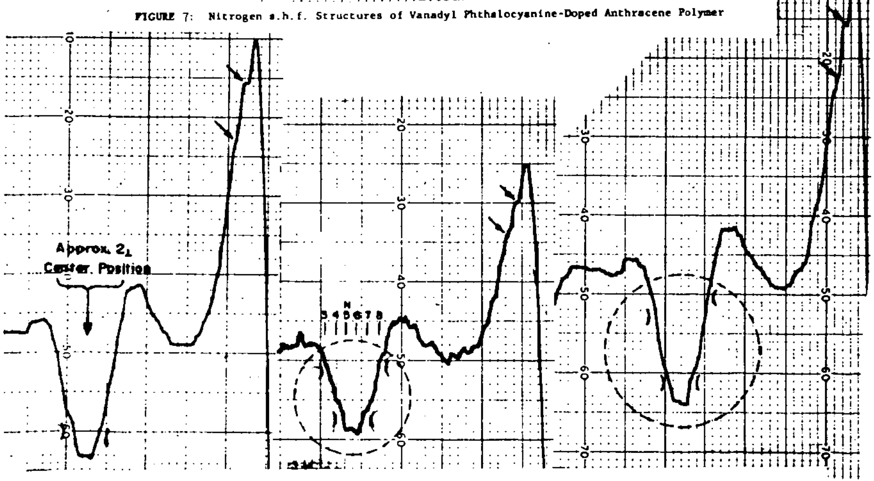

FIGURE 8: Repeated Scans of the No. $2_\perp$ Region of a Bachaquero (VX) Asphaltene (Poorly Resolved Nitrogen Lines).

FIGURE 3: Nitrogen s.h.f. Lines Superimposed on Vanadium Lines (Typical Case).

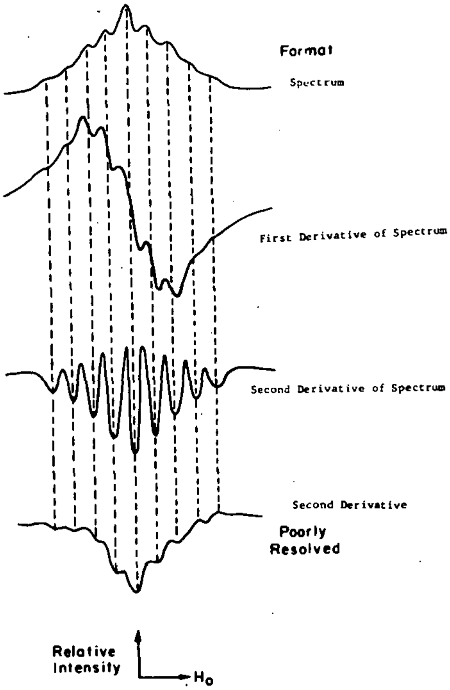

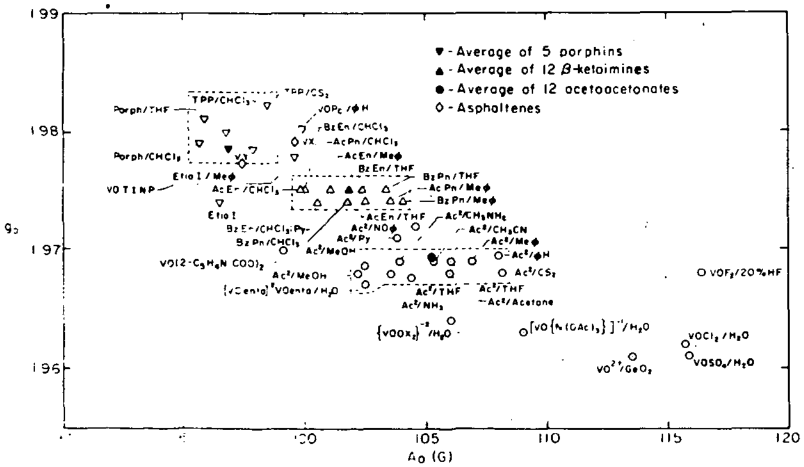

FIGURE 1 : Relationship Between g_o and A_o for a Series of Vanadyl Ligands

Application of Luminescence Spectroscopy to the Analysis of Fuels

Harold F. Smith

Perkin-Elmer Corporation, Norwalk, Connecticut

Luminescence spectroscopy is based on the absorption and reemission of light by a molecule, ion or atom. It is of great analytical utility because the emitted light is characteristic of the electronic structure of the emitting species. The phenomenon of luminescence is not a newly discovered one. The first monograph on luminescence was written by Liceti[1] in 1640. In 1845 Herschel[2] reported on the luminescence characteristics of quinine sulfate. Stokes[3] in 1852 observed that in all cases the light emitted from a molecule was at longer wavelengths than that which it absorbed. His observation was termed the "Stokes shift" and has since become well understood. In 1895 Weidman and Schmidt[4] and in 1907 Stark and Mayer[5] reported the first systematic study on luminescence of aromatic molecules.

Lommel[6] in 1877 first reported on the quantum efficiencies of certain molecules, and in 1907 Nichols and Merritt[7] discussed their observations of the interesting "mirror image" relationship between absorption and emission spectra. From the preceding observation it is apparent that the luminescence properties of molecules have been known for a long time. The successful exploitation of luminescence had to wait, however, until other areas of technology were sufficiently advanced to permit the observation and measurement in a controlled and quantitative manner.

That fluorescence and phosphorescence techniques are being accepted rapidly in all areas of analytical chemistry is emphasized by referring to the 1964 and 1966 Analytical Chemistry Annual Reviews[8,9] covering the four-year period from December 1961 to December 1965, in which 1,049 references to a large variety of analytical applications of fluorescence and phosphorescence are contained.

Before proceeding into the discussion of specific applications of fluorescence and phosphorescence, the relationship of these phenomenon to each other and the absorption process should be shown (Fig. 1).

In both fluorescence and phosphorescence spectroscopy one may determine two different kinds of spectra (Fig. 2). The difference between these two spectra is that the emission spectrum is obtained by spectrally recording the light emitted from a sample while being excited by some selected wavelength of light. An excitation spectrum on the other hand is obtained by measuring the intensity of emitted radiation from a sample at a specific wavelength as the excitation light is varied continuously.

For example, Figure 3, the absorption spectrum of a 1 ppm anthracene solution, and Figure 4, the excitation and emission spectra of the same sample, show great structural similarity. The emission bands are all at longer wavelength than the absorption band, but the excitation bands fall at exactly the same wavelength as the absorption bands. A significant point is that the excitation spectrum of a molecule gives the same information as its absorption spectrum.

troscopy in fuels analysis is the method for qualitatively and quantitatively determining anthracene and napthalene at low concentrations in a benzene-type matrix. The three aromatic types represent the majority of aromatic molecules in fuels.

Experimental

All standard samples were prepared using reagent grade anthracene and naphthalene after recrystallization from a saturated hydrocarbon. The matrix was made from a 50/50 volume/volume mixture of toluene and o-xylene, spectroquality from Matheson, Coleman and Bell.

The spectra were run on a Hitachi-Perkin-Elmer MPF-2A Fluorescence Spectrophotometer. High quality, low-fluorescence, silica sample cells were used for obtaining the data.

Discussion of Results

A sample containing 10 ppm naphthalene and 10 ppm anthracene in the matrix was prepared and the qualitative emission spectra of the sample determined at several excitation wavelengths. Figure 5 shows the emission spectra obtained from the sample excited at 270mμ and at 280mμ. The principal emission, Spectrum A, is observed in the region between 360 and 440mμ, with a low intensity emission band in the 300 to 340mμ range. The emission between 380 and 440mμ arises from the anthracene whereas that in the 300 to 340mμ region arises from the naphthalene. Spectrum B in this figure was taken from the sample without removing it from the instrument. The only change was the excitation wavelength from 270 to 280mμ. Some rather dramatic changes in the spectrum are evident. The overall intensity of both band systems has been increased greatly and the ratio of the naphthalene to anthracene emission has completely reversed. It is apparent from this spectrum that one could easily determine the concentration of each of these components independently of the other in this aromatic matrix. One cannot do such an analysis by absorption spectroscopy.

The spectrum shown in Figure 6 was from the sample excited at 290mμ. In this case the naphthalene intensity continued to increase sharply, whereas the anthracene decreased. The spectra shown in Figure 7 show the anthracene intensity increasing and the naphthalene intensity fading. The Spectrum A was produced by exciting the sample at 300mμ whereas Spectrum B was produced by the 310mμ excitation.

The series of spectra shown in Figure 8 were run while exciting with 320, 330 and 340mμ excitation respectively and in these spectra all evidence of naphthalene presence was lost. The significance of the behaviour noted in Figures 6, 7 and 8 is that one can take a mixture of aromatic hydrocarbons and produce different spectra dependent on the wavelength of excitation. By choosing the appropriate excitation wavelengths, one can emphasize the presence of one component relative to the others and in many cases completely eliminate the appearance of any component other than the one of specific interest.

Our next point of concern was ability to selectively excite the three aromatic types, benzene, naphthalene and anthracene, individually. For this experiment the sample containing 10 ppm naphthalene and 10 ppm anthracene in the o-xylene-toluene matrix was diluted 1:100 with isooctane giving concentrations of 0.1 ppm naphthalene, 0.1 ppm anthracene and 1% o-xylene-toluene. The series of three spectra shown in Figures 9, 10 and 11 were obtained by exciting this solution with 20, 290 and 350mμ radiation respectively. Figure 9 shows the emission spectrum of the benzene-type aromatics. Figure 10 is that of naphthalene and Figure 11 is that of anthracene. One not only can qualitatively identify these three aromatic types, but can determine their approximate concentration by simply altering the excitation wavelength and measuring the emission from each aromatic type independently of the others.

While the data shown in the preceding discussion indicate the qualitative applicability of luminescence spectroscopy to the basic types of aromatic molecules found in petroleum and coal based fuels, it does not provide an insight into the usefulness of the technique for quantitative analysis. Hercules[10] has shown that luminescence intensity and concentration are related as follows:

$$S(F)_\lambda = f(\Theta)\,g(\lambda)\,I_o\,\phi_f\,abc\left[1 - \frac{abc}{2!} + \frac{\overline{abc}^{2}}{3!} - \cdots \frac{\overline{abc}^{n}}{(n+1)!}\right.$$

Where abc are the molar absorptivity, cell path and concentration respectively; $f(\Theta)$ is the solid angle of interception of radiation by the detector; $g_{(\lambda)}$ is the quantum conversion factor for the detector which is a function of wavelength; I_o is the intensity of the exciting radiation and 0_f is the quantum efficiency of the molecule. There are two concentration regions where this arrangement may be greatly simplified. The one of greatest interest to the analytical chemist is the one in which the concentration of fluorescent materials is small. In such case abc 0.05. This allows us to write Equation 1 as

$$(S_F)_\lambda = f(\Theta)\,g(\lambda)\,I_o\,\phi_f\,abc$$

From this equation it may be seen that the relationship between fluorescence intensity and concentration will be linear through a point of maximum concentration, $C_{max} = \frac{0.05}{(a)_\lambda b}$, where $(a)_\lambda$ is the molar absorptivity of the compound at the wavelength of excitation. It should be emphasized that this concentration is not the maximum at which useful data may be obtained. Beyond this level the curve relating fluorescence intensity to concentration is not linear. A calibration curve relating concentration to fluorescence intensity can be used to extend the range of useful analysis over at least another order of magnitude.

The other extreme condition where equation one may be simplified is that of very high concentration of absorbing and emitting molecules such that the absorption of incident radiation is almost complete. In that case, equation one may be reduced to

$$(S_F)_\lambda = f(\Theta)\,g(\lambda)\,\phi_f$$

showing that the detector signal is independent of fluorescer concentration. This condition is important in determining quantum efficiencies for quantum counters and scintillation counters. Analysis under these conditions is most effectively done by using front surface illumination and viewing of the sample. With this geometry, penetration effects and self-absorption problems are minimized. This geometry is generally required when the fluorescence or phosphorescence spectrum of a solid, opaque or highly turbid sample is analysed. Using the front surface viewing geometry even raw crude oil samples may be excited and their luminescence observed.

As indicated by the terms in Equation (1) there is an intermediate concentration range for each absorber and fluorescer at which the intensity concentration relationship will become nonlinear. One generally observes that the fluorescence intensity approaches a limiting value as the concentration is increased. The principal precaution, therefore, in using luminescence techniques for quantitative analysis is to realize that there is a range above which the concentration intensity curve will become nonlinear, and if it is required to work in the nonlinear region, a sufficient number of standard points be taken to accurately describe the intensity concentration curve.

Curves showing the intensity concentration relationship for naphthalene and anthracene in Figures 12 and 13. The naphthalene standards were prepared in o-xylene-toluene matrix. Each contained 10 ppm anthracene. The anthracene standards were prepared in the same matrix and each contained 10 ppm of naphthalene. The curves are practically linear in the lower concentration range, but begin to deviate from linearity at the higher end of the range.

In order for a measurement technique to be useful for quantitative analysis, stability of the measurement system must be such that good repeatability is possible. Unfortunately, the feeling exists that fluorescence measurement is imprecise. Admittedly, this has been true in many cases but it was an equipment rather than a technique limitation. Figure 14 shows an example of excellent repeatability. The three spectra of a 10 ppb anthracene sample are superimposed. One would be hard pressed to show better repeatability by any other analytical technique.

Summary

Luminescence spectroscopy has broad application in the analysis of fuels and related products. All aromatic types are subject to analysis by fluorescence or phosphorescence. It is possible by using the incremental excitation technique to obtain spectra of each aromatic type completely independent of the others present and, therefore, more effectively analyze for components of mixtures.

application in the analysis
types are subject to
It is possible by using
to obtain spectra of each aromatic
others present and, therefore, more
for components of mixtures.

Bibliography

1. I. B. Berlman, "Handbook of Fluorescence Spectra of Aromatic Molecules" p. 2, Academic Press, New York, 1965.
2. J. Herschel, Phil. Trans. Roy. Soc. (London) 135, 143 (1845).
3. G. G. Stokes, Phil. Trans. Roy. Soc. (London) 142, 463 (1852).
4. E. Wiedeman and G. C. Schmidt, Ann. Physik., 56, 18 (1895).
5. J. Stark and R. Meyer, Physik. Z. 8,250 (1907).
6. E. Lommel, Pogg. Ann. 160, 75 (1877).
7. E. L. Nichols and E. Merrit, Phys. Rev. 31, 376 (1910).
8. C. E. White, Analytical Chemistry Annual Reviews, Part One, 116R, 1964.
9. C. E. White, Analytical Chemistry Annual Reviews, 155R, 1966.
10. D. M. Hercules, Analytical Chemistry, 38, 29A, 1966.

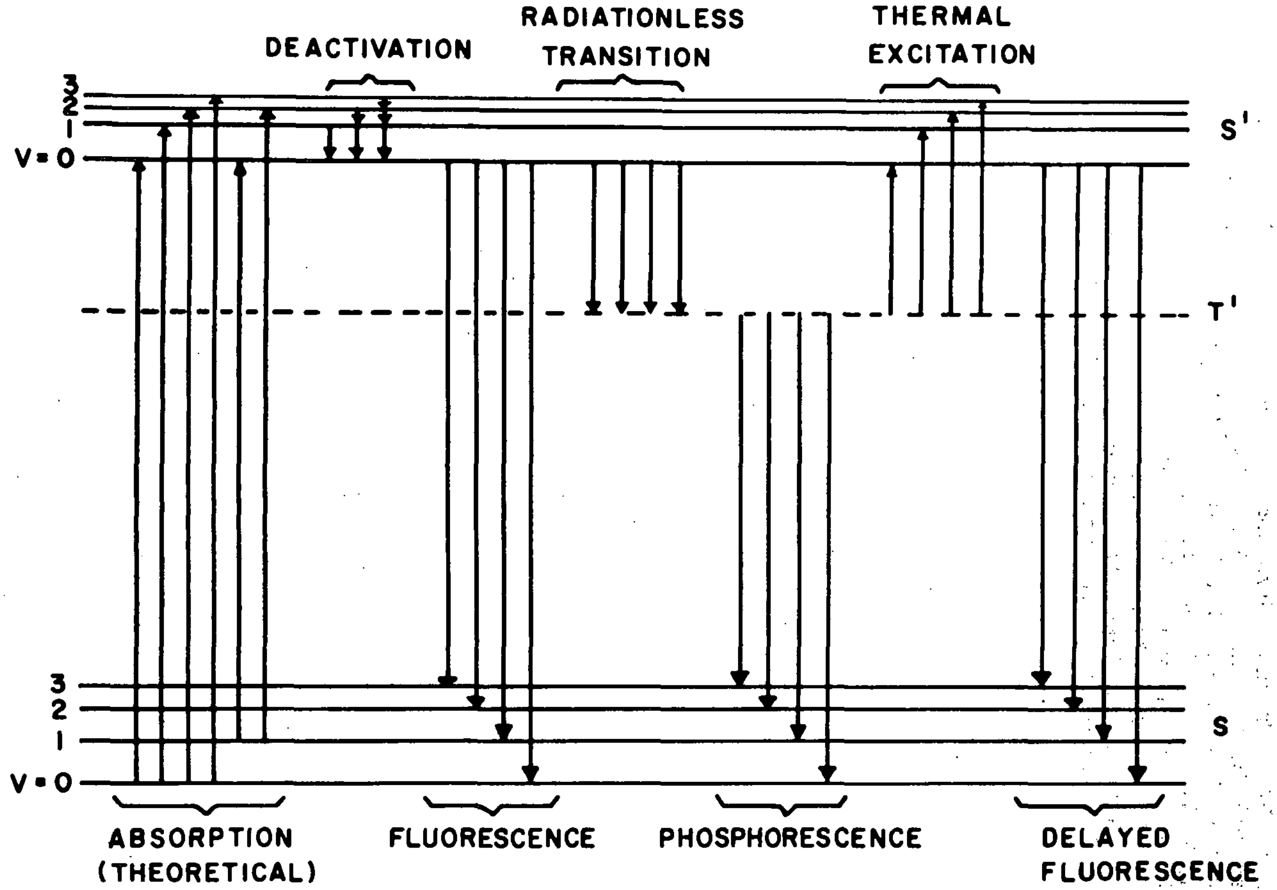
DEACTIVATION
RADIATIONLESS TRANSITION
THERMAL EXCITATION
3
2
1
V = 0
S'
T'
3
2
1
V = 0
S
ABSORPTION (THEORETICAL)
FLUORESCENCE
PHOSPHORESCENCE
DELAYED FLUORESCENCE

FIGURE 1

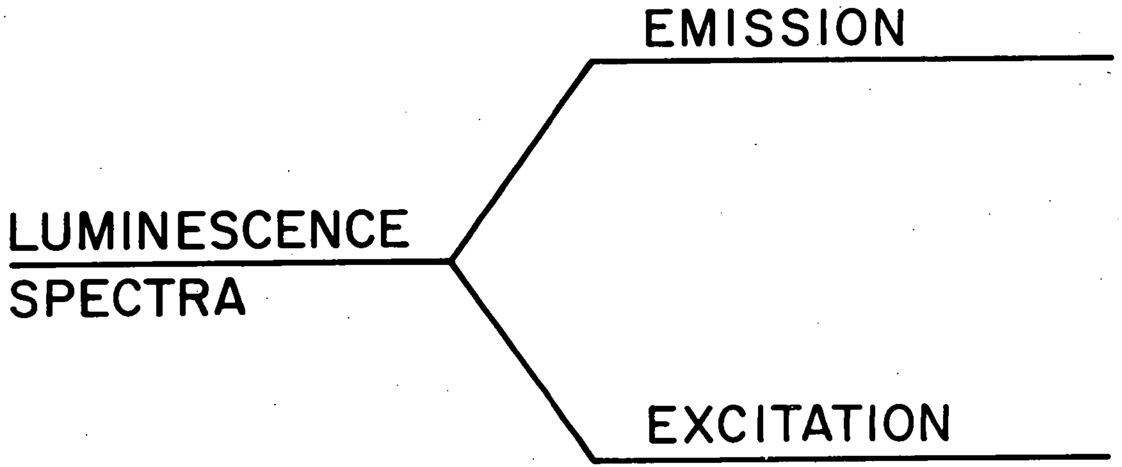
LUMINESCENCE
SPECTRA
EMISSION
EXCITATION

FIGURE 2

SAMPLE ANTHRACENE
ORIGIN -
SOLVENT EtOH
CONC. 0.1 PPM

CELL PATH 100 MM
REFERENCE EtOH
OPERATOR SCP
REMARKS

SLIT WIDTH .25 MM @ 350
RESOLUTION
SCAN SPEED

CURVE NO.
ORD. EXP. ST 5 / T
PEN RESPONSE 3
DATE 2-20-67

UV

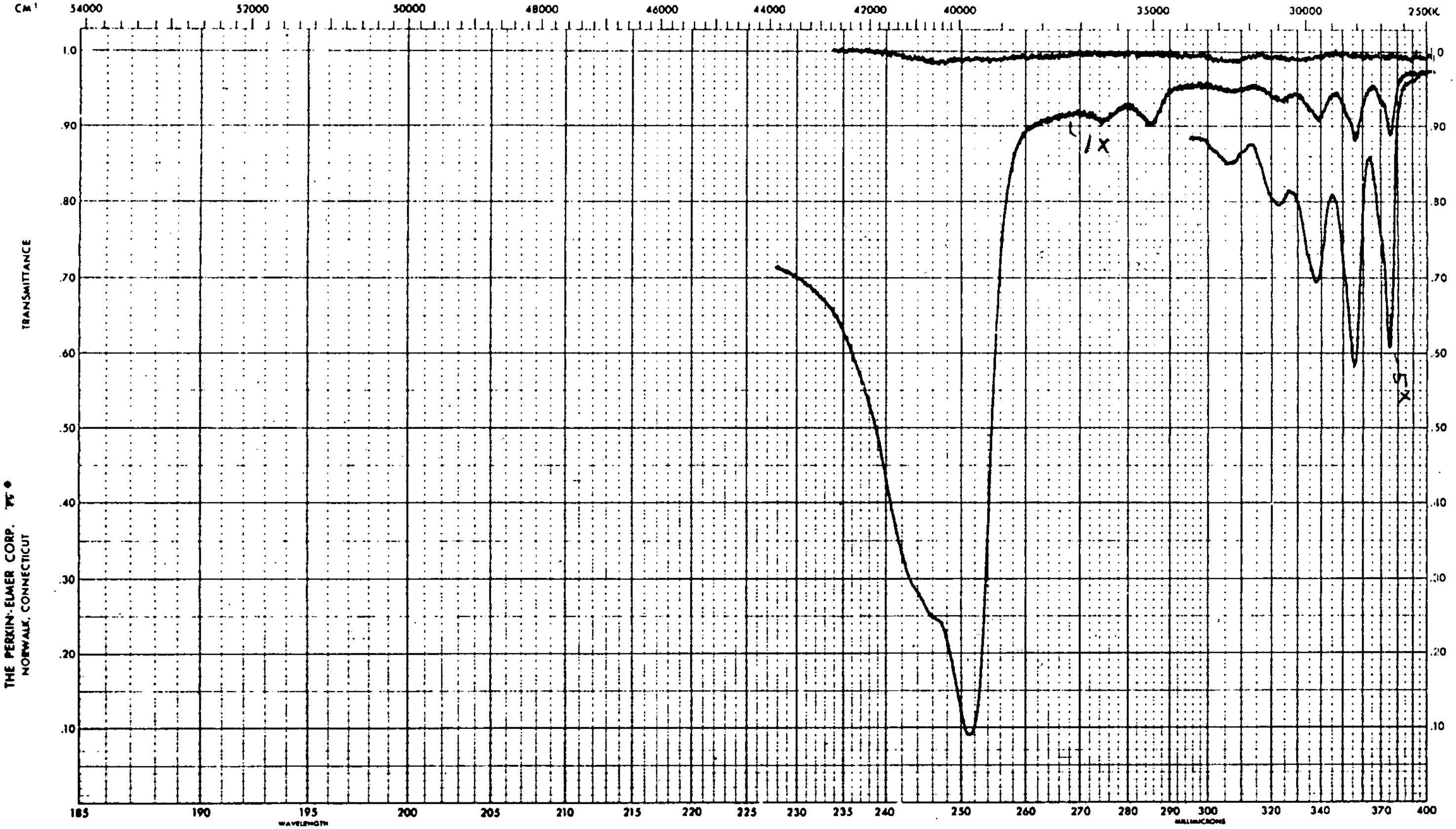

FIGURE 3

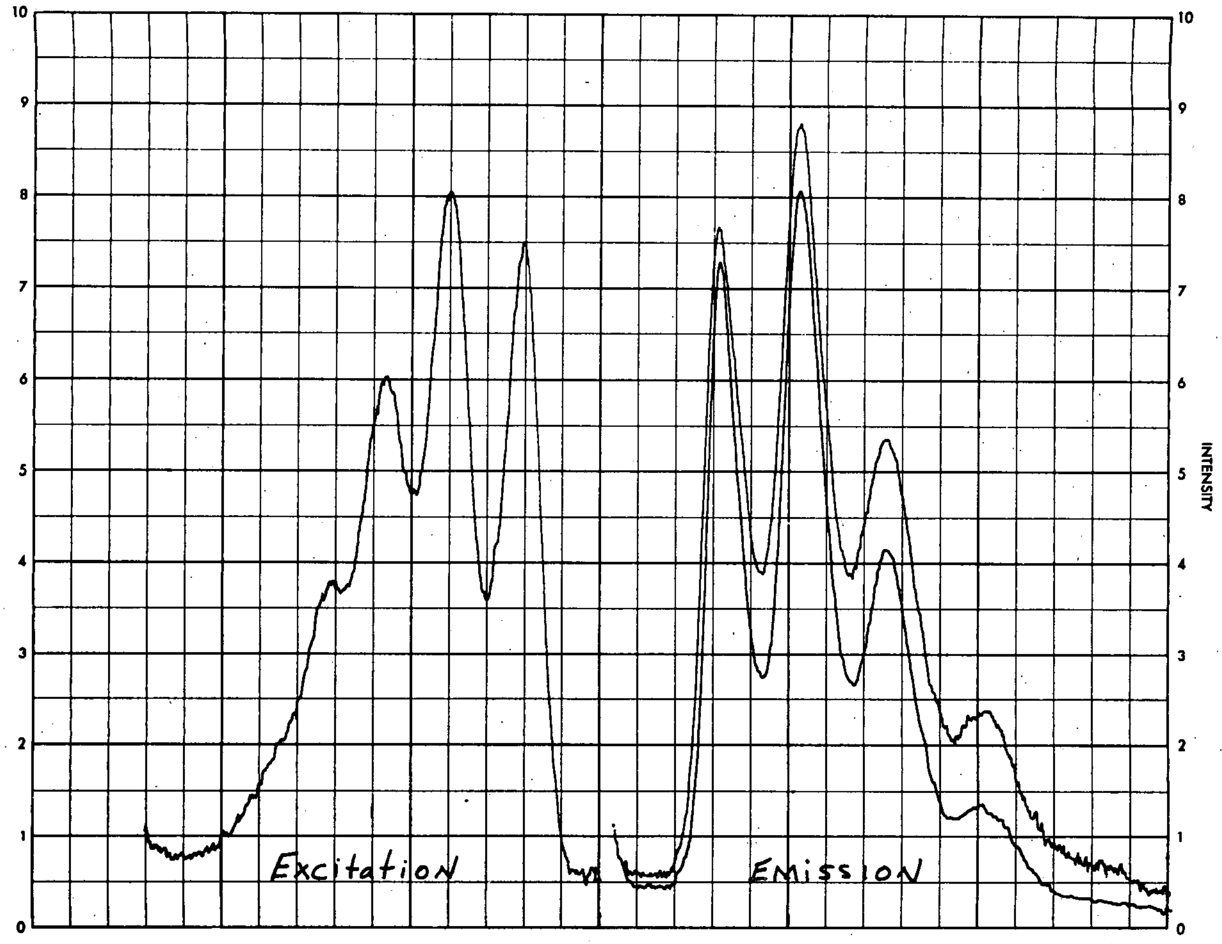

FIGURE 4

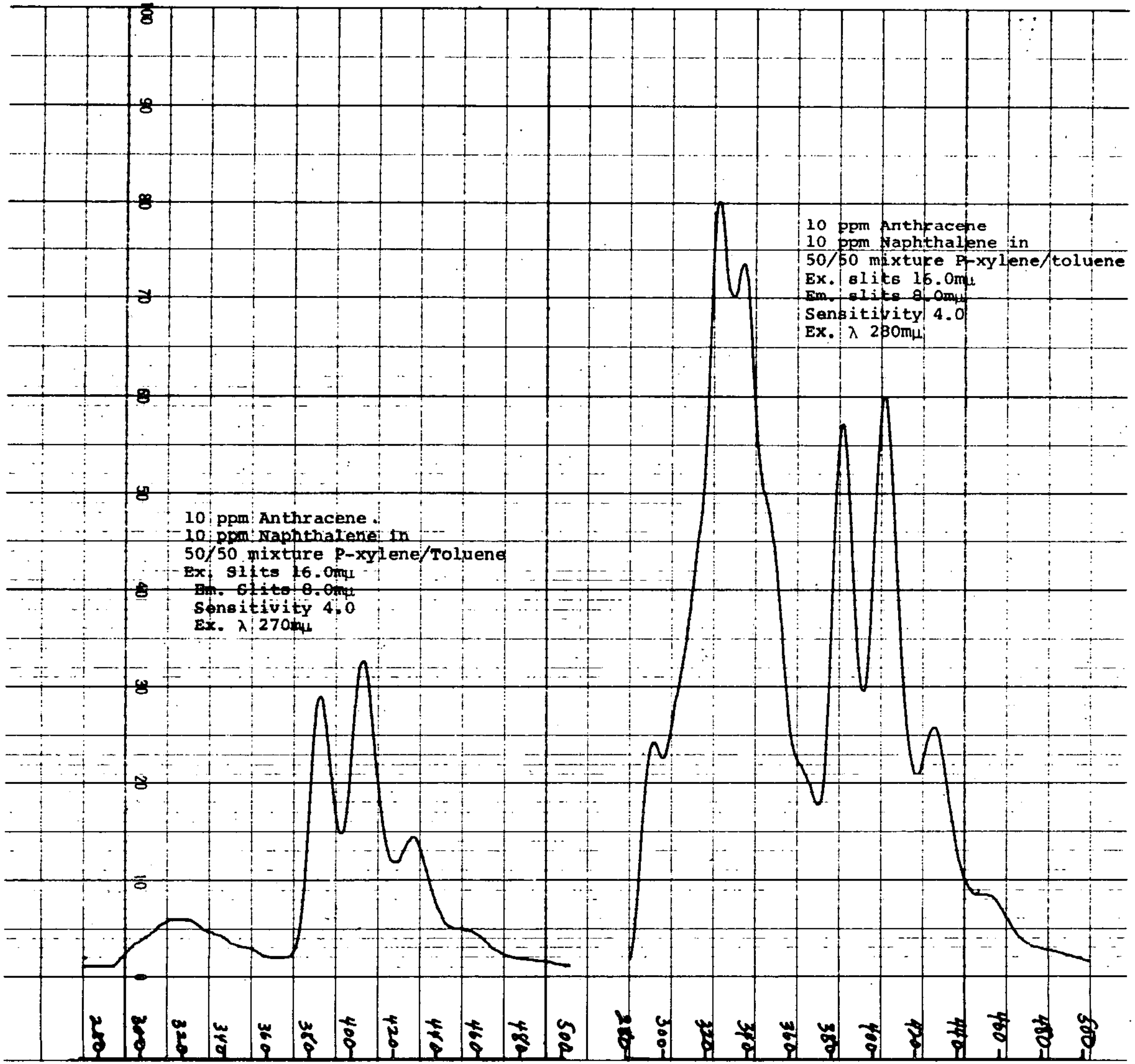
10 ppm Anthracene
10 ppm Naphthalene in
50/50 mixture P-xylene/Toluene
Ex. Slits 16.0mμ
Em. Slits 8.0mμ
Sensitivity 4.0
Ex. λ 270mμ
10 ppm Anthracene
10 ppm Naphthalene in
50/50 mixture P-xylene/toluene
Ex. slits 16.0mμ
Em. slits 8.0mμ
Sensitivity 4.0
Ex. λ 280mμ
100
90
80
70
60
50
40
30
20
10
0
280
300
320
340
360
380
400
420
440
460
480
500
280
300
320
340
360
380
400
420
440
460
480
500

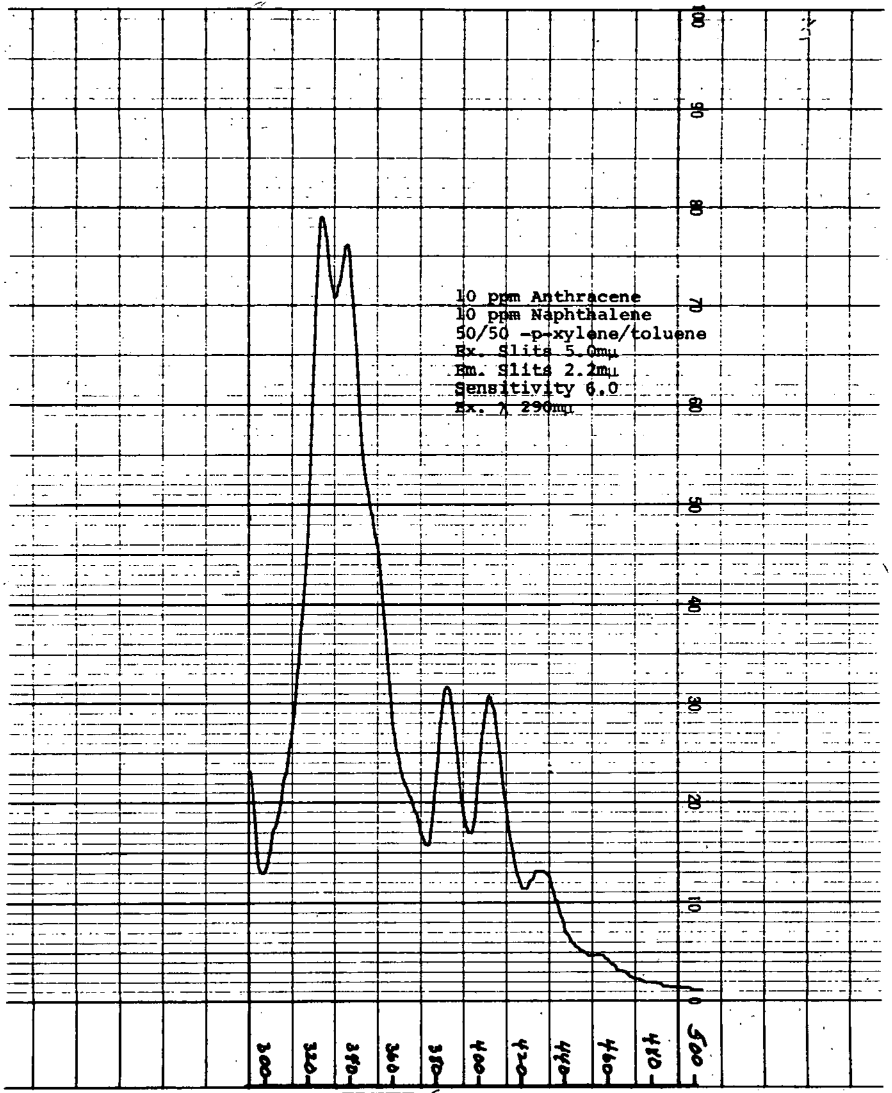

10 ppm Anthracene
10 ppm Naphthalene
50/50 -p-xylene/toluene
Ex. Slits 5.0mμ
Em. Slits 2.2mμ
Sensitivity 6.0
Ex. λ 290mμ

FIGURE 6

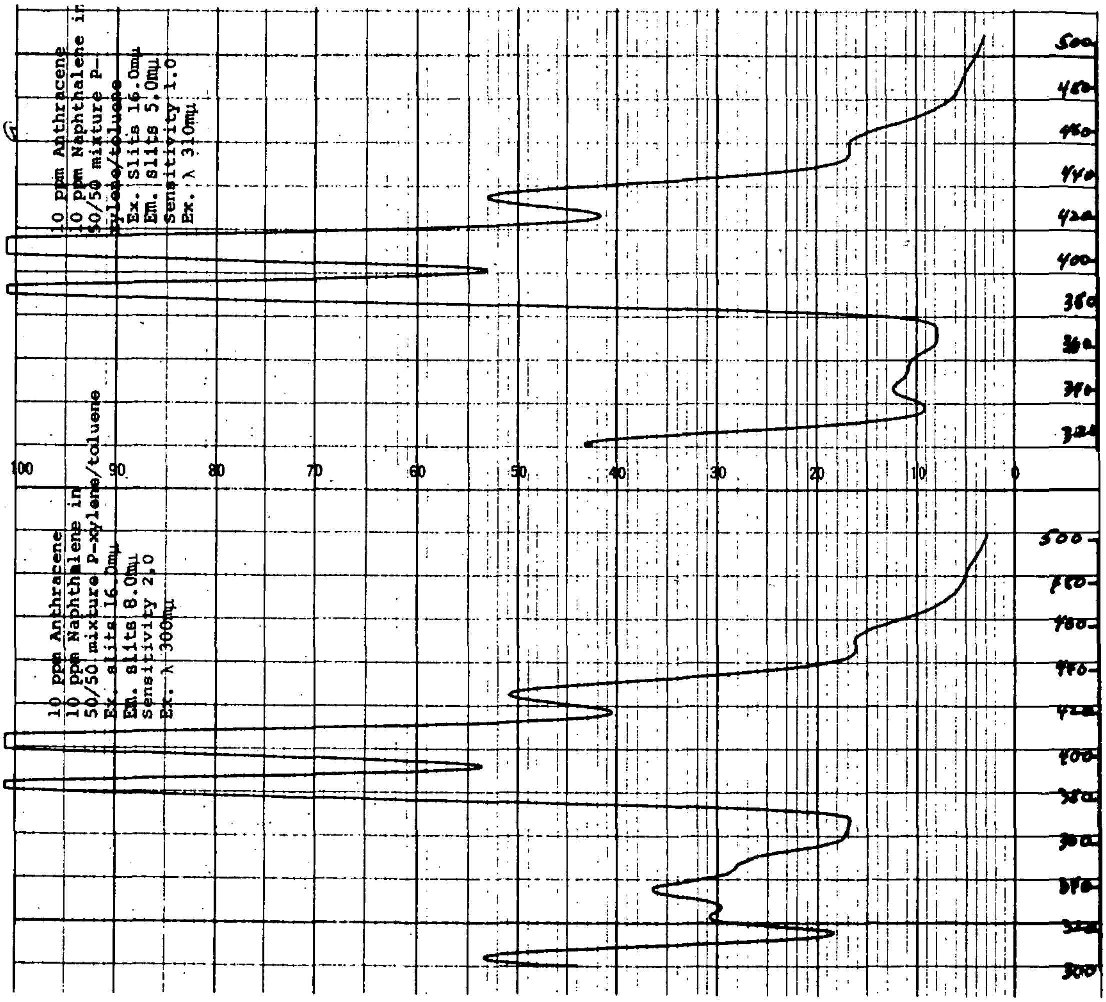
10 ppm Anthracene
10 ppm Naphthalene in
50/50 mixture P-
xylene/toluene
Ex. Slits 16.0mμ
Em. Slits 5.0mμ
Sensitivity 1.0
Ex. λ 310mμ
10 ppm Anthracene
10 ppm Naphthalene in
50/50 mixture P-xylene/toluene
Ex. slits 16.0mμ
Em. slits 8.0mμ
Sensitivity 2.0
Ex. λ 300mμ
100
90
80
70
60
50
40
30
20
10
0
500
480
460
440
420
400
380
360
340
320
500
480
460
440
420
400
380
360
340
320
300

FIGURE 7

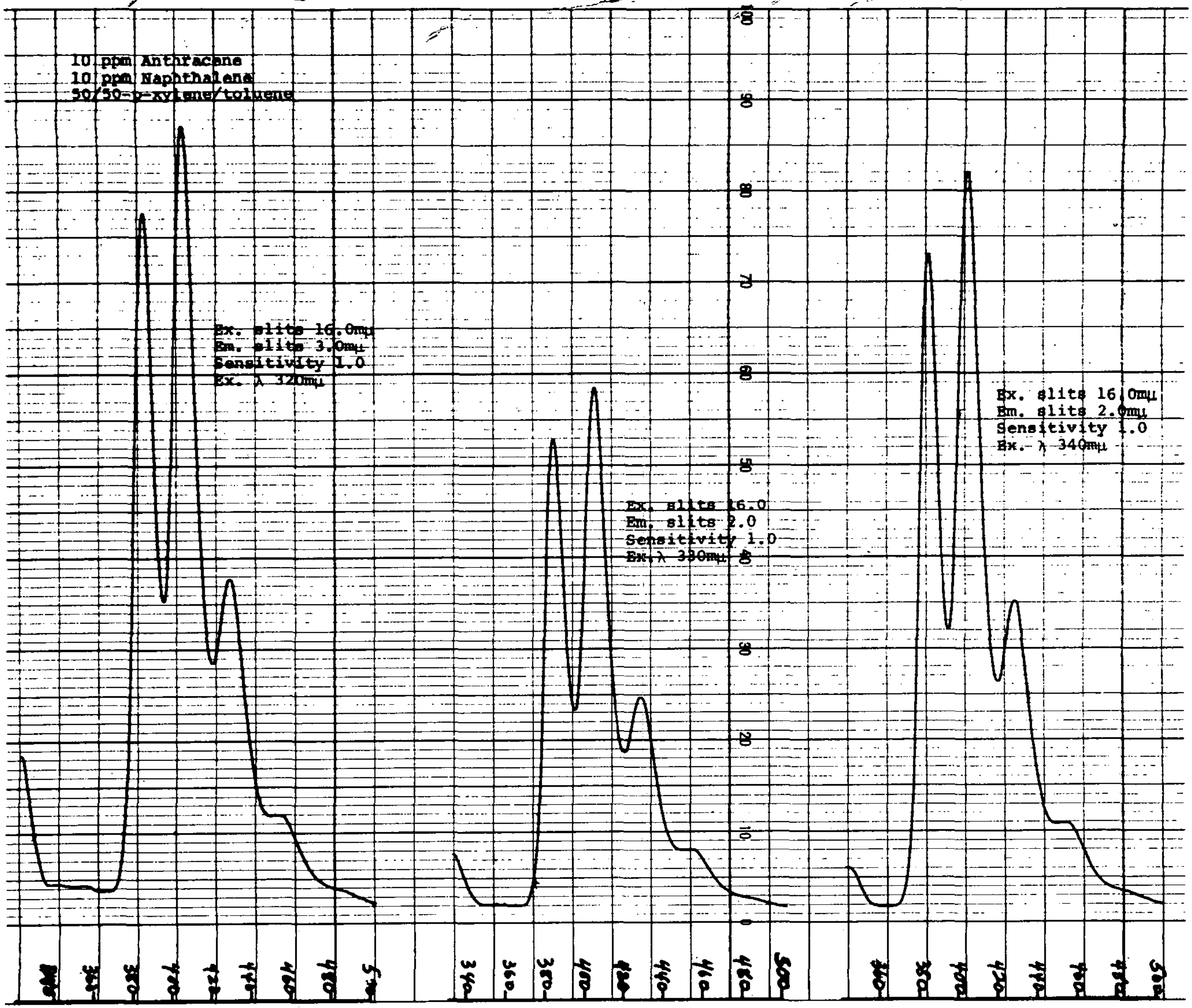
10 ppm Anthracene
10 ppm Naphthalene
50/50-p-xylene/toluene
Ex. slits 16.0mμ
Em. slits 3.0mμ
Sensitivity 1.0
Ex. λ 320mμ
Ex. slits 16.0
Em. slits 2.0
Sensitivity 1.0
Ex. λ 330mμ
Ex. slits 16.0mμ
Em. slits 2.0mμ
Sensitivity 1.0
Ex. λ 340mμ
100
90
80
70
60
50
40
30
20
10
0
360
380
400
420
440
460
480
500
340
360
380
400
420
440
460
480
500
360
380
400
420
440
460
480
500

FIGURE 8

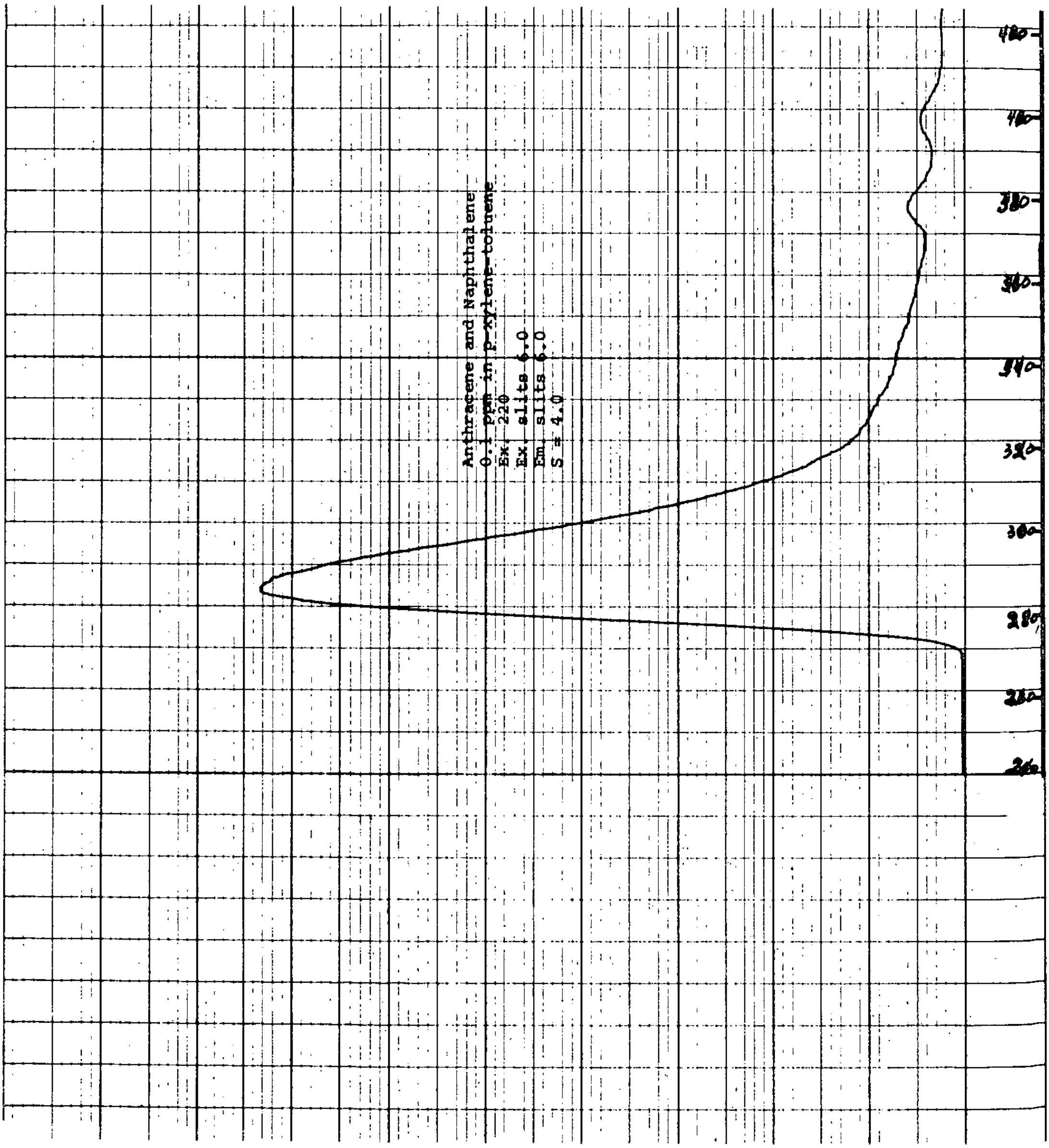
Anthracene and Naphthalene
0.1 ppm in p-xylene-toluene
Ex. 220
Ex. slits 6.0
Em. slits 6.0
S = 4.0
420
400
380
360
340
320
300
280
260
240

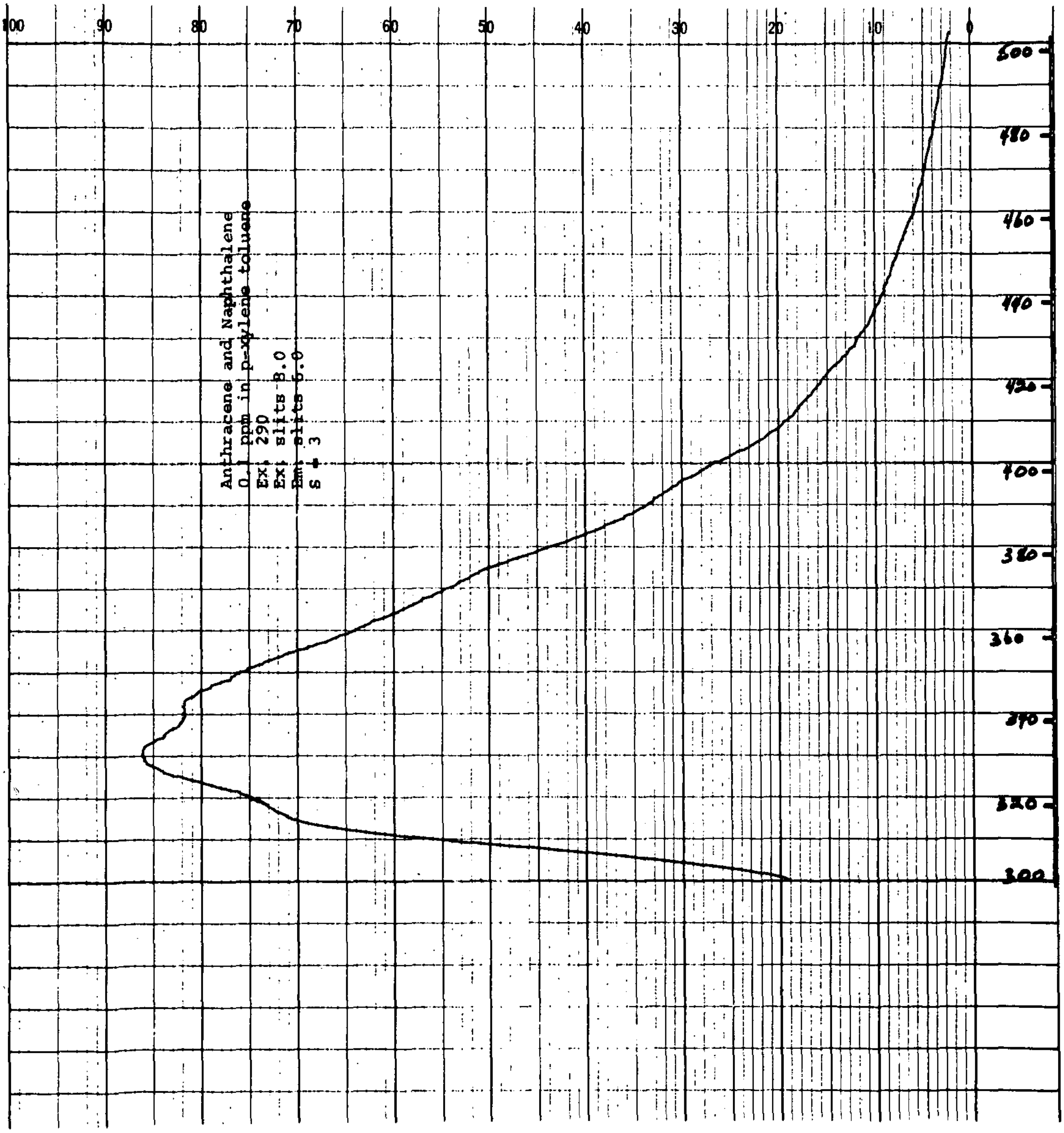

100
90
80
70
60
50
40
30
20
10
0
500
480
460
440
420
400
380
360
340
320
300
Anthracene and Naphthalene
0.1 ppm in p-xylene toluene
Ex. 290
Ex. slits 8.0
Em. slits 6.0
S = 3

FIGURE 10

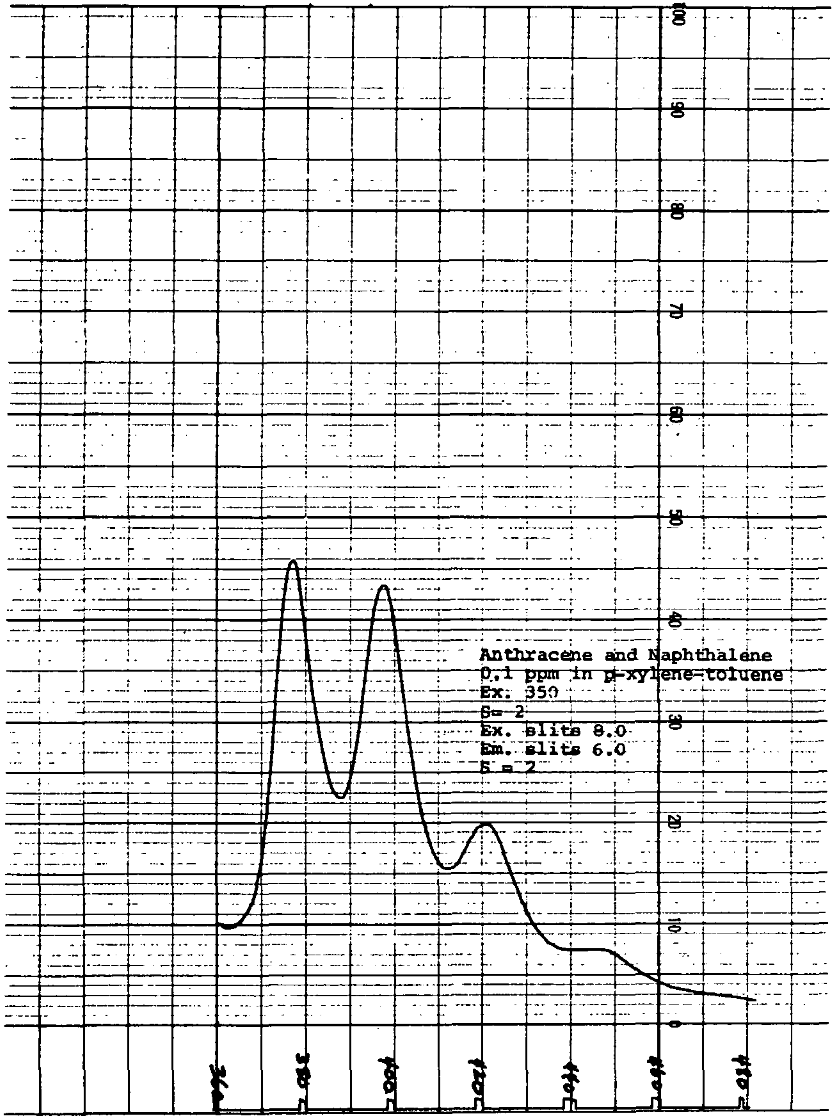
100
90
80
70
60
50
40
30
20
10
0
360
380
400
420
440
460
480
Anthracene and Naphthalene
0.1 ppm in p-xylene-toluene
Ex. 350
S= 2
Ex. slits 8.0
Em. slits 6.0
S = 2

FIGURE 11

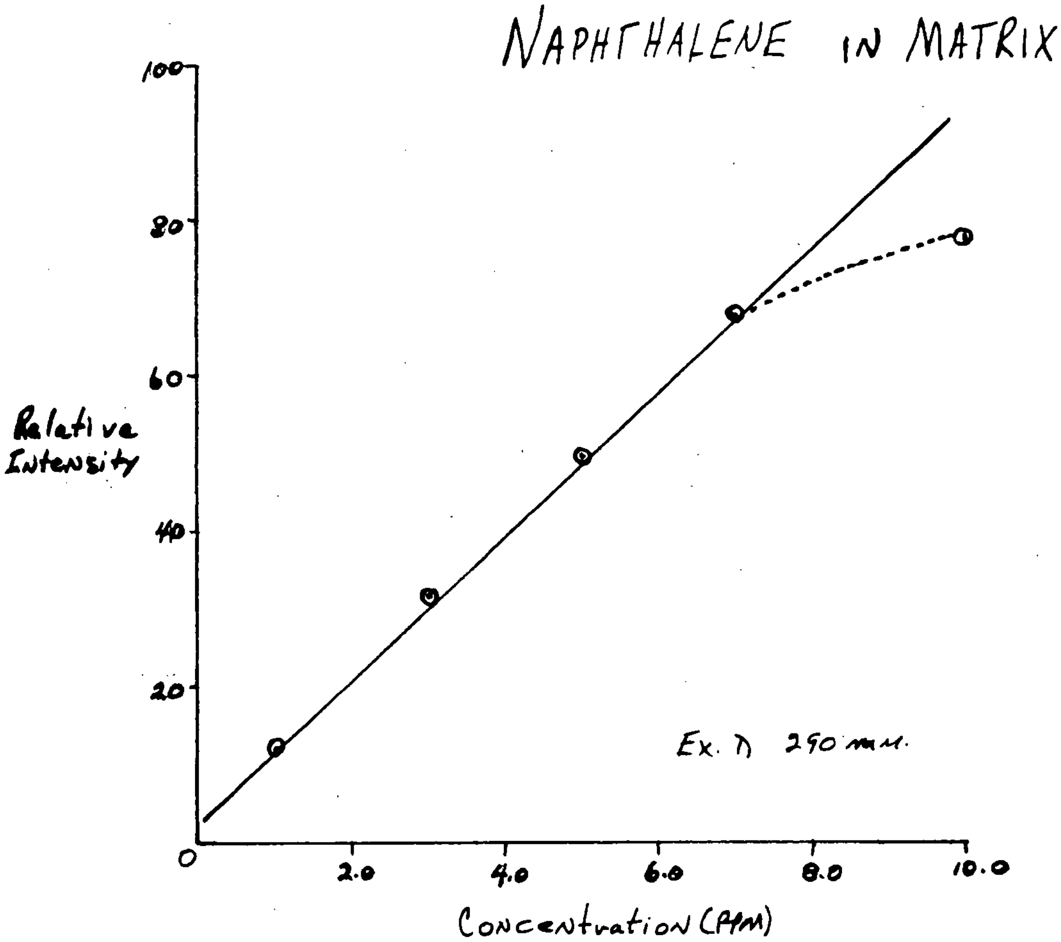
NAPHTHALENE IN MATRIX
Relative Intensity
100
80
60
40
20
0
2.0
4.0
6.0
8.0
10.0
Concentration (PPM)
Ex. λ 290 mμ.

FIGURE 12

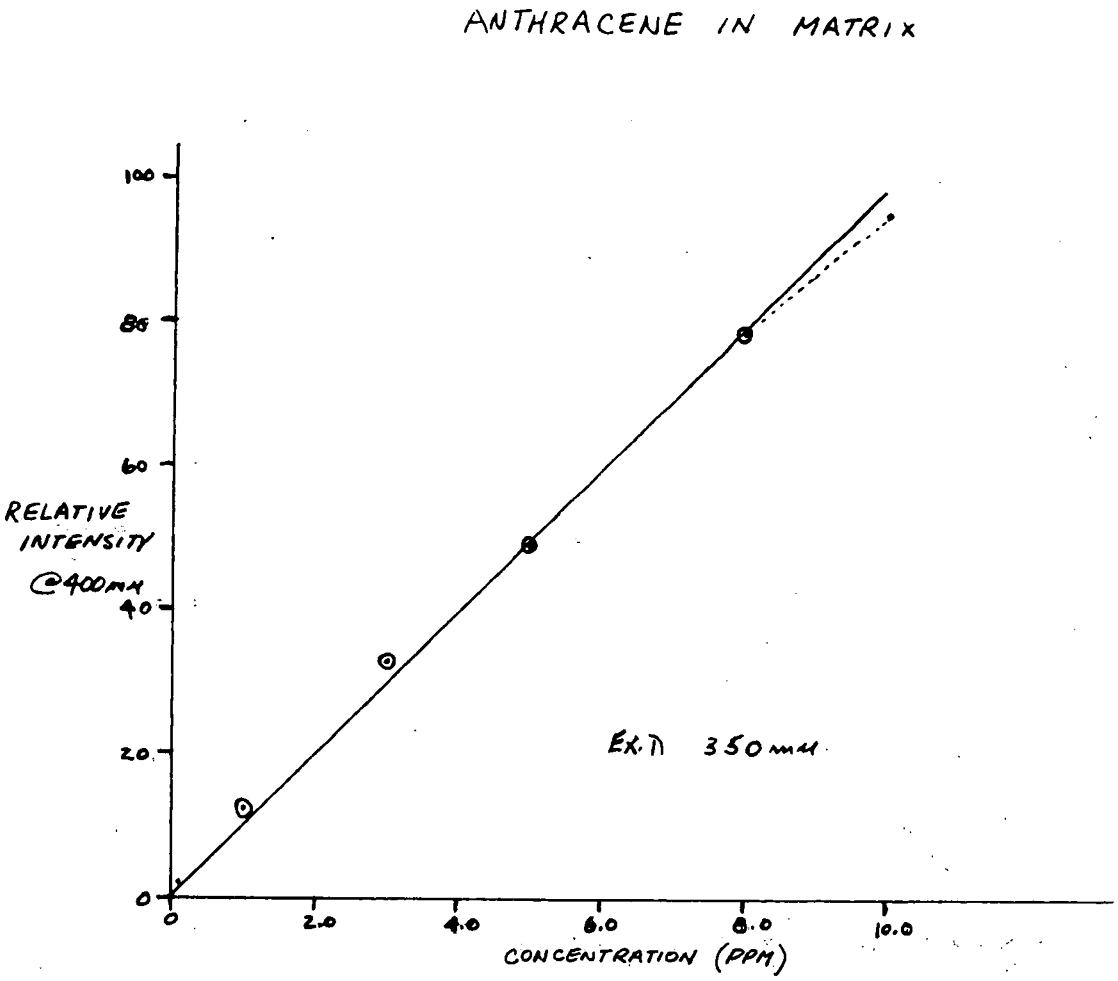
ANTHRACENE IN MATRIX
RELATIVE INTENSITY @400mμ
100
80
60
40
20
0
0
2.0
4.0
6.0
8.0
10.0
CONCENTRATION (PPM)
EX.λ 350mμ

FIGURE 13

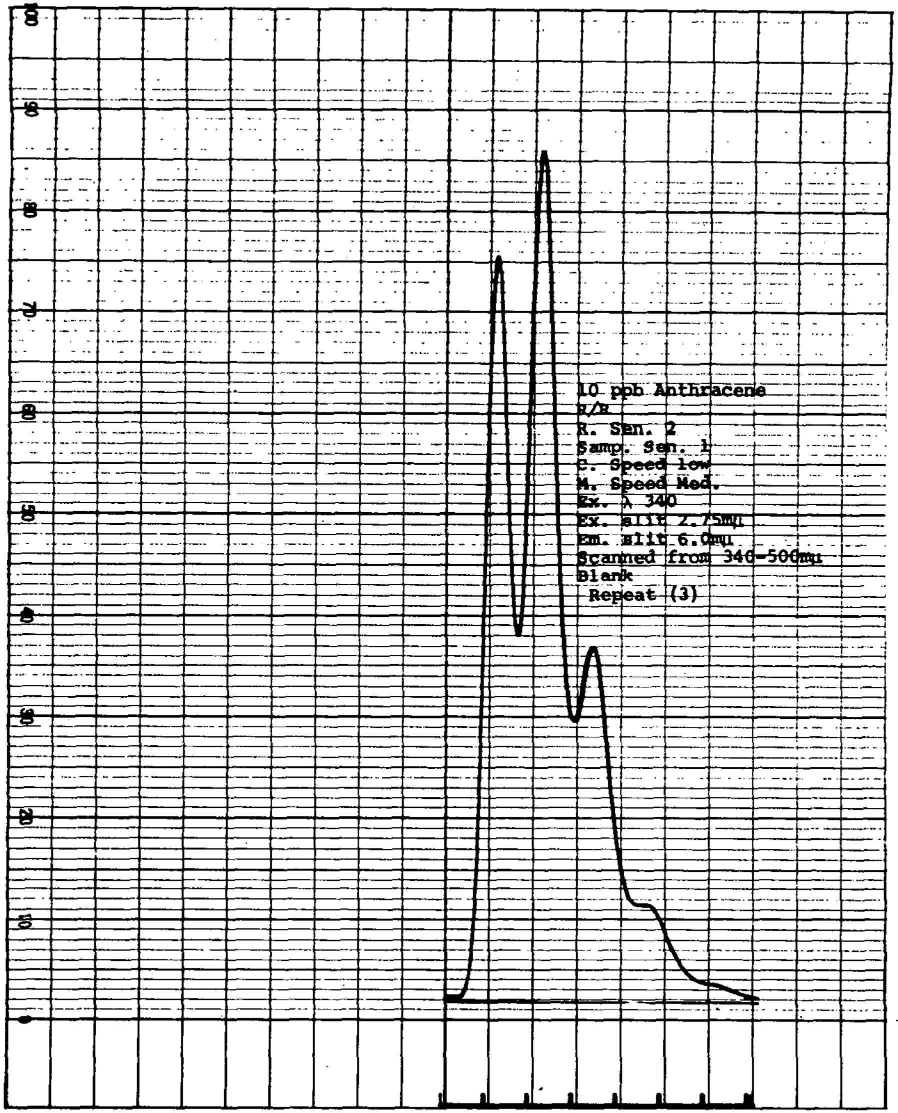
10 ppb Anthracene
S/R
R. Sen. 2
Samp. Sen. 1
C. Speed low
M. Speed Med.
Ex. λ 340
Ex. slit 2.75mμ
Em. slit 6.0mμ
Scanned from 340-500mμ
Blank
Repeat (3)
100
90
80
70
60
50
40
30
20
10
0

DOUBLE RESONANCE MODULATED MICROWAVE SPECTROSCOPY

G. W. Flynn*, O. Stiefvater, and R. Volpicelli

Research Systems Inc., 236 Grove St., Lexington, Mass.

I. Introduction

A large number of molecular systems which have measurable vapor pressures at dry ice or room temperature can be studied by microwave spectroscopy. In general it is necessary that these molecules possess a permanent dipole moment (usually greater than 0.1 Debye) and have rotational states with energy level spacings which correspond to frequencies in the microwave spectral range (8-40 GHz, or 0.29 - 1.33 cm^{-1}). Most molecules have been studied in the microwave range with a "standard" Hughes and Wilson Stark-modulated spectrometer.[1] In this sytem the molecule is placed in a waveguide cell at a pressure of 10-100 μ of Hg. Microwave radiation is passed through the cell and absorbed by the molecular system at frequencies corresponding to the energy level separations of certain pairs of rotational states. It is important to realize that this resonance absorption for levels i, j with $E_i - E_j = hv_{ij}$ (where E_i, E_j are the energies of states i,j and h isPlanck's constant) involves only two levels(we neglect here possible overlap between two or more transitions and degeneracies). In order to enhance the sensitivity for detection of the absorbed microwave radiation, a large electric field (0-2000V/cm) is applied to the gas in the cell. The interaction of the molecular dipole moment with this field causes a shift in the rotational energy level spacings and a consequent shift in the microwave absorption frequencies. The large electric field is modulated in square wave fashion, usually at 100KHz, and hence the absorption of radiation is also modulated at the same frequency and can be detected with a phase sensitive detector.

The standard Stark spectrometer can be characterized as a single resonance device because it involves the resonant absorption for only a single line (one pair of rotational energy levels). It is also possible to simultaneously irradiate a gaseous system with two microwave radiation fields with frequencies corresponding to two different rotational resonances of the molecule. Such experiments have been pursued by several authors[2-4] in Stark modulated spectrometers where the basic detection scheme still involves the molecular Stark effect. However, when two microwave fields are applied to a gaseous sample, it is possible to eliminate the standard high voltage Stark modulated cell by modulating one of the microwave fields instead.[5,6] This last spectroscopic scheme has been characterized as double resonance modulated microwave spectroscopy and constitutes the main concern of this abstract.

II. Theoretical Considerations

The theoretical treatment used here assumes that the resonance lines are pressure broadened. The average lifetime of a rotational state is taken as the mean time between collisions. Only three rotational energy levels, 1, 2, 3 with energies $E_1<E_2<E_3$ are considered. The transitions $1\rightarrow2$ and $2\rightarrow3$ are assumed to be allowed with dipole moment matrix elements μ_{12} and μ_{23} and resonance frequencies $\omega_0' = 2\pi\nu_{12}$, $\omega_o = 2\pi\nu_{23}$. Two radiation fields are allowed to impinge upon the gaseous sample, a strong field $E' = E_o'\cos\omega' t$ and a weak field $E = E_o \cos\omega t$ with ω' near ω_o' and ω near ω_o but $|\omega'-\omega| > 1$ GHz. (See figure 1a) τ is defined to be the average collision lifetime for the states 1, 2, 3 and n_1, n_2, n_3 are the number of molecules per cm^3 in states 1, 2, 3 for the gas at thermal equilibrium. It is useful to define the parameters $x = (\mu_{23}E_o)/(2\hbar)$ and $y = (\mu_{12}E_o')/(2\hbar)$.

All double resonance experiments of interest in this work are such that the transitions induced by the fields E and E' occur between pairs of rotational levels which have one common energy level (i.e. level 2 for $1 \rightarrow 2$, $2 \rightarrow 3$). The power in the radiation field E' is taken to be sufficient to "saturate the transition $1 \rightarrow 2$. This is equivalent to saying $|y|^2\tau^2 >> 1$. The power in E however is assumed to be so low that the $2 \rightarrow 3$ transition is not "saturated" $(|x|^2\tau^2 << 1)$. Physically, saturation corresponds to a situation where the rate of transitions induced by a radiation field between two levels is such that the population difference between the levels involved in the transition is no longer described by the thermal equilibrium value.

The main features of microwave modulated double resonance spectroscopy are: (1) the strong (high power) field E' is used to modulate the gaseous molecular sample by interacting with the energy levels 1 and 2; (2) the modulation produced by E' causes small but readily detectable changes in the absorption of radiation from the weak field E by transitions between the levels 2 and 3; (3) the signal detected consists essentially of the power absorbed from the weak field E; (4) the strong field E' is blocked from the crystal receiver and is never detected.

Javan[7] in a classic paper has given a mathematical description of a three level system interacting with two radiation fields. The theory is directly applicable to microwave double resonance but the mathematical details are too complex to present here. Therefore only a very qualitative and intuitive description will be given in what follows.

For weak radiation fields it is generally true that only single quantum transitions can take place in a molecular system due to absorption of radiation. Thus a molecule can absorb a photon from field E and go from state 2 to state 3. In the presence of a very large field such as E' at the 1 → 2 molecular resonance frequency and a weaker field E at the 2 → 3 molecular resonance frequency, it is possible for a molecule in state 1 to simultaneously absorb a photon from both E' and E and make a transition to state 3 directly via a double quantum transition. Such transitions are allowed due to the strong quantum mechanical mixing of states 1 and 2 by E'. In a double resonance experiment the power absorbed from E consists of two terms: (1) power absorbed by molecules making the usual single quantum transition 2 → 3; (2) power absorbed by molecules making a two quantum jump from 1 → 3.

In a microwave modulated double resonance spectrometer the field E' is square wave modulated between the values $E' = E_0' \cos \omega' t$ $\omega_1' = \omega_0'$ and $|\omega_2' - \omega_0'| = 20$ MHz. In such a situation, for power levels in the E' field of the order of one watt or less, $E' = E_0' \cos \omega_2' t$ generally has only a small effect on the molecular system because ω_2' is so far from ω_0'. Thus it is possible to take $E' = 0$ for half the square wave cycle without introducing much error.[8] If phase sensitive detection locked to the modulation frequency of E' is used to detect the power absorbed from E, the power absorbed from E during the $E' = 0$ half of the modulation cycle will be essentially identical to an ordinary single resonance absorption. The power absorbed during the $E' = E_0 \cos \omega_0' t$ half cycle will have the double resonance shape predicted by Javan's theory.

III. Pressure Dependence and Intensity of Double Resonance Signal

In the case where E' is only an 0.1 watt field at the J=0-1 resonance frequency the lineshape for the OCS J=1-2 transition will have the appearance shown in figure 1b. As the pressure increases the signal "height" S will decrease and the "line width" will increase in a somewhat complex manner.[9]

Using a computer to simulate line shapes in OCS, the "line intensity" S for the J=1→2 transition with an 0.1 Watt pump field at the J=0-1 resonance frequency has been determined as a function of pressure. These calculations correspond to the line shape shown in figure 1b. A table of S versus pressure and τ is given in Table 1 below for this case.

Table 1

S (arbitrary units)	P (μ of Hg)	τ* (sec x 10^{+6})
3.15	2	12.40
3.19	10	2.48
3.03	20	1.24
1.05	100	0.248
0.27	200	0.124

*Δν = 12 MHz/mm, full width at half height, see ref. 10.

At low pressure, for E' a 1 Watt pump field, it is possible to compare the theoretical intensity S_1 (Figure 1c) with that which can be obtained from a single resonance Stark modulated spectrometer. When the S_1 and S_2 lines are well resolved, S_1 is very similar to a single resonance absorption and it might be expected that the intensity is the same as that for the equivalent Stark modulated line. This is not true normally and the theoretical intensity is expected to be less in general for the double resonance spectrometer. The problem which arises here has to do with the effect of the pumping radiation on various molecular M states (M is the projection of the total angular momentum J on a space fixed axis). This effect becomes small as higher J values are studied and is treated in detail elsewhere.[9] There are also some practical technical problems to be considered in comparing Stark and double resonance spectrometers. Because of the absence of a Stark plate in the double resonance system, the double resonance wave guide cell can easily be made about five times as long as the corresponding Stark cell thus enhancing the signal intensity by a substantial amount. Finally, there are some subtle intensity effects in a double resonance spectrometer which arise from the rate of relaxation of the rotational states and may lead to some enhancement in signal intensity over the Stark case. These effects should be negligible in most cases.[9]

IV. Experimental Results

Several molecules have been investigated in the present experiments using a double resonance modulated spectrometer similar to that of reference 6. Only the results for propionaldehyde are considered here. For this molecule the $2_{11} \rightarrow 3_{12}$ ($\omega_0/2\pi = 33,347$ MHz) transition was observed while the $2_{02} \rightarrow 2_{11}$ ($\omega_0'/2\pi = 13474.9$ MHz) transition was pumped. The line shape corresponded to that shown in Figure 1b. Figure 2 is a plot of the signal height S (see Figure 1b) as a function of pressure for pure propionaldehyde.

It can be seen that the signal height begins to fall off drastically for pressures in excess of about 25μ of Hg. This behavior is qualitatively similar to that predicted using computer simulated line shapes for the molecule OCS (see Table 1).

The reason for the initial rise in the signal height in the pressure range 0-20 μ of Hg is readily understood by the following considerations. For pressures below about 10 μ of Hg the linewidth of the signal is not determined by collision processes and hence the theoretical discussion presented earlier does not apply to this region. Before pressure broadening sets in, the linewidth will generally be a constant (determined by the modulation frequency, temperature, and cell dimensions) and the line intensity will increase directly as the density of the sample. This is similar to the situation observed in a Stark spectrometer except that for the Stark case the maximum signal height is independent of pressure in the pressure broadened range. For the double resonance case the line intensity drops in the pressure broadened range because of incomplete modulation.

For gas samples which are mixtures of several components (all or only one of which have a microwave spectrum) curves similar to that shown in Figure 2 are observed for a given component. The peak of the signal generally occurs at a different pressure than that for the pure sample due to the difference in collision cross sections for the various constituents of the sample. It is worth noting that the double resonance technique serves as an unambiguous identification method for a molecule in the presence of many other molecules. This is because the observation of a double resonance signal for a given microwave pump and observation frequency requires that the sample have a resonance at each of these respective frequencies and that these resonances must have a common energy level. That such a series of circumstances might arise for more than one molecule is highly unlikely.

V. Conclusions

1. At moderate or low pressures (about 20μ of Hg) it is expected that a microwave modulated double resonance spectrometer will have a better signal to noise ratio than a Stark modulated spectrometer provided the double resonance waveguide cell is at least several times longer than the Stark cell.

2. At high pressures, due to incomplete modulation, the double resonance technique is less advantageous than the Stark technique.

3. The double resonance technique is extremely useful for identification of molecules in a mixed sample due to the highly selective nature of the double resonance phenomenon.

REFERENCES

* Department of Chemistry, Columbia University, New York, N.Y.

1. K.B. McAfee, R.H. Hughes, and E.B. Wilson, Jr. Rev. Sci. Inst. 20 821 (1949)
2. A. Battaglia, A. Gozzini, and E. Polacco, Nuova Cimento 14, 1076 (1959)
3. T. Yajima and K. Shimoda, J. Phys. Soc. Japan 15 1668 (1960)
4. A.P. Cox, G.W. Flynn, and E.B.Wilson, Jr. J.C.P. 42 3094 (1965)
5. A. Battaglia, A. Gozzini, and E. Polacco, Arch. des Sciences, Switzerland 13, F A S C 171 (1960)
6. R.C. Woods III, A. Ronn, and E.B. Wilson, Jr., "A Double Resonance Microwave Spectrometer" (to be published)
7. A. Javan, Phys. Rev. 107 1579 (1957)
8. Sometimes, however, the small effects introduced by the off resonant field ω_2' can be readily detected even when $|\omega_2' - \omega_0'| \sim 500$ MHz (O. Stiefvater, unpublished results).
9. G. W. Flynn (to be published)
10. Molecular Microwave Spectra Tables, NBS Circular 518.

Figure 1.

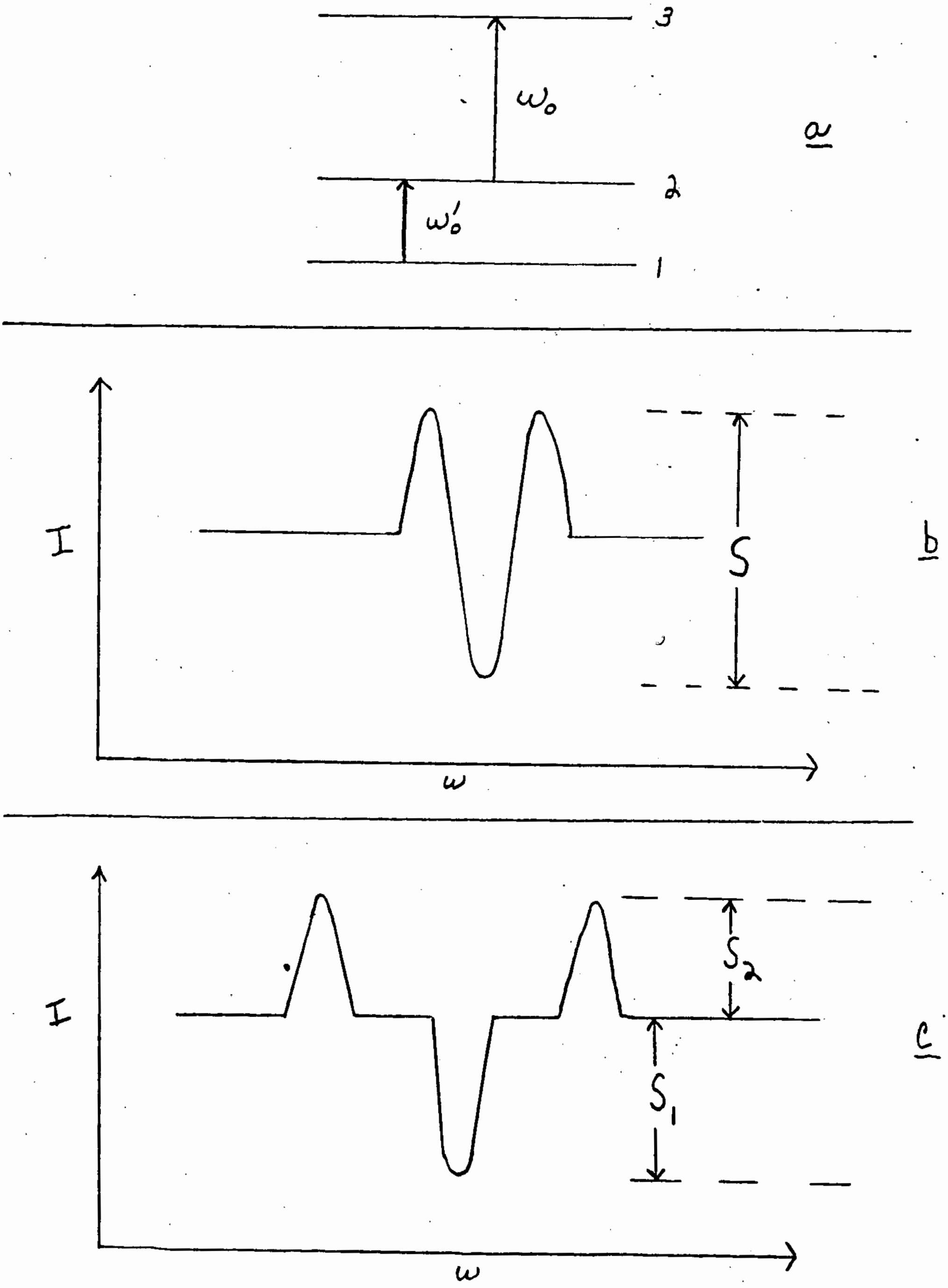
3
ω₀
2
ω₀′
1
a
I
S
b
ω
I
S₂
S₁
c
ω

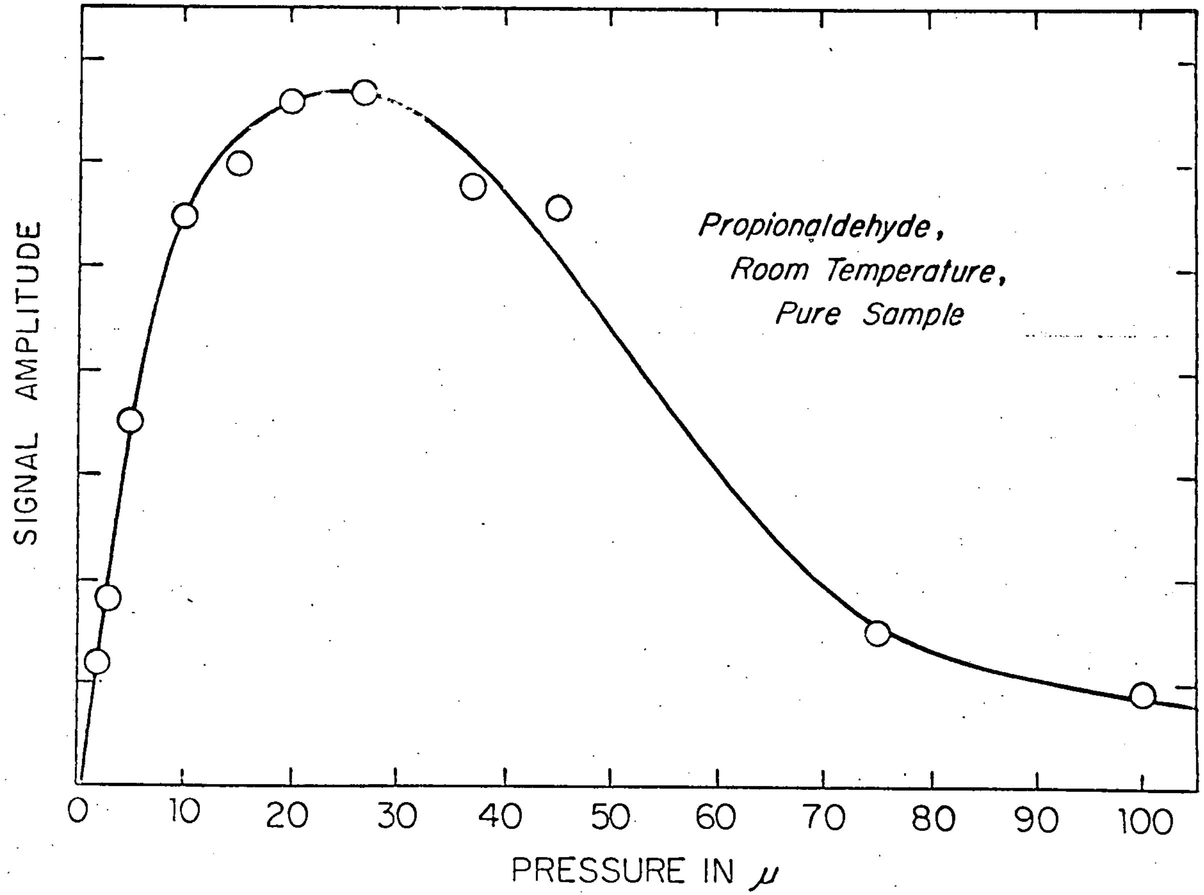
SIGNAL AMPLITUDE
Propionaldehyde,
Room Temperature,
Pure Sample
0
10
20
30
40
50
60
70
80
90
100
PRESSURE IN μ

Figure 2.

INVESTIGATIONS IN NQR SPECTROSCOPY

William L. Truett

Wilks Scientific Corporation, So. Norwalk, Conn.

NQR Spectroscopy refers to that branch of spectroscopy in which energy is absorbed by various atomic nuclei in the region from ∿ 1-1000 Mc/s. A full and excellent discussion of all the theoretical and experimental aspects of the subject has been given by Semin[1]. Among the more important nuclei which show the effect are Cl^{37}, Cl^{35}, Br^{81}, Br^{79}, I^{127}, Sb^{121}, Sb^{123}, Al^{27}, N^{14}, Ga^{69}, Ga^{71}, and V^{51}; in all 131 isotopes can absorb RF energy.

The precise position of the absorption depends upon the electron density about the nucleus and the number of allowed absorption bands upon the nuclear spin. In general with nuclei of spin 3/2, one line will be observed from each chemically distiguishable nucleus. Thus with Cl^{35}, spin 3/2, Table I summarizes the number of bands to be expected in the indicated structures.

TABLE I

STRUCTURE	ABSORPTION BANDS
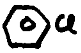	1
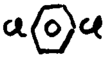	1
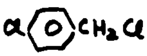	2
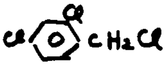	3

Until recently nqr spectra could be obtained only with considerable difficulty due to the wide range of frequencies over which any particular isotope might absorb (50-100 Mc/s) and the slowness of search due to the frequent necessity of adjusting the oscillators used. The instrument developed by Peterson and Bridenbaugh[2] has made a dramatic difference in the ease of search over wide ranges by an essentially automatic and unattended spectrometer.

In addition to the components customarily present in an oscillator of the superregenerative sort, the Peterson instrument contains an electro-mechanical servo loop which serves to stabilize the oscillator over wide ranges by feeding back a voltage to the grid of the oscillator tube, customarily a 12AU7, which results in a stabilized output at constant noise. Thus, searches are readily conducted over ranges of 20-40 Mc/s which contain the vast majority of organo chloro compound absorption bands, or 200-300 Mc/s which contain the vast majority of organo bromo compounds; the time required for such searches is 2 to 4 hours.

Some additional refinements to the Peterson spectrometer have been noted by Graybeal[3], but full detials on relative performance have not been published.

Previous examination of the quantitative aspects of nqr spectroscopy has largely been limited to determination of the effect of impurities on the peak intensities of absorption bands[4] with minor references to the utility of peak intensities to determine the relative numbers of chemically different nuclei present in a molecule[5,6]. Relatively minor references will be noted in papers concerned with nqr spectroscopy with regard to sample size. It is apparent from papers containing absorption data on large numbers of compounds[1,7] that while chemical shifts comparable in principle to those observed in nmr spectra are present, splittings due to the effects of neighboring atoms are not present.

Unfortunately, a type of splitting is encountered which has to do with the fact that spectra can be determined only upon crystalline solids and is designated crystal splitting. It is due to the fact that chemically equivalent nuclei in a crystalline lattice may be physically non equivalent by virtue of relative lattice positions. Normally, it can be recognized by the extent of the splitting ∿0.2 Mc/s, and the equal intensities of the two bands[8]. In certain cases it simplifies the interpretation of a spectrum for it has been found that virtually all trichloromethyl groups show a trio of bands of equal intensity separated by about 0.1-0.2 Mc/s.

Examination of mixtures of p-dichlorobenzene and p-dibromobenzene along the lines noted by Dean[9] give very similar results using the Wilks Scientific Corporation NQR-1A NQR Spectrometer. Additional examples of p-dichlorobenzene and γ-hexachlorocyclohexane indicates that the peak height is an excellent way to determine the concentration of impurities present in a crystal of a chloro compound in the range from 0.01 to 1.0%, and that calibration curves of the sort generally useful in quantitative infrared measurements can easily be constructed.

With regard to the amount of sample required it has been found that employing the NQR-1A it is possible to determine usable spectra of p-dichlorobenzene on samples of 25-50 mg., although routinely 500mg will suffice for any unknown. It has been found that in general a much smaller sample, 100mg, routinely suffices for any bromo compounds where the absorption frequencies are much higher, while compounds that absorb at frequencies near 5 Mc/s will require 1000mg routinely for detection.

Careful examination of a number of spectra of diverse types of organic chloro compounds makes it apparent that nqr spectra can be used to determine the relative numbers of the different types of chloro atoms present. It has been found that peak height alone is sufficient to this end and that integration of the area is unnecessary. Thus, with 2,4-dichlorophynoxy acetic acid we find two bands of matched intensity, Spectrum 1. A molecule of γ-hexachlorocyclohexane is known to contain 3 axial and 3 equitorial chloro atoms, and due to their spatial arrangement there are effectively 4 types of chloro atoms present. The spectrum shows 4 lines of a 1:2:2:1 peak height relationship which fits the known structure[10].

Unfortunately, instruments of the Peterson type cannot be used routinely for the measurement of the spectra of nitrogen compounds due to saturation phenomena precisely encountered in other types of resonance measurements. The use of other types of oscillators such as the Robinson or P-K-W oscillator[11,12] can furnish data on many types of nitrogen compounds.

At the present time there are relatively few examples in the literature of the use of nqr to determine the structure of an organic molecule; Kozima has used this technique to differentiate between the chlorination products of cyclohexane, 2,2-dichlorocyclohexane and 2,6-dichlorocyclohexaneone[13].

Application of the nqr technique to γ-hexachlorocyclohexane has been noted above. A similar study of β-1,2,3,4,5,6-hexachlorocyclohexane revealed that only a single strong band is observed near 37.0 Mc/s. This agrees with the known structure in which the chloro atoms are all trans and all possess the equitorial configuration. It is of interest to note that the only easily attained isomer of 1,2,3,4,5,6-hexabromocyclohexane has a very complex spectrum and is clearly not related to the β-chloro isomer above.

γ-1,2,3,4-tetrachloro - 1,2,3,4-tetrahydronapthalene has been the subject of a recent nmr investigation[14] and has the configuration noted symbolically below:

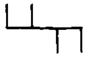

An nqr spectrum of this compound shows two bands of equal intensity at 35 and 36.5 Mc/s and is in agreement with the nmr assignment.

The nqr spectrum of 2,4-dichlorobenzotrichloride, Formula I, might be expected to show three bands representing the three types of chloro atoms

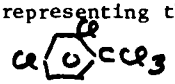

present in a 1:1:3 intensity, with probable splitting of the band due to the trichloromethyl group into a triplet. The actual spectrum (Spectrum 2) shows the expected 3 bands, however, the band at 39.0 Mc/s which is due to CCl_3 is split into a distinct doublet at a 2:1 intensity. A reasonable interpretation of this effect is that the ortho chloro group is interferring sterically with the free rotation of the trichloromethyl group. As a result of this the two chloro atoms of the trichloromethyl group nearer the ortho chloro group are different from the one which is farther.

If collection of data of the sort in references 1 to 7 are studied, it is possible to develop correlation charts of the Colthrup type which have proved so popular in infrared spectroscopy. In such a chart it will be noted that in the case of organic chloro compounds that a range of 30-55 Mc/s embraces virtually all classes of chloro compounds. Acid chlorides show bands near 30 Mc/s while N-chloro compounds lie at the other end of the range near 55 Mc/s. Aromatic and aliphatic chloro compounds absorb near 34-35 Mc/s for the simple types while the more highly substituted types absorb at higher frequencies, for example; the trichloromethyl group near 39Mc/s. Spectra of compounds containing as many as 5 chemically different chloro atoms have shown five distinct bands.

REFERENCES

1. Semin, G.K., and Fedin, E.I., "Use of Nuclear Quadrupole Resonance in Chemical Crystallography." Available through Consultants Bureau, New York (1964) 227 West 17 Street, New York, New York. Unlisted chapters in the Mossbauer Effect and Its Applications in Chemistry, V. I. Gol'danskii.

2. Peterson, G.E., and Bridenbaugh, P.M., The Review of Scientific Instruments, 35, 698 (1964).

3. Graybeal, J.D., and Croston, R.P., The Review of Scientific Instruments, 38, 122 (1967).

4. Duchesne, J., and Monfils, A., Compt. Rend., 238, 1801 (1954).

5. Holmes, R.R., Carter, R.P., and Peterson, G.E., "Molecular Structures of PCl_4F, PCl_3F_2 and PCl_2F_3: Pure Chlorine Nuclear Quadrupole Resonance and Low Temperature F^{19} NMR Spectra," The Journal of Chemical Physics, 3, 1748 (1964).

6. Lorenzo, J.V.D., and Schneider, R.F., Inorganic Chemistry, 6, 766 (1967).

7. Hooper, H.O., and Bray, P.J., The Journal of Chemical Physics, 33, 334 (1960).

8. Dewar, M.J.S., and Lucken, E., Journal of Chemical Society, 426 (1958)

9. Dean, D., The Journal of Chemical Physics, 23, 1734 (1955).

10. Brame, E.G., Analytical Chemistry (In press).

11. Schempp, E., and Bray, P.J., The Journal of Chemical Physics, 46, 1186 (1967)

12. O'Konski, C.T., "Nuclear Quadrupole Resonance Spectroscopy," Determination of Organic Structures as Physical Matters, 2, Ch. 11, Academic Press, New York (1962).

13. Kozima, K., and Saito, S., "Nuclear Quadrupole Resonance of di-Chlorocyclonexanone, " The Journal of Chemical Physics, 31, 560 (1961).

14. De la Mare, P.B.D., et al, Journal of Chemical Society 3, 827 (1966).

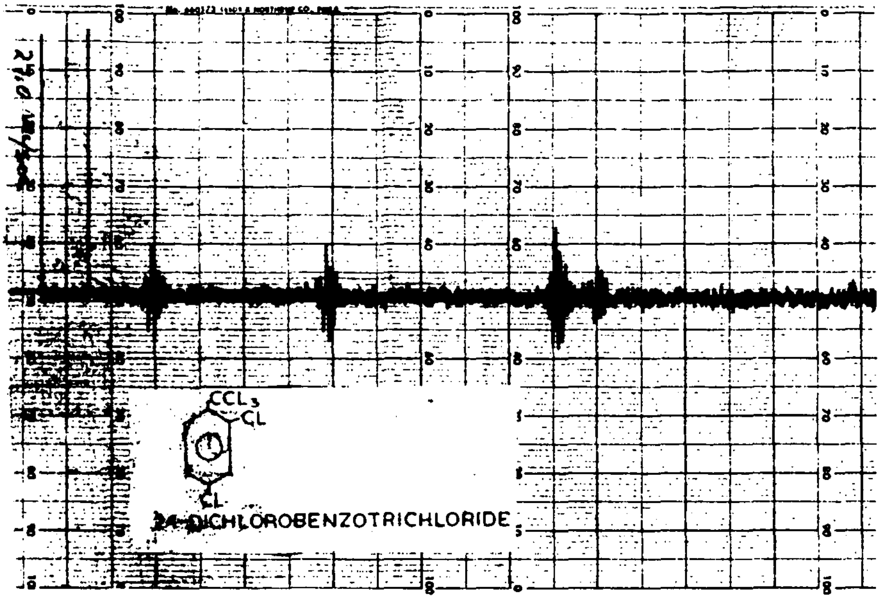

SPECTRUM 1

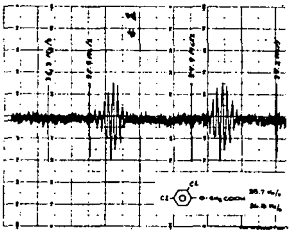

SPECTRUM 2

MÖSSBAUER SPECTROSCOPY: PRINCIPLE AND PRACTICE

Carl W. Seidel

Nuclear Science & Engineering Corporation
Pittsburgh, Pennsylvania 15236

ABSTRACT

Mössbauer Spectroscopy has started to come into its own as an analytical tool. In order to understand what has been accomplished and the potential applications of the Mössbauer Effect, one must understand nuclear resonance absorption and how it is effected by the environment of the absorbing nucleus. The perturbation of the nuclear energy levels of Mössbauer nuclides and the resultant characteristics of Mössbauer spectra are reviewed. This includes the isomer shift and its dependence on the electron density about the nucleus, quadrupole splitting and magnetic hyperfine splitting as well as the temperature dependence of these properties. Correlations of the above properties with the ionic state, electronegativity of a bonding component or with theoretical electron density calculations can be accomplished. The Debye-Waller factor for both the source and absorber material places certain restrictions on the ability to observe the Mössbauer Effect with all possible Mössbauer nuclides. Two typical Mössbauer spectrometer systems are described. One utilizes a constant velocity mode of operation for obtaining data, at one velocity at a time. The other utilizes a constant acceleration mode of operation which scans the chosen velocity range repetitively, storing the counting data in a multichannel analyzer. The basic detection system is the same for both systems but the readout devices may differ. Application of Mössbauer Spectroscopy in the study of surface effects such as adsorption and the study of the bonding of some organo metallic compounds will be discussed.

Another technique has been added in the field of spectroscopy. This new method of analysis depends upon the observance of nuclear resonance absorption which in turn depends upon the recoil free emission and recoil free absorption of gamma rays, or the Mössbauer effect. The term Mössbauer Spectroscopy has been applied to this new and very useful instrumental method which complements the more established techniques of NMR, ESR and x-ray diffraction.

The theory behind the Mössbauer effect has been fully described by Mössbauer (23), Frauenfelder (24) and Wertheim (3) and will not be described in detail here. Certain nuclides (Mössbauer nuclides) exhibit a nuclear decay scheme where the transition from the first excited nuclear level (and sometimes second excited nuclear levels) to the ground state may occur with the recoilless emission of a gamma ray. This gamma ray is uniquely capable of raising a similar nucleus in the same type environment from the ground state to the first (or second) excited nuclear level by recoilless absorption (resonant absorption). Most of the elements that have one or more of these Mössbauer nuclides are shown on the accompanying chart (Fig. 1). The resonant absorption process depends on the fact that the emitting (source) and absorbing (sample) species are bound in a crystal lattice.

Resonance absorption may be destroyed by employing the Doppler effect. If we move either source or absorber relative to the other we may alter the conditions necessary for resonance absorption. Essentially what happens is that by moving either the source or absorber toward the other (a positive Doppler velocity) we increase the energy of the gamma ray as seen by the absorbing species. By moving one away from the other (a negative Doppler velocity) we decrease the energy of the gamma ray as seen by the absorbing species. A complete Mössbauer spectrum would therefore be the plot of the rate of transmission of the gamma ray through the absorbing sample as a function of this Doppler velocity. The resonant condition results in a noticeable decrease in transmission (resonant peak). The parameters of such a spectrum include M (or $\mathcal{E}$), the percent decrease in transmission (magnitude of the peak) at the resonant velocity and Γ, the width of the resonant peak at half maximum as shown in Fig. 2.

Resonance absorption occurs at zero velocity only if both the emitting and absorbing species are in the same physical environment. If this is not true then the resonance absorption may occur at a non-zero velocity. This displacement of the resonance from zero velocity is called the chemical or isomer (I.S.=δ) (Fig. 3). The isomer shift value is a linear function of the s electron density and for Fe-57 decreases with increasing s electron density (1). The d electron density affects the isomer shift mostly by shielding the s electron from the nucleus. Adding d electrons to the atom of interest decreases the electronic charge density at the nucleus, an effect just the opposite of that resulting from the addition of s electrons. The contribution to the shift from the p electrons is very small (3).

Since the electron density at the nucleus is a function of the oxidation state of the absorbing atom and of the electronegativity of its nearest neighbors we have a means of qualitatively identifying compounds, determining oxidation states and structural information concerning the absorbing material. For example, in Fig. 4 we can see how different tin (IV) halides give very noticeably different isomer shifts. The SnF_4 gives a quadrupole splitting because of the inhomogeneous field of surrounding F atoms (it is believed to have a polymer like structure).

Quadrupole splitting (QS=Δ= distance between the two resonance peaks) is due to the interaction of the inhomogeneous electric field at the nucleus (due to the environment) with the electric quadrupole moment of the excited nucleus. The result is a doublet or two resonant peaks. This occurs because the first nuclear excited level splits into two sublevels and two transitions (of slightly different energy) may occur (Fig. 5). Quadrupole splitting may be related quantitatively to the oxidation state and the nature of the chemical bonding of the absorbing atom (1). It also may be used as a method of determining the symmetry of crystals and crystal distortion incurred by substitution in the compound as shown in Fig. 6. The isomer shift of a quadrupole split spectrum is taken as the displacement of centroid from zero velocity. In Fig. 6 the isomer shift of the nitroprusside is different than that of the ferrocyanide due to the fact that the s electron density about the iron atom has changed when one of the ligands changed.

Another interaction, that of the nuclear magnetic moments and the external or intermolecular magnetic fields results in magnetic hyperfine splitting (MHS) of the spectra (a nuclear Zeeman effect). (Fig. 7) In the case of iron we may obtain a spectrum with six resonances. Identification of magnetically ordered structures and determination of Curie and Néel temperatures for many materials may be accomplished by studying their MHS spectra (3). The MHS of rare earth intermetallic compounds has been used to determine the magnetic properties and structure of these materials (25).

Double six line spectra may be obtained when the iron present in the absorber may be in either of two different environments (having different nearest neighbors) or two different crystal structures (tetrahedral and octohedral) where the internal magnetic field is different at each site. A composite of a six line and a one or two line spectrum may occur when two forms (magnetic and nonmagnetic) of a material such as Fe_2O_3 are present in the absorber.

The isomer shift for split spectra is recorded by taking the centroid of the spectrum and measuring its displacement from zero velocity.

Mōssbauer spectra may not always be as uncomplicated as one of the three basic forms described. But combinations and perturbations of the basic forms can usually be separated into component factions (basic forms) with little difficulty, (especially with computer curve fitting programs) providing a wealth of information about the absorber sample. Generally it may be said that the area under the resonance peak is proportional to the amount of the element under investigation in a particular type of sample (22). Mōssbauer Spectroscopy can provide quantitative information as well as qualitative information about the sample.

Examples of some of the information obtained using Mōssbauer spectroscopy may be shown with a few typical spectra. We have seen the different isomer shifts of the tin (IV) halide compounds. In most iron compounds a quadrupole splitting is typical, as shown in Fig. 8 (a wide splitting for ferrous and a narrow splitting for ferric compounds).

Many different iron compounds have their isomer shifts and quadrupole splittings listed in a table compiled by Fluck et al. The accompanying diagram (Fig. 10) shows certain band locations on the velocity axis where isomer shift and quadrupole split values may be found. The influence of temperature on these values is generally linear from -120°C to +80°C (1). The influence of pressure varies according to the crystal structure (22).

Temperature dependence of the electric quadrupole splitting and isomer shift values can provide much information on chemical structure and bonding (26). For example, the sixth electron in excess of the half filled shell in ferrous compounds (d^6) causes a sharp temperature dependence on the quadrupole splitting. At the lower temperature the lowest molecular orbital is most populated and therefore we find the highest quadrupole splitting. As the temperature rises all molecular orbitals are populated equally and ΔE approaches zero. The d^5 configuration for iron has a much smaller temperature dependency. Brady, Duncan and Mok have reported the temperature dependence on a number of high and low spin iron compounds (27).

Pressure dependence of Mōssbauer spectra may be much smaller than temperature dependence unless the material can be significantly compressed to alter the bond lengths or the environment of the absorbing nucleus. If all the bonds were symetric and changed equally with pressure the electron density would change resulting in an isomer shift. Quadrupole splittings may change with pressure if asymmetry is present in the absorber. Mōssbauer Spectroscopy may thus detect small asymmetries which are not measurable by x-ray diffraction (28).

Other studies of isomer shifts have been made on iron compounds (13), iron organic compounds (14), tin compounds (2,15,16), and iodine compounds (17).

Studies on the bonding of clatherates (Kr) and rare gas compounds (3) have been made using Mössbauer Spectroscopy. Structural data on many compounds such as iron carbonyls, ferrates, dipyridyl iron complexes and SnF_4 (polymer-like structure) (1, 2) have also been studied using this new non-destructive method of analysis.

Wertheim and co-workers have correlated the isomer shift values of Fe-57 as a function of 3d and 4s electron charge density (13). Their diagram is shown in Fig. 9 and it provides a useful aide in determining electron charge density for compounds of interest.

Since most of the original work in the field of Mössbauer Spectroscopy has been with iron, many potential applications of this technique in the non-destructive testing of metals and alloys have already been discussed (5, 6). Mössbauer Spectroscopy may be used in quality control or for the study of alloy structure and its relation to the magnetic hyperfine fields of the alloy. Corrosion and certain surface defects on metals or gas absorption on metal surfaces (e.g. catalysts) may also be studied using this technique. Mineral assay methods are being developed since certain minority ingredient can usually be detected in a host matrix (2).

Many of the above studies require thick samples which prohibit transmission type experiments. Therefore a scattering technique is used. This requires that both the source and detector be on the same side of the absorber (shielded from one another). The re-emitted radiation (from the decaying resonantly excited absorber nucleus) is detected and instead of a decrease in counting rate at resonance we observe an increase in detection of the Mössbauer gamma ray, resulting in a Mössbauer spectrum just the inverse obtained in a transmission experiment.

Investigation of iron compounds has extended the use of Mössbauer Spectroscopy to the field of biology. Gonzer, Grant and Kregzde (10) have studied hemoglobin and some of their results are shown on Fig. 11. The different spectra result from different ligands bound to the central iron atom. A more extensive study of hemoglobin has recently been published by Lang, et al. Other work has been done with heme and hemin compounds (12) ferrodoxin (11) and iron porphyrins (8).

Iodine is another element that has recently allowed Mössbauer Spectroscopy to be used in the biological field.

Cryogenic techniques (to provide a stiff matrix) have been developed that allow the experimenter to study species stable or more easily available in solution. Some of these techniques and the general application of Mössbauer Spectroscopy in Biology were the subject of discussion at a 1965 symposium (9).

The study of other Mössbauer elements is discussed extensively in recent publications (18, 19, 22). A new index of all publications concerning Mössbauer investigations has recently been published (20). This Mössbauer Effect Data Index has the compilation of all the data obtained and lists the parameters by nuclide.

Although many applications have been found using Mössbauer Spectroscopy, the field is just blossoming. Most of the results must be interpreted on an empirical basis. Spectra must be compiled and instruments compared to a standard reference point in order that the values obtained by different investigators be correctly interpreted.

It is interesting to note that the National Bureau of Standards in the United States now offers a standard reference crystal of sodium nitroprusside which gives a sharply defined quadrupole split spectra. The distance between the peaks (in mm/sec.) provides an accurate calibration of the investigators velocity scale. Dr. J. J. Spijkerman of the NBS Laboratory has authored a recent review article on Mōssbauer Spectroscopy which provides a compilation of publications for 1965, categorized by element with comments on the nature of each study, as well as an excellent list of references(22). Another excellent review was recently published by Greenwood in England (26).

It is obvious from the expanding number of publications that the Mōssbauer Effect is becoming a more effective analytical technique. The fact that Mōssbauer Spectroscopy has been accepted as a member of the spectroscopy family is also obvious from the availability of commercial Mōssbauer Effect Spectrometers.

Commercial and homemade Mōssbauer Spectrometers may be divided into two basic types, mechanical (usually constant velocity) and electro-mechanial (usually constant acceleration). The mechanical systems are many and include precision lathes, cam devices, pulley arrangements and piston type drives. All of these devices are limited to the relatively low velocities (usually less than 2 cm/ sec.) but may be used to study most iron and tin systems. A precision lathe type of Mōssbauer Spectrometer that is commercially available (Fig. 12) moves either the source or absorber at a given velocity (between 0.05 and 15 mm/sec.). This instrument employs a synchronous motor, and a ball-disc integrator transmission system to vary the velocity. An o-ring coupling moves the precision machined steel lead screw which in turn moves the source or absorber stage. When operating a constant velocity system, taking data for one velocity at a time, one must be very careful that the detection electronics do not drift or the resultant spectrum will be worthless.

An electromechanical transducer is the type of instrument used for a constant acceleration type of Mōssbauer Spectrometer. A voltage signal (triangular, sawtooth or sinesoidal) is transformed into a velocity in the transducer. Thus the transducer may sweep through a spectrum of velocities (from the maximum in one direction through zero to a maximum in the other directions) during each cycle. A feedback system corrects for any deviation from the reference voltage signal.

When operating at constant velocity the data is accumulated in one or two scalers. A multichannel analyzer operating in the multiscaler mode is required when operating at constant acceleration. Each channel will represent a scaler for a given velocity. Therefore the motion of the transducer must be synthronized to the MCA while it is advancing through its channels. Synchronization is most frequently established by slaving the Mōssbauer spectrometer to the MCA by deriving the reference velocity signal from the address register of the MCA.

The National Bureau of Standards system uses the analog signal from the address register to drive the transducer, with a maximum velocity of 20 cm/sec. (commercial units are available up to 60 cm/sec.) (Figs. 13A, B). A constant velocity mode of operation is also included in the NBS system.

The usual detection system used with a Mōssbauer Spectrometer would include a detector, a high voltage supply pre-amplifier, a linear amplifier, single channel analyzer scaler and timer. A multichannel analyzer capable of operating in the multiscaler mode should be included if operating in the constant acceleration mode. This mode of operation is favored because it averages any small electronic drift problems in the detection system. The type of detector chosen depends upon the gamma ray of interest. Gas filled proportional counters are generally used below 40 Kev.

Velocity spectra may be obtained directly from the MCA by using an x-y recorder. Digital data is obtained with a typewriter or paper readout system. This is necessary if you wish to perform a computer analysis of the data.

Cryogenic accessories to cool both source and absorber during Mössbauer experiments are sometimes necessary. Cooling is required in order to measure the Mössbauer effect in systems containing certain nuclides (ones with low Debye temperatures). Many commercially available dewars are designed to contain different cryogenic liquids including helium. Another system available provides cooling by the Joule-Thomson expansion of hydrogen gas. Control of gas pressure allows temperature variation from 16°K to 70°K to better than ± 0.5°K. In any cryogenic system one must be extremely careful that the unit does not introduce any vibration to the source or absorber or resonance absorption may be destroyed.

Mössbauer sources for many nuclides are also available commercially and may vary in composition. Some may be electroplated (Co-57 on copper, palladium or platinum) or just potted in plastic (Sn-119m as $BaSnO_3$). Absorbers are easily made by mounting the sample (foil or powder) between two sheets of 5 mil mylar with the help of double backed tape. Cryogenic mounts are usually metallic for better heat conduction properties.

Studies into the bonding of organo metallic compounds (especially organo-tin compounds) have been fairly numerous. Interpretation of isomer shift values and a compilation of different data has been summarized in two papers by Herber et al (29, 30). Fig. 14 shows how the Mössbauer parameters for a number of tin compounds may be grouped. Various organo-tin compounds fall in the crosshatched areas.

A recent investigation into the bonding of iron in coal using Mössbauer Spectroscopy was done by Lefelhocz and Kohman of Carnegie-Mellon University and Friedel of the Bureau of Mines in Pittsburgh (31). Various coal samples were run to study the organically bound iron in the coal. Their preliminary work confirms that the iron sulfide in coal consists mainly of pyrite and indicates that non-pyrite iron is in a high spin iron (II) state having octohedral coordination.

The Mössbauer spectra obtained by Lefelhocz et al. could not be compared directly to any other reported spectra. Some spectra with similar δ and Δ values has led them to believe that the iron may be bound to heterocyclic nitrogen aromatic groups in the coal macerals or possibly in a clay-like silicate mineral or gel.

Another area of usefulness for Mössbauer Spectroscopy is the investigation of catalysts and their functions. Very little has been published on this type of work. NSEC has recently been working with a number of companies in this area. Initial results have shown different Mössbauer patterns for new and used catalysts of iron oxides as well as complex iron compounds. Both magnetic and non-magnetic forms may sometimes be present in different ratios for the new and used catalysts. Hopefully future work will include investigation of these catalysts in working systems to see what influence adsorption (and perhaps reaction) may have on the Mössbauer Spectrum.

Some work has been done on adsorption studies using the Mössbauer effect. Flinn and co-workers studied iron on the surface of Al_2O_3 (32). An anisotropy of thermal vibration relative to the surface was observed. This resulted in unequal peaks in the quadrupole split spectrum. The large quadrupole split also indicated that the iron was present in a highly assymetric electrical field. The amplitude of vibration was greatest along the axis of the electric field gradient (normal to the surface) compared to that parallel to the surface.

Other adsorption studies have been made by Burton, Goodwin and Frauenfelder at the University of Illinois (33) and by Shpinel and co-workers in Russia (34) and others (35, 36, 37). Comparisons were made between atoms in the bulk of the matrix, in the surface of the matrix and on the surface of the matrix. Variations of the resultant spectra with temperature for each type sample were used to explain the surface dynamics of an atom. It is hoped that Mössbauer Spectroscopy will prove more useful in the study of the surface dynamics, chemical states and magnetic properties of adsorbed particles (including very thin films).

This explanation of Mössbauer Spectroscopy, description of equipment available and the examples of the applications that have been given are all too brief. Much new information concerning the elements we are able to study has been obtained using this very sensitive analytical technique. Some of this information can be obtained by no other method. Other information compliments what has been obtained using NMR, ESR and x-ray diffraction and other analytical techniques. Therefore, we can look forward to increased references to data obtained from Mössbauer spectra and further refinement of Mössbauer Spectroscopy.

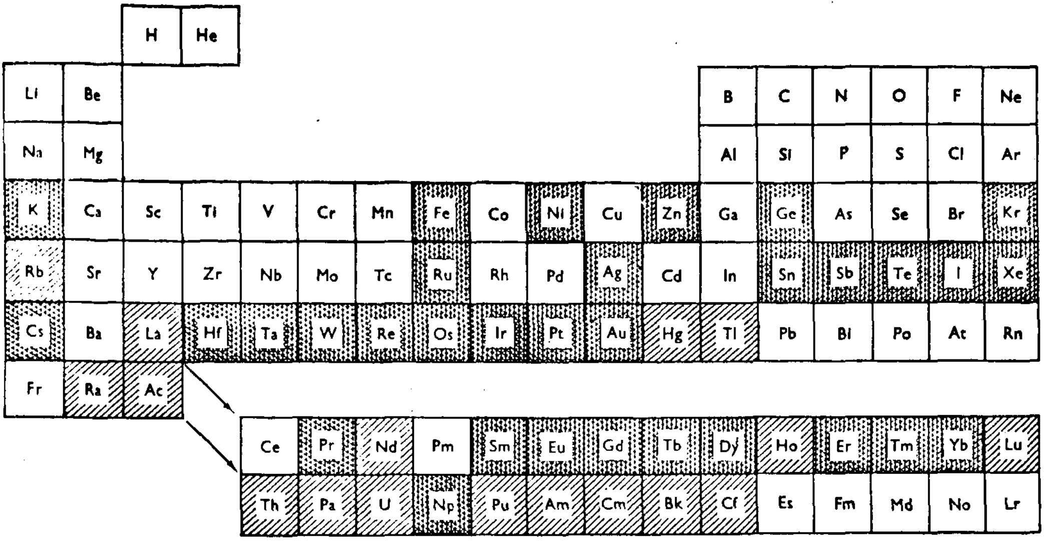

		H	He														
Li	Be											B	C	N	O	F	Ne
Na	Mg											Al	Si	P	S	Cl	Ar
▩ K	Ca	Sc	Ti	V	Cr	Mn	▩ Fe	Co	▩ Ni	Cu	▩ Zn	Ga	▩ Ge	As	Se	Br	▩ Kr
▨ Rb	Sr	Y	Zr	Nb	Mo	Tc	▩ Ru	Rh	Pd	▩ Ag	Cd	In	▩ Sn	▩ Sb	▩ Te	▩ I	▩ Xe
▩ Cs	Ba	▨ La	▩ Hf	▩ Ta	▩ W	▩ Re	▩ Os	▩ Ir	▩ Pt	▩ Au	▨ Hg	▨ Tl	Pb	Bi	Po	At	Rn
Fr	▨ Ra	▨ Ac															
				Ce	▩ Pr	▨ Nd	Pm	▩ Sm	▩ Eu	▩ Gd	▩ Tb	▩ Dy	▨ Ho	▩ Er	▩ Tm	▩ Yb	▨ Lu
				▨ Th	▨ Pa	▨ U	▩ Np	▨ Pu	▨ Am	▨ Cm	▨ Bk	▨ Cf	Es	Fm	Md	No	Lr

▩ Mössbauer effect observed (32 Elements)

▨ Mössbauer effect predicted (17 Elements)

Fig. 1. Occurrence of the Mössbauer Effect (26)

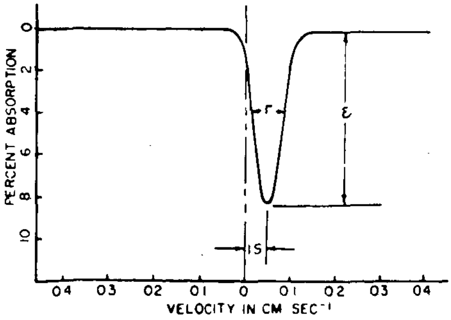

Fig. 2. Typical Mössbauer spectrum. (4)

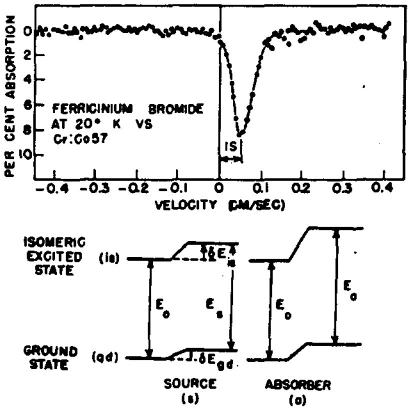

$$\delta = \frac{4\pi}{5} Z e R^2 \frac{\Delta R}{R} \left(|\psi_a|^2 - |\psi_s|^2 \right)$$

Fig. 3. Isomer shift. The effect of the electric monopole interaction is to shift nuclear levels without separating the magnetic sublevels. The shifts are very small as compared to the total energy of the gamma ray, 10^{-12} Eγ. (7)

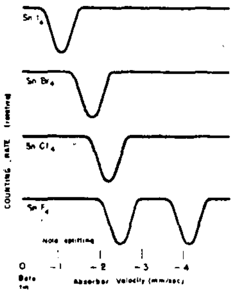

Fig. 4. Mössbauer spectra can contain more than one line, if energy levels are split by interaction that depends on nuclear orientation. In this case SnF_4 spectrum is doublet because Sn^{119} electric moment interacts with inhomogeneous field of surrounding F atoms.(2)

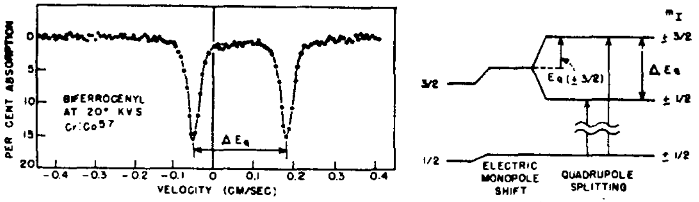

$$\Delta E_q = \frac{eqQ}{2}$$

Fig. 5. Quadrupole splitting. The interaction of the nuclear quadrupole moment, Q, with the gradient of the electric field, eq, is illustrated for nuclear ground-state spin $I_{gd} = 1/2$ and for isomeric-state spin $I_{is} = 3/2$; the diagrams are applicable to Fe^{57}, Sn^{119}, and Tm^{169}, among other isotopes. For the ground state, or any state with $I = 1/2$, Q is inherently zero. An example of a pure quadrupole Mössbauer absorption spectrum is shown. (7)

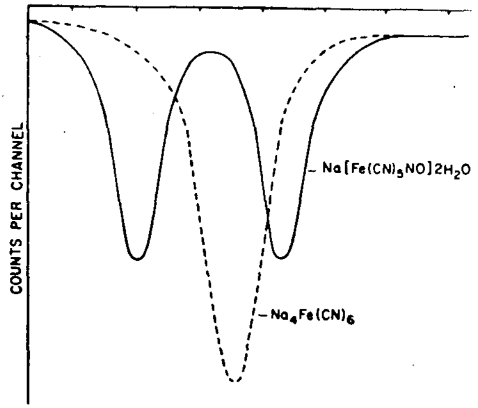

Fig. 6. Mössbauer spectra of an octahedrally symmetric complex $[Na_4FeCCN)_6]$ and of a distorted octahedral complex $[Na_2[Fe(CN)_5NO]\cdot 2H_2O]$, showing the effect of a non-vanishing electric field gradient at the Mössbauer lattice point. (4)

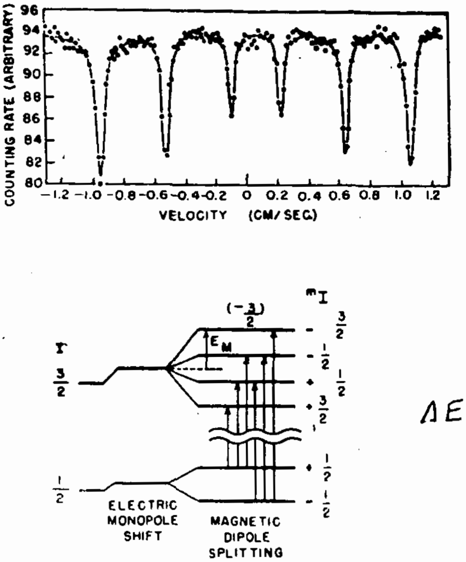

$\Delta E_M = \mu \frac{H}{I}$

Fig. 7. Magnetic hyperfine splitting for $I_{gd} = 1/2$, $I_{is} = 3/2$. As a result of the selection rule, $\Delta m = 0, \pm 1$, only six of the possible eight lines are observed. The graph shows the Fe^{57} hyperfine splitting of FeF_3, which corresponds to a field of 620,000 oersteds.(7)

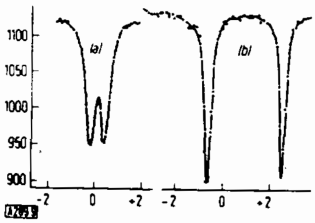

Fig. 8. Mössbauer spectra (a) of $FePO_4 \cdot 4\,H_2O$ and (b) of $FeSO_4 \cdot 7\,H_2O$ (1)
Ordinate: transmission [arbitrary units]
Abscissa: velocity of the source relative to the absorber [mm/sec]

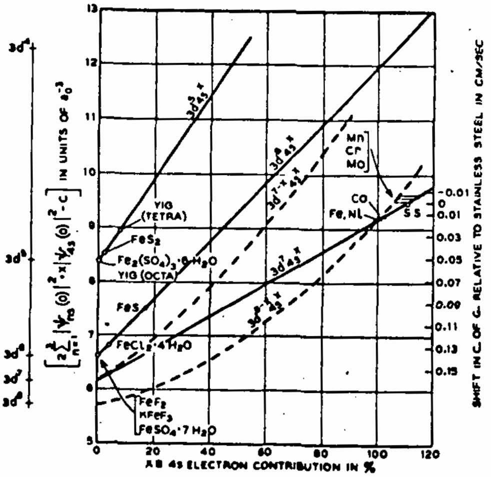

Fig. 9. A possible interpretation of the Fe^{57} Mössbauer isomer shifts in various solids. The total s-electron density is plotted as a function of the percentage of $4s$ character for various d-electron configurations. The reasons for placing the experimental data on given theoretical curves are discussed in the text. The constant $C = 11\,873\ a_0^{-3}$. (13)

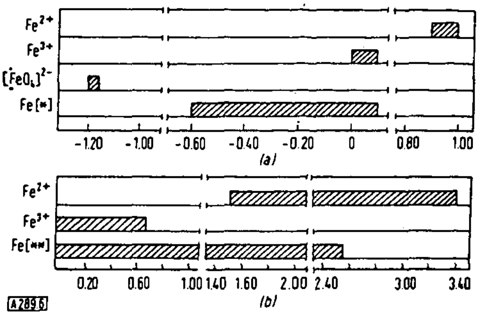

Fig. 10. (a) Values for the isomeric shifts and (b) values for the quadrupole splittings of Mössbauer lines in ferrous and ferric compounds. (1)

Radiation source: ^{57}Co in platinum at 25 °C.

Abscissa: Velocity of the source relative to the absorber [mm/sec].

Fe [*] = iron in complexes and metals.

Fe [**] = iron in complexes.

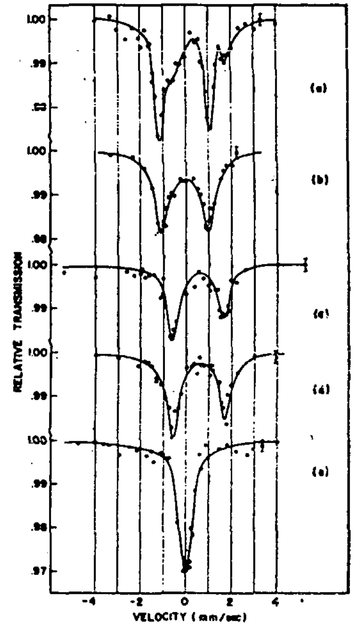

Fig. 11. Mössbauer absorption spectra with a source of Co^{57} diffused into Pt and kept at room temperature and absorbers of (*a*) rat red cells at 4°K and isotopically enriched with Fe^{57}, (*b*) crystalline rat oxyhemoglobin at 77°K, (*c*) human CO_2-hemoglobin (in a CO_2 atmosphere) at 77°K, (*d*) human hemoglobin (in a N_2 atmosphere) at 77°K, and (*e*) human CO-hemoglobin (in a CO atmosphere) at 77°K. We have used the standard notation that source approaching absorber is positive velocity. (10)

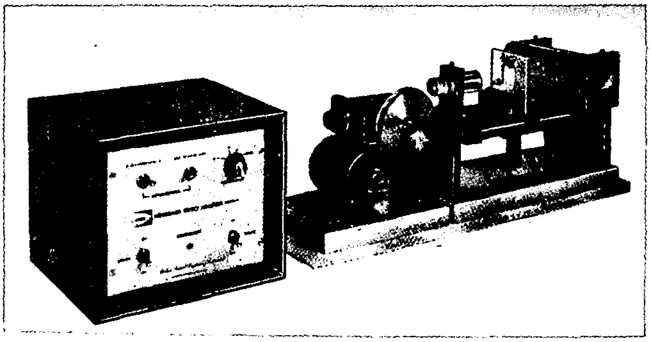

Fig. 12. A Constant Velocity Mössbauer Effect Analyzer

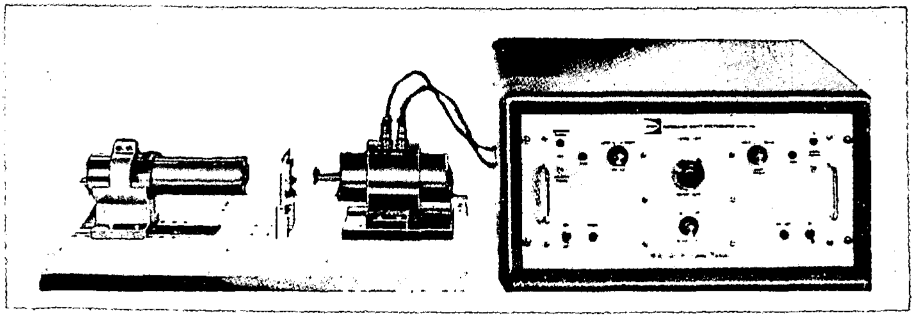

Fig. 13. A Constant Acceleration Mössbauer Effect Spectrometer

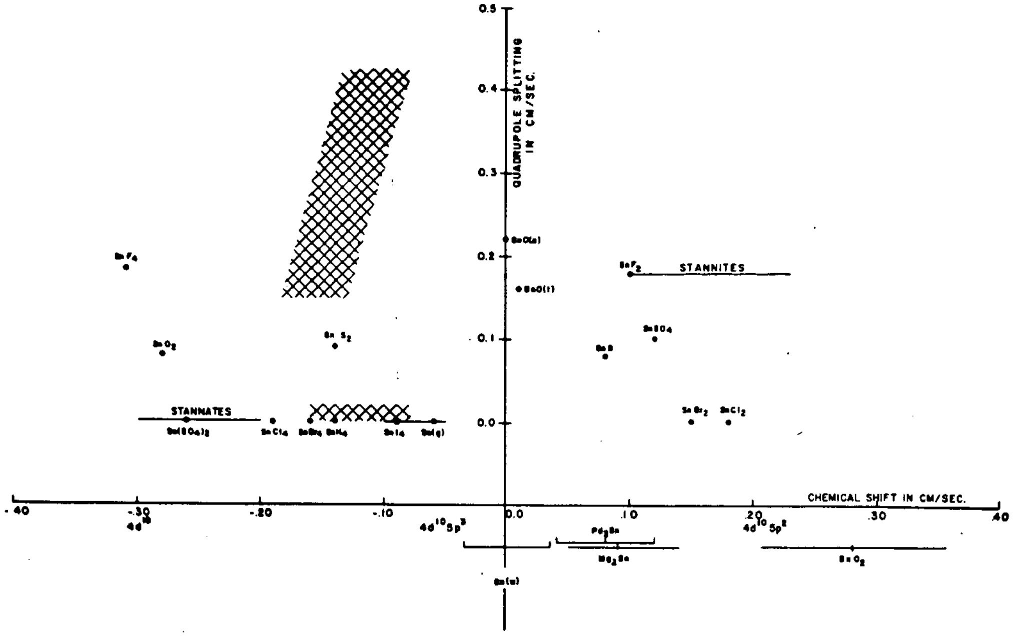

Fig. 14. Correlation diagram of the quadrupole splitting and chemical shift values for Tin Compounds at 78°K (38)

References

1. Fluck, E., Kerler, W., Neuwirth, W., Angew. Chem. 75, 461 (1963).
2. Goldanskii, V.I., Intern. Science & Tech., December (1963).
3. Wertheim, G.K., "Mössbauer Effect, Principles and Applications", Academic Press, New York, 1964.
4. Herber, R.H., J. Chem. Ed. 42, 180 (1965).
5. Johnson, C.E., Ridout, M.S., Cranshaw, T.E., Madsen, P.E., Phys. Rev. Letters 6, 450 (1961).
6. Wertheim, G.K., Phys. Rev. Letters, 12, 24 (1964).
7. Wertheim, G.K., Science 144, 253 (1964).
8. Maling, J.E., Neissbluth, M., "Mössbauer Resonance Studies in Iron Porphyrins and Heme-proteins", in Electronic Aspects of Biochemistry, B. Pullman, Ed., Academic Press (1964).
9. Kettering Foundation Symposium, March 1965, A. San Pietro, Ed., Antioch Press (1965).
10. Gonser, U., Grant, R.W., Kregzde, J., Science 143 (1964).
11. Pillinger, W.L., Stone, J.A., AEC Report DP878 (1964).
12. Bearden, A.J., Moss, T.H., Caughey, W.S., Beaudreau, C.A., Proc, Nat. Acad. Sci. 53, 1246 (1965).
13. Walker, L.R., Wertheim, G.K., Jaccarino, V., Phys. Rev. Letters 6, 98 (1961).
14. Herber, R.H., King, R.B., Wertheim, G.K., Inorg. Chem. 3, 101 (1963).
15. Bryukhanov, V.A. et al, Soviet Phys. JETP (English Translation), 16, 321 (1963); see also ibid 16, 310 (1963); 16, 879 (1963).
16. Cordey-Hayes, M., J. Inorg. and Nuclear Chem. 26, 915 (1964).
17. DeWaard, H., DePasquall, G., Hafemeister, D., Phys. Letters 5, 217 (1963); Rev. Mod. Phys. 36, 358C (1964).
18. Fluck, E., "The Mössbauer Effect and Its Application in Chemistry" in Advances in Inorganic Chemistry and Radiochemistry - Vol. 6, Emeleus, H.J. Sharpe, A.G., eds., Academic Press, New York (1964).
19. Proceedings of the 3rd International Conference on the Mössbauer Effect, Rev. Mod. Physics 36, #1 Part II (Jan. 1964).
20. Muir, A.H. et al, "Mössbauer Effect Data Index", 1958-1965 Interscience - John Wiley and Sons, New York City (1967).
21. Lang, G., Marshall, W., Proc. Phys. Soc. 87, 3 (1966).
22. DeVoe, J.R., Spijkerman, J.J., Anal. Chem. - Annual Reviews 38, 382R (1966).
23. Mossbauer, R.L., Ann. Rev. Nuclear Sci. 12, 123 (1962).
24. Frauenfelder, H., "The Mössbauer Effect"; W. A. Benjamin Inc., New York (1962).
25. Nowik, I., Bell Telephone Laboratories, Murray Hill, New Jersey (to be published).
26. Greenwood, N.N., Chemistry in Britain 3, No. 2 56-72 (1967).
27. Brady, P.R., Duncan, J.F., Mok, K.F., Proc. Royal Soc. (London) 287A, 343-62, (1965).
28. Christ, B.W., Spijkerman, J.J., Giles, P.M., Ruegg, F.C., Trans. Met. Soc. of AIME (Tech. Letter to be published).
29. Herber, R.H., Stoeckler, H.A., Reichle, W.T., J. Chem. Phys. 42, 2447 (1965).
30. Herber, R.H., Nuclear Sci. Abstr. 19 No. 8 13518 (1965).
31. Lefelhocz, J.F., Friedel, R.A., Kohman, T.P., (Submitted to Geochimica et Cosmochimica Alta April 1967).
32. Flinn, P.A., Ruby, S.L., Kehl, W.L., Science 143, 1434 (1964).

33. Burton, J.W., Frauenfelder, H., Goodwin, R.P., Nuclear Sci. Abstracts No. 20 40078 (1965).

34. Karasev, A.N., Polak, L.S., Shlikhter, E.B., Shpinel, V.S., Kinetika i Kataliz 6 710 (1965).

35. Kundig, W. et al, Phys. Rev. 142 327 (1966).

36. Suzdalen, I.P. et al, J.E.T.P. 22, 979 (1966).

37. Hobson, M.C., Nature 214 79 (1967).

38. Spijkerman, J.J., Symposium on "The Mössbauer Effect and Its Application in Chemistry" to be published in the Advances in Chemistry Series (1967) by A.C.S.